Luigi Ciotti

Competition Between Transport Phenomena in a Reaction-Diffusion-Convection System

Phd Thesis

Relatore: Prof. Mauro Rustici

Scuola di Dottorato
in Scienze e Tecnologie Chimiche
XIII Ciclo
Direttore: Prof. G. B. Suffritti

Università degli Studi di Sassari
Facoltà di Scienze Matematiche, Fisiche e Naturali
Dipartimento di Chimica
Novembre 2011

A Cinzia e a nostro figlio Pietro

Sommario

La presente tesi è costituita da tre parti principali.

Nella prima parte è riportata una breve introduzione alla scienza non lineare, all'analisi non lineare e alla termodinamica del non equilibrio. Vengono inoltre illustrati i concetti di cinetica chimica delle reazioni oscillanti, con particolare riferimento alla reazione di Belousov–Zhabotinsky .

Nella seconda parte viene descritta la formulazione del modello matematico reazione–diffusione–convezione (RDC), usato nelle simulazioni numeriche per lo studio degli scenari di transizione al caos degli oscillatori chimici, e la relativa traduzione in un opportuno linguaggio di programmazione.

Nella terza parte, i metodi impiegati per la caratterizzazione del sistema e i dati ottenuti. Ciò che si osserva è una sequenza distinta e caratteristica di biforcazioni, ascrivibile allo scenario di tipo RTN, in cui un regime quasiperiodico si trasforma in un regime con raddoppiamento del periodo nella via al caos chimico. L'influenza esercitata in maniera opposta dai due parametri sulla dinamica del sistema suggerisce che esista una sorta di competizione tra i fenomeni di trasporto, nella fattispecie diffusione e convezione. Viene anche rilevato un comportamento simmetrico tra oscillazioni chimiche e caos spazio-temporale. Questo lascia ipotizzare che i due aspetti siano una manifestazione dello stesso fenomeno, rafforzando l'ipotesi che le oscillazioni chimiche e le instabilità dovute ai fenomeni di trasporto siano all'origine del caos deterministico per questo tipo di sistemi. Parallelamente, è stato portato avanti uno studio di dinamica molecolare per il calcolo dei coefficienti di diffusione degli intermedi attivi nella reazione Belousov–Zhabotinsky , cioè $HBrO_2$ and Ce(III), per mezzo del mean square displacement e della funzione di autocorrelazione delle velocità. I dati ottenuti hanno permesso una comprensione più approfondita della competizione idrodinamica osservata.

Abstract

This doctoral dissertation consists of three main parts.

In part one, a general overview of the basic concepts of nonlinear science, nonlinear analysis and non-equilibrium thermodynamics is presented. Kinetics of chemical oscillations and the well known Belousov–Zhabotinsky reaction are also illustrated.

In part two, a Reaction–Diffusion–Convection (RDC) model is introduced as a convenient framework for studying instability scenarios by which chemical oscillators are driven to chaos, along with its translation to an opportune code for numerical simulations.

In part three, we report the methods and the data obtained. We observe that distinct bifurcation points are found in the oscillating patterns as Diffusion coefficients (d_i) or Grashof numbers (Gr_i) vary. Singularly there emerge peculiar bifurcation paths, inscribed in a general scenario of the RTN type, in which quasi–periodicity transmutes into a period-doubling sequence to chemical chaos. The opposite influence exhibited by the two parameters in these transitions clearly indicate that diffusion of active species and natural convection are in 'competition' for the stability of ordered dynamics. Moreover, a mirrored behavior between chemical oscillations and spatio-temporal dynamics is observed, suggesting that the emergence of the two observables are a manifestation of the same phenomenon. The interplay between chemical and transport phenomena instabilities is at the general origin of chaos for these systems.

Further, a molecular dynamics study has been carried out for the calculation of diffusion coefficients of active species in the Belousov–Zhabotinsky reaction, namely $HBrO_2$ and Ce(III), by means of mean square displacement and velocity autocorrelation function. These data have been used for a deeper comprehension of the hydrodynamic competition observed between diffusion and convective motions for the stability of the system.

Acknowledgments

Before starting this academic adventure, I knew it would be a hard task dealing with a doctoral research project in a theoretical field, significantly different from my everyday job as an analytical chemist. Nonetheless, the wish to return – nine years later – to some fascinating problems encountered in my undergraduate studies and the desire to breathe again an academic atmosphere brought me to this decision; but I am not sure if this project would have been equally successful without the support of a very friendly and affectionate working group. The research activity for my doctoral dissertation has been, in fact, a very stimulating endeavor but, apart from scientific advantage, I will always remember the last four years for the personal enrichment. For this reason I would like to spend some words for the people who made special this experience and are today a part of my life.

First and foremost I want to thank my Advisor Prof. Mauro Rustici for having accepted me as a PhD student in the Nonlinear Dynamics Group, for the excellent example he has provided as a friend and mentor, other than as professor, and for having invited me to his wonderful dinners (which, regrettably, I could not reciprocate!).

But this project owes a lot to two friends. I would like to express my gratitude to Dr. Marco Masia, for having taken time out from his busy schedule to serve as my co-advisor: his expertise, understanding, and patience added considerably to my doctoral experience. Also, I would like to thank my PhD colleague Marcello, whose indefatigable effort provided the indispensable ingredients to be churned into the cauldron. I truly appreciated the amount of time and energy that they invested in guiding me throughout this work, the many conversations – as enlightening as always – and their support in the most critical moments. I owe them my eternal gratitude.

Thanks also to Emiliano for his stimulating, lively and friendly presence. I wish we had spent some more time working together but I hope we will have a further occasion in the future.

Lastly, I would like to thank my mother, who raised me with a love for science and supported me in all my pursuits, and my friend Annamaria, the best teacher I have ever had.

I am also particularly grateful to my friends Richard and Monica, who were so kind to read the whole manuscript thoroughly and correct the English spelling and grammar, and to Alessandro, Angelo e Pierpaolo, for the support they provided me through this long project: without their love, encouragement and editing assistance, I would not have finished this thesis.

Luigi Ciotti

30th November, 2011

Indice

Elenco delle figure

Elenco delle tabelle

Parte I

Introduction

Order from disorder

Among the several advances of the 20th century, nonlinear science is exceptional for its generality. Indeed, it plays a key role in almost every branch of modern fundamental and applied research. Its first goal is to provide the concepts and techniques for an unified description of a particular, but wide, class of phenomena where simple deterministic systems generate complex behaviors, with the emergence of unattended temporal dynamics and spatial patterns.

Our scientific knowledge is often based on the assumption that in a natural system, subject to external and well defined conditions, individual effects can be unambiguously traced back to particular causes. In other words, a compound cause is viewed as the algebraic sum of a collection of simple causes, each of which can be uniquely linked to a particular effect. The total effect responding to the total cause is then considered to be just the linear sum of the constituent effects.

For its undoubted charm, this idea, along with its corollaries of reproducibility and unlimited predictability, mastered for a long time our way of thinking and gradually led us toward an idea of a linear world. Although attractive and reassuring, this idea is slowly changing because it can give only a partial view of the natural world. In many situations, and mainly in daily life, we can observe in fact radical deviation from these proportional laws. In simple terms, considering the cooperation between the different elements of a system, nonlinear science recognized that the whole is more than a sum of its parts, providing a context for consideration of phenomena like tsunamis (tidal waves), biological evolution, atmospheric dynamics, and the electrochemical activity of a human brain, among many others.

Nonlinear science introduces a new way of thinking, based on an interchange between qualitative and quantitative techniques, topological and geometric considerations, deterministic and statistical aspects. The fundamental laws of microscopic (Newton and Schröedinger equations) and macroscopic physics (Navier-Stokes and mass-action law) are inadequate for the comprehension or the formulation of complexity induced by the evolution of nonlinear systems. On the other hand dissipative structures, negative entropy, autoorganization, attractors, fractals, Lyapunov exponents, are part of a new vocabulary proposed by modern nonlinear science and provide a new pragmatic way to tackle a challenge where the classic approach fails.

The evolution of the state variables of a system, obeying to the classical laws of physics, is described by a system of differential equations first order in time along with spatial derivatives (laplacian and gradient). These can be ordinary (ODE), like Hamilton or chemical kinetic equations, or partial (PDE), like fluidodynamic or reaction-diffusion equations. In the last case, typical for a macroscopic description, we have to deal with infinite degrees of freedom, which are the values of state

variables (now fields) in every point of the space as a function of time. In some cases we can reduce them to a finite number of variables by means of the well known Galerkin's reduction method: the fields are described as Fourier series and equations for amplitude are truncated to the first normal modes, providing an ODE system for amplitudes of every mode important for the description of our system. A general form for these equations is given by

$$\frac{\partial X_i(\mathbf{r},t)\}}{\partial t} = F_i(\{X_j(\mathbf{r},t)\},\{\nabla^k X_j(\mathbf{r},t)\},\ \mu) \tag{1}$$

where μ are *control parameters* and play an important role in the behavior of a dynamic system: they are related to the internal structure of the system (diffusion coefficients, viscosity) and regulate also the way by which the system communicates with the external environment (thermal constraints, residence time, etc.). Although the problem described by our ODE system is *deterministic* (we can predict the evolution for every time t, once initial values X_i at the time t_0 are known), it requires an infinite amount of data specifying initial conditions in a precise way. In practice, it has nonsense value, because measurements performed by an observer are always of finite precision. This is not only an instrumental, but also a natural limit for knowledge, according to Heisenberg's uncertainty principle. Such a dynamic system has in principle an infinite number of variables, i.e., the values of fields $X_i(\mathbf{r},t)$. Sometimes discretization or reduction can be very difficult and such systems are often solved via numerical integration.

In the phase space Γ our system will be represented by a small region of volume $\delta\Gamma_0$, rather than a point, whose extension is given by the precision of measurements. For the observer, the points inside this region represent the same macroscopic state. Thanks to the idea of statistic ensemble (Gibbs, 1902) we can introduce the function ρ, the density of probability, expressed as the ratio between the probability that the system is in a determined state to the number N of states available, when the region of space is very small

$$\rho = \frac{1}{N}\lim_{\delta\Gamma_0\to 0}\frac{\delta N}{\delta\Gamma} \tag{2}$$

In order to forecast the probability of occurrence of certain values of state variables X_i, we have to solve an equation for ρ. The theorem of uniqueness (appendix V) states that the number of trajectories in the phase space must be conserved. This signifies that ρ can be considered as a trajectory density and, in analogy to the mass density for a fluid, we can write the following relation between probability (or trajectory) density and evolution laws:

$$\frac{dln\rho}{dt} = -\nabla\mathbf{F} \tag{3}$$

which can be integrated, giving

$$\frac{1}{t}\ln\frac{\rho_t}{\rho_0} = -\frac{1}{t}\int_0^t dt'\nabla\mathbf{F} = -(\bar{\nabla\mathbf{F}})_t \tag{4}$$

where $(\bar{\nabla\mathbf{F}})_t$ is the temporal average. Equations 3 and 4 are the starting point for the classification of dynamical systems into two main categories, *conservative* and *dissipative*:

- if $(\bar{\nabla}\mathbf{F})_t = 0$, $\rho_t = \rho_0$; trajectory density is conserved and the system is said to be *conservative*;
- if $(\bar{\nabla}\mathbf{F})_t < 0$, $\rho_t < \rho_0$; trajectories will contract in the phase space and tend to regions with lower dimension: the system is said to be *dissipative*.

Dissipative structures are among the new concepts introduced by nonlinear science, i.e., ordered structures when a system is far from its thermodynamic equilibrium. The mechanism of formation of dissipative structures cannot be explained in terms of classical thermodynamics or statistical mechanics used for equilibrium structures. One of the first numerical studies for dissipative systems was carried out in the early

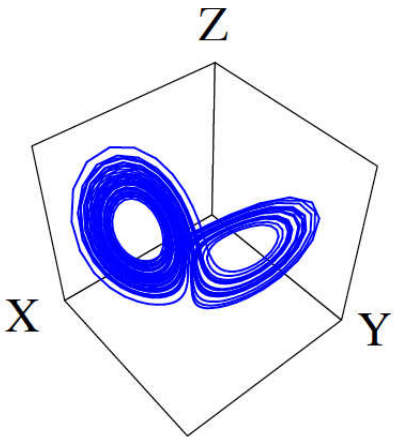

Figura 1: the Lorenz's chaotic attractor

1960's by Edward Norton Lorenz Lorenz, 1963, an american mathematician and meteorologist, who was trying to understand the failures of linear prediction techniques for weather forecasts. Using one of the world's first mass-produced computers to simulate atmospheric dynamics, he found that long aperiodic trajectories could be produced quite robustly.

Then, in one of history's most serendipitous episodes of computer rounding error, he found that the aperiodicity was paired with sensitive dependence on initial conditions. He then reduced the atmosphere simulation to a differential equation in three variables that produced the *Lorenz's attractor* (figure 37). Lorenz later gave a lecture entitled *Predictability: Does the Flap of a Butterfly Wings in Brazil set off a Tornado in Texas?*, which caused the concept of sensitive dependence on initial conditions to become popularly known as the *butterfly effect* (figure 2). Chaos describes a system that is predictable in principle but unpredictable in practice. In other words, although the system follows deterministic rules, its time evolution appears random. In dynamic systems theory, the term chaos is applied to deterministic systems that are aperiodic and that exhibit sensitive de-

Figura 2: the butterfly effect

pendence on initial conditions. Sensitivity means that a small change in the initial state will lead to progressively larger changes in later system states. Because initial states are seldom known exactly in real-world systems, predictability is severely limited. The concept of chaos has been used to explain how systems that should be subject to known laws of physics, such as weather, may be predictable in the short term but are apparently random on a longer time scale.

The study carried out for this doctoral dissertation has been focused on the numerical study of nonlinear dynamics encountered in a reaction–diffusion–convection system. When kinetics has an autocatalytic mechanism as a source of nonlinearity, the Belousov–Zhabotinsky reaction becomes a particular case.

The Belousov–Zhabotinsky reaction is the most studied oscillating reaction, used as laboratory model for more complex systems in biology and biophysics, that exhibits a plethora of dynamical phenomena under opportune conditions, when the system is far from its thermodynamic equilibrium. Complex temporal evolution and ordered dissipative structures, observed in experiments and emerging as particular solutions of our modelization, has been investigated by means of nonlinear analysis techniques.

Further,molecular dynamics simulations have been carried out for the calculation of an important dynamical property of our system: the diffusion coefficient of the intermediate species participating in the Belousov–Zhabotinsky reaction.

0.1 Non-equilibrium Thermodynamics

The second principle of Thermodynamics in its classic form introduces the entropy state function S. In isolated systems entropy increases for irreversible processes and is zero at equilibrium

$$\frac{dS}{dt} \geq 0 \tag{5}$$

According to Rudolf Clausius's postulate, the entropy of the universe is increasing: it would necessarily imply that the whole universe is devoted to a thermic death, in contradiction of what we can directly observe in the actual instant and what we can deduce from the past.

Figura 3: Ilya Prigogine

While Clausius formulated his second principle in the early 1850s, Charles Darwin founded his own evolution theory by observing that the history of our planet evolved by increasing its grade of *complexity*. How then would it be possible to conjugate the two theories? Is it probable that both Clausius and Darwin were right? A first reply to this question could be to conceive the biological life beyond the physical laws, deeming the existence of life in our planet as an highly improbable event that found an autosustainable way to be. This hypothesis has been made by Jacques Monod (Nobel Prize in Medecine, 1965) in his book *Chance and Necessity*. On the other hand, Ilya Prigogine (Nobel Prize in Chemistry, 1977, figure 3) tried to reply to the question operating inside the physical laws Prigogine, 1947. Non-equilibrium has been considered, for a long time, only as a perturbation able to hinder the onset of equilibrium. We can deal, indeed, with a new class of phenomena considering a process far from its thermodynamic equilibrium.

0.1.1 Dissipative structures

If we apply, for instance, a thermal gradient to a cell containing a mixture of two different gases, we can observe an enrichment of one gas near the hottest wall, while the second stays by the coldest. As a result, entropy of the system is lower than it would be in a homogenoeus mixture: in this case non-equilibrium could became a *source of order*. Let us consider, as a further example, a thin layer of a fluid between two horizontal plates in a gravity field. The two plates have two different temperatures T_0 and T_1 so that $T_0 \geq T_1$. When $\Delta T = T_0 - T_1 = 0$ the fluid reaches the thermodynamical equilibrium, characterized by homogeneous temperature and absence of motion. Suppose that we now increase the thermal gradient such that $\Delta T = T_0 - T_1 > 0$. This condition will move the system away from equilibrium and heat will flow from the hottest to the coldest wall. When ΔT is weak the fluid will stay at rest: an observer moving along the horizontal plane will feel uniform temperature and density.

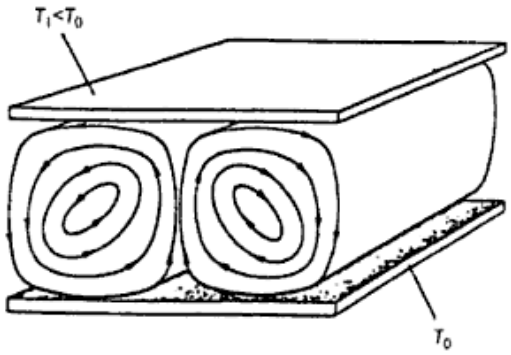

Figura 4: Qualitative view of convection Bénard cells

If ΔT exceeds the critical value ΔT_c, a motion of the fluid is observed, characterized by the presence of convection cells, the so-called Bénard cells (Figure 48). These cells have typical dimension and geometry. Also velocity, temperature and density at a fixed point are time dependent. We can further observe that two contiguous cells rotate in opposite direction: therefore, in a determined point of the space, a small element of volume can exist in two different states, in the sense that it can be part of a cell rotating in clockwise and counterclockwise direction at the same time. The rotating direction is choosen by local thermal fluctuations: it is then impossible to predict the rotation trend. This phenomenon causes a symmetry breaking associated with the sense of rotation. In other words Bénard's convection destroys the translational symmetry in the horizontal direction. We have therefore formation of order starting from disorder. The emerging structures are said *dissipative structures* Nicolis, 1995; Nicolis e Prigogine, 1977.

0.1.2 Isolated systems

Isolate systems do not exchange energy or matter with the external environment. For such systems we have that $dS > 0$: an entropy increase is associated with a disorder increase, because the system doesn't trend to the formation of organized structures, but to equilibrium structures.

In statistical mechanics, i.e. thermodynamic laws reinterpreted on a microscopic basis, we have the Boltzmann's order principle for isolated systems:

$$S = k_B ln\Omega \tag{6}$$

where k_B is the Boltzmann's constant and Ω is the number of complexions. In other words statistical interpretation, according to the second principle, forecasts a maximization of the number of the microstates accessible by the system.

0.1.3 Closed systems

For closed systems, which have only energy exchange with external environment, the situation is very similar and could be valued considering the free energy function F, defined as

$$F = E - TS \tag{7}$$

where E is the energy of the system and T is the temperature. F reaches the minimum value at equilibrium. There is then a competition between energy E and entropy S. At low temperature the contribution of S is negligible and a minimum of F corresponds to a minimum of E. For increasing temperature the system will move toward higher entropy states.

The first step in the redefinition of the problem is to understand that Boltzmann's order principle is not adapted to describe dissipative structures, because they are not equilibrium structures. These new structures can appear only when we operate far from the thermodynamic branch, characterized by a maximum of entropy S and a minimum of free Gibbs energy F. Non-equilibrium thermodynamics leads us to formulate a sufficient condition for the stability of the thermodynamic branch. If this condition it is not satisfied, the thermodynamic branch will become unstable and the system can evolve toward new structures implying a *coherent behavior*.

0.2 Open Systems

In order to heal the apparent contrast between classic thermodynamics and the organization observed in biological life, it is necessary to consider *open* systems, by analyzing non-equilibrium states from a different point of view.

A thermodynamic system is said to be open when it has an exchange of matter and energy with the external environment. Biological systems are open. The extended version of the second principle of thermodynamics, applicable to open systems, was formulated by Ilya Prigogine in 1945. The entropy variation dS in a time interval dt can be regarded as the sum of two terms

$$dS = d_e S + d_i S \tag{8}$$

where $d_e S$ is the flow of entropy due to energy and matter exchange with the environment, while $d_i S$ is the entropy production due to irreversible processes in the internal system (i.e. diffusion, thermal conduction, chemical reactions). The second principle requires $d_i S \geq 0$. For an isolated system $d_e S = 0$, therefore $dS = d_i S \geq 0$. Open systems differ from isolated ones by the $d_e S$ term, the external entropy flow. Contrarily to $d_i S$, that cannot be negative, the $d_e S$ term does not have a fixed sign. We can then imagine some situations where the system reaches an entropy state lower than the initial state because of a negative entropy flow from the environment.

$$\Delta S = \int_\Gamma dS < 0 \tag{9}$$

This state, highly improbable from a classical thermodynamic point of view, can be indefinitely held if the system reaches a stationary state $dS = 0$, or $d_e S = -d_i S < 0$. Theoretically, if we give a sufficient amount of negative entropy to our system, it is possible to decrease the entropic content in order to have creation of ordered structures, avoiding a violation of the second principle. This contribution must happen far from equilibrium conditions, otherwise $d_i S$ and $d_e S$ are zero. This is of great concern for living beings: for example biosphere as a whole is a non-equilibrium system, because it is fed with a solar energy flow; cellular membranes are supplied with different chemical reactions and have gradients of chemical substances. Summarizing, we can deal with thermodynamic systems characterized by two main trends:

- tendence to equilibrium with a high grade of disorder
- tendence to a stationary state characterized by a cooperative and coherent behavior of the different parts

Without entering into the details of thermodynamic study, it is possible to demonstrate that the creation of coherent ordered structures occurs far from equilibrium in an open system, when it obeys to nonlinear laws, while destruction of order is observed at the equilibrium or thereabouts.

0.3 Nonlinear Systems

The insability of the thermodynamical branch in open systems gives rise to the possibility of studying a plethora of uncommon phenomena, like autoorganization and chaotic dynamics. We briefly introduce here the basis for a nonlinear dynamics approach. From a mathematical point of view an operator $\mathbf{F}$ is linear if

$$\mathbf{F}(f+g) = \mathbf{F}(f) + \mathbf{F}(g) \tag{10}$$

and

$$\mathbf{F}(af) = a\mathbf{F}(f) \tag{11}$$

where a is a constant and f, g are functions. If $\mathbf{F}$ does not satisfy equations 120 and 121, the operator is nonlinear. In a linear system the effect of the combined action of two separate causes is simply the overlap of the single effects. On the other hand, in a nonlinear system the overlapping principle is no longer valid and the combined actions of two separate causes can lead to new situations. One of the most surprising features of nonlinear systems is the phenomenon of *bifurcation*. We illustrate this concept by considering the very simple example of the *hoop*. We consider (figure 40) a rigid vertical ring of radius r in a field of gravity.

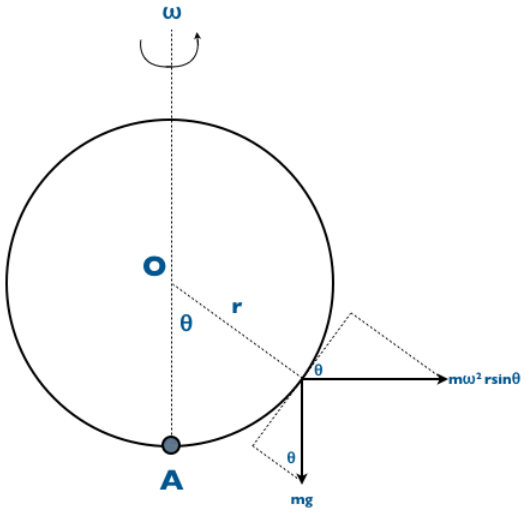

Figura 5: A mass m on a vertical rotating hoop

A mass m is initially placed at an angle θ from the lower end of the vertical diameter and is allowed to move along the ring with no friction. As long as the ring as a whole is at rest, it will perform a periodic motion around position A (if $\theta \neq 0$) or will remained fixed for ever on A (if $\theta = 0$), the equilibrium state of our simple device. Now let the ring be rotated around its vertical diameter with a constant angular velocity ω, as a result of an external constraint (here an appropriately applied torque). Experiment shows that as long as ω is small the mass still oscillates around the same equilibrium position A as before. But, beyond a critical threshold ω_c the situation changes completely and the mass oscillates around a new equilibrium position corresponding to a nonzero value of the angle θ. Actually there exist two such equilibria, placed symmetrically around the vertical diameter. There is no preference for either of the equilibria to be choosen: the choice is dictated by the initial position and velocity of the mass which, in many respects, is governed by chance.

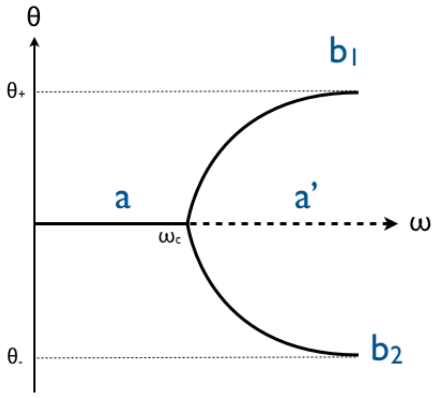

Figura 6: Bifurcation of new equilibria θ_+ and θ_-

Still, in a given experiment only one of these equilibria will be realized and the mass will accordingly oscillate around it. To the observer, this will appear as an asymmetric realization of a perfectly symmetric physical situation, a symmetry breaking in other words, like the Bénard cells rotation, the particular symmetry being broken here being the reflection symmetry around the vertical diameter.

It is convenient to organize this information on a diagram (figure 41) in which the equilibrium position θ, characterizing the state of our system, is plotted against the angular velocity ω - the constraint acting on the system. Below the threshold ω_c only one position is available, corresponding to $\theta = 0$ (branch a in figure 41). Beyond ω_c this state cannot be sustained. We express this in figure 41 by the dashed line along the branch a'. For each $\omega > \omega_c$ two new equilibria become available and we obtain two branches of states b_1 and b_2 which merge with a at $\omega = \omega_c$ but separate from it at $\omega \neq \omega_c$. This is the phenomenon of *bifurcation* and ω_c is said to be a bifurcation point. The new solutions emerging from this scenario can be stationary (*transcritic* and *pitchfork* bifurcations) or time-periodic (*Hopf* bifurcations). For more details, see appendix V.

The action of an external periodic force on a nonlinear oscillator of the kind depicted in figure 40 gives rises, under certain conditions, to an aperiodic motions of the mass m referred to as *deterministic chaos*. A more detailed description of this characteristic signature of nonlinear systems will follow in the next sections and appendix V Nicolis, 1995; Strogatz, 1994.

0.4 The Phase Space

The temporal evolution of a dynamic system can be described by the system variables set in an n-dimensional space Γ called the *phase space*. Due to the experimental impossibility to exactly know the position of a point with an infinite precision, in the phase space the initial state will not be a point but a finite element of volume $\delta\Gamma_0$. For an observer the points contained in $\delta\Gamma_0$ represent the macroscopic state of the experimental system. From every point, viewed as a different initial condition, a trajectory starts in the phase space. The envelope of all these

trajectories is called the *phase portrait* and in three dimensional space has a tubular or cylindric shape (figure 42).

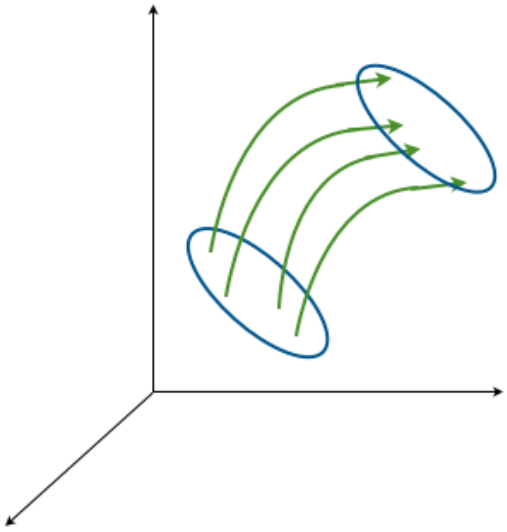

Figura 7: Trajectories in the phase space for a dynamic system

It is important to evaluate how the dimension of the volume varies with time. A rigorous description of the evolution of $\delta\Gamma_0$ in terms of divergence of the trajectory flow $\mathbf{F}$ is reported in appendix V. Here we use the conclusions of that derivation, in order to define *dissipative systems*. A dynamic system is said to be *conservative* if the relative volume in the phase space is conserved and $\nabla\cdot\mathbf{F} = 0$, while dissipative systems show a decrease with time in the phase space volume and $\nabla \cdot \mathbf{F} < 0$. From this it arises that trajectories starting from a determined volume in the phase space will trend to a subset, called the *attractor*. Attractors are objects limited and enclosed in the phase space, whose dimension d is strictly inferior than the space dimension n (we then exclude the Γ space from this category). Attractors can be monodimensional (fixed points), bidimensional and periodic (limit cycles) or with higher dimensions (quasiperiodic and *fractal* attractors). It is important to note that a non-dissipative system cannot have attractors.

A very important theorem, that plays a decisive role in the phase portrait structure, is the *Theorem of Existence and Uniqueness*. In the phase space Γ given $\mathbf{X_0}$ as a non-singular point, belonging to a certain open subset U and satisfying Lipschitz's condition

$$| \mathbf{F}(\mathbf{Y}) - \mathbf{F}(\mathbf{X}) | \leq k \, | \mathbf{Y} - \mathbf{X} | \tag{12}$$

for some $k < \infty$, thus exists an interval $t_0 < t < t_0 + T$ such that in U there is a unique solution $\mathbf{X}(t; \mathbf{X_0}, t_0)$ for the equation

$$\frac{d\mathbf{X}}{dt} = \mathbf{F}(\mathbf{X}, \mu) \tag{13}$$

where $\mathbf{F}$ is the evolution law, $\mathbf{X}$ are the degrees of freedom of the system and μ is a set of *control parameters*.

0.4.1 One variable system

When phase space is monodimensional, attractors must have dimension $D = 0$ and therefore only **fixed points** can exist. In terms of the original differential equation 121, fixed points represent equilibrium or steady solutions, since $d\mathbf{X}/dt = 0$.

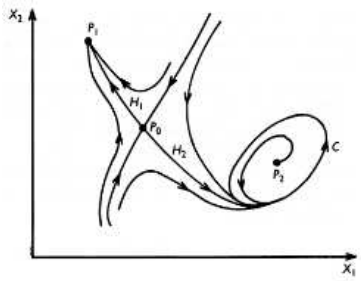

Figura 8: fixed points and a limite cycle

0.4.2 Two variables system

Since $n = 2$ attractors in the phase space can have fixed points with $D = 0$ and **limit cycles** with $D = 1$ (figure 36). While fixed points identify a stationary behavior, limit cycles indicate a *periodic* motion. Trajectories combining two fixed points are *heteroclines*, while a curve that starts from a fixed point and comes back to it is a *homocline*. The Existence and Uniqueness Theorem has an important corollary stating that intersections between trajectories are possible only if the intersection point is also singular. This constraint is particularly severe in a bidimensional phase space, where it is has an important topological consequence. If a closed line C exists, every trajectory inside C will stay trapped in there for ever. If in C exists some singular point, a trajectory will move toward it eventually, otherwise it will approach the closed orbit. For a vectorial field in a plane, this corollary is known as *Poincaré–Bendixson Theorem*.

0.4.3 Three variables system

Besides fixed points and closed curves, in this case other attractors exist without violating the Theorem of Uniqueness, such as simple and k–fold **torus** (torus with $k \geq 2$ holes). It is possible to demostrate that a k–fold torus must possess at least $2k - 2$ fixed points, implying that there is no torus other than the simple one free of fixed points. In the phase space a torus can be parametrized by two angular coordinates ϕ and ψ and the resulting motion will be *biperiodic*, with periods T_1 and T_2 (figure 9).

If T_1 and T_2 have an integer ratio, such as

$$\frac{T_1}{T_2} = \frac{p}{q} \qquad \forall\ p, q \in \mathbb{Z} \tag{14}$$

the motion can be reduced to a periodic one and will be represented by a closed curve winding p and q times along the two angular directions of the torus. On the other hand, if $\frac{T_1}{T_2}$ is irrational, the resulting motion will be *quasiperiodic*, characterized by a helix winding along the torus without ever closing to itself and without any self-intersections. A two-dimensional torus embedded in a three-dimensional space consitutes the natural prototype of quasiperiodic behavior. Such behavior is encountered in a large classe of nonlinear systems under nonequilibrium constraints. A valid method for classifying a toroidal attractor is the *Poincaré's map*, that plots

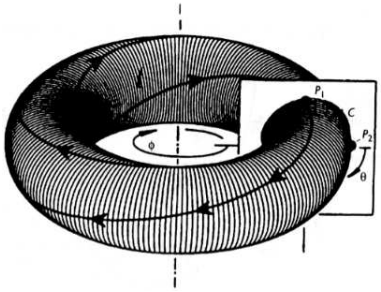

Figura 9: 2–torus

the intersections of a quasiperiodical dynamics with an opportune surface (the so called Poincaré's surface).

0.4.4 Fractals

Our exploration of the geometry of the phase space has led us to identify different kind of attractors as prototypes of stationary behavior (fixed point), periodic behavior (closed curve) and quasiperiodic behavior (torus). When dimension $n \geq 3$, corresponding motion is **chaotic** and manifolds other than attractors of conventional geometry exist, sometimes called *strange attractors* or *fractals* Mandelbrot, 1982. Roughly speaking, fractals are complex geometric shapes with fine structure at arbitrarily small scales.

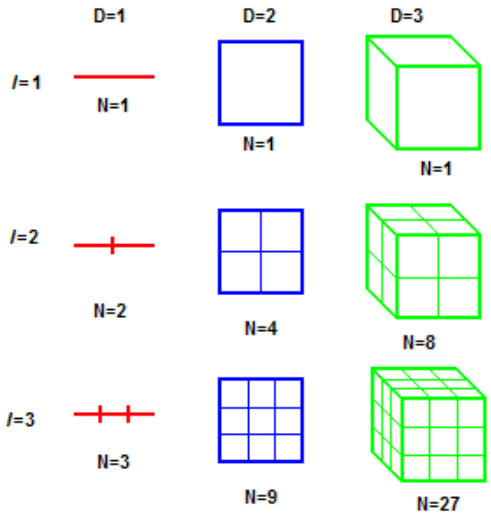

Figura 10: euclidean dimensions

Usually they have some degree of self-similarity. In other words, if we magnify a tiny part of a fractal, we will see features reminiscent of the whole: sometimes similarity is exact, more often it is only approximate or statistical. Fractals are of great interest because of their exquisite combination of beauty, complexity and endless structure. They are reminiscent of natural objects like mountains, clouds, coastlines, shells and broccoli in a way that classical geometrical shapes like squares and cones can't match (figure 11). The intrinsic dimension D of such objects is not an integer. The canonical algorithm to construct fractals mimics a process of successive fragmentation. If we take an object with linear size equal to 1 residing in Euclidean dimension D, and reduce its linear size by the factor $1/l$ in each spatial direction, it takes N number of self similar objects to cover the original object (figure 10)

$$N = l^D \tag{15}$$

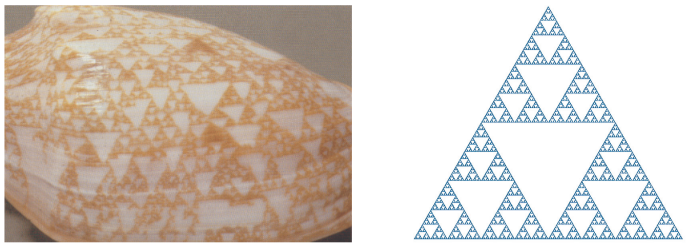

(a) a shell of *Volutidae* family **(b)** Sierpinsky's triangle

Figura 11: natural patterns and fractals

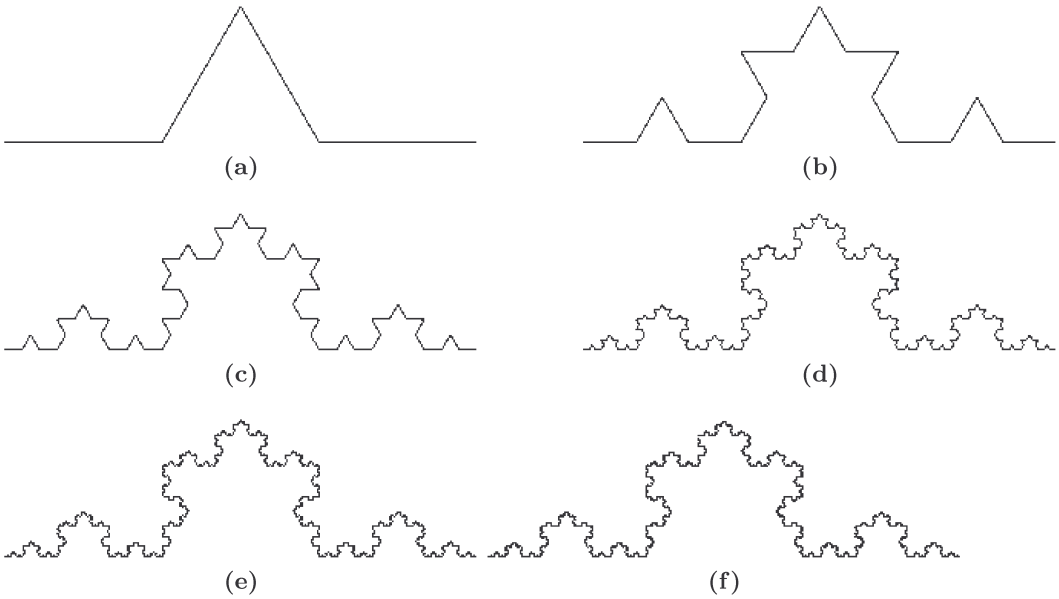

Figura 12: construction of a fractal by successive fragmentation

The dimension D is then defined by

$$D = \frac{\log N(l)}{\log l} \tag{16}$$

and it is still equal to its topological or Euclidean dimension.

By applying the above equation to fractal structures, we can get its fractal dimension as a non-whole number as expected.

$$D = \lim_{\epsilon \to 0} \frac{\log N(\epsilon)}{\log (1/\epsilon)} \tag{17}$$

where $N(\epsilon)$ is the number of self-similar structures of linear size ϵ needed to cover the whole structure.

For instance, the fractal dimension of Von Koch's curve (figure 12) is given by

$$D = \lim_{\epsilon \to 0} \frac{\log N(\epsilon)}{\log (1/\epsilon)} \tag{18}$$

$$D = \lim_{k\to\infty} \frac{\log 4^k}{\log 3^k} = \frac{\log 4}{\log 3} \approx 1.2619$$

since from a segment of linear size l, four self-similar segments of side $\epsilon = l/3$ are constructed, and so forth.

0.5 Deterministic Chaos

Chaos has been routinely observed in controlled laboratory experiments. Chemical reactions, optical systems such as lasers, and fluid dynamics experiments have been designed to exhibit chaotic dynamics. The existence of chaos in natural phenomena is more controversial. Celestial mechanics can be approximated using Newton's laws to high precision. Since n-body gravitational systems contain chaotic trajectories for $n \geq 3$, chaotic orbits of celestial bodies are probably pervasive in the solar system. In other areas such as population dynamics, weather and climate, the issue is clouded due to the question of whether the process can be convincingly modeled as a deterministic system. A system is said to be chaotic when it shows an irregular and unpredictable evolution, along with sensitivity to initial conditions. It is worth noting that chaotic dynamics is very different from a random walk, the first being governed by an internal structure that regulates its dynamic evolution. In the phase space, a chaotic system has its own attractor, while random dynamics fill the space as noise does. A very efficient way to characterize deterministic chaos is by means of *Lyapunov exponents* (see appendix V): they measure how trajectories originating from close points diverge after a time t in the phase space. We can now give the following definitions

- a deterministic system is chaotic if it shows aperiodic behavior and sensitivity to initial conditions;
- in the phase space chaotic dynamics are confined in a compact attractor, with dimension $2 < d \leq n$ and geometry compatible with fractal manifolds, according to the Theorem of existence and uniqueness (see appendix V);
- a chaotic system has a positive Maximal Lyapunov Exponent ($MLE > 0$);
- temporal data series for chaotic dynamics have a characteristic FFT spectrum with a wide band at low frequency values.

0.6 Transition scenarios to chaos

If a nonlinear system has chaotic dynamics, then it is natural to ask how this complexity develops as control parameters vary. The identification and description of routes to chaos has had important consequences for the interpretation of experimental and numerical observations of nonlinear systems. If an experimental system appears chaotic, it can be very difficult to determine whether the experimental data comes from a truly chaotic system, or if the results of the experiment are unreliable because there is too much external noise. Chaotic time series analysis provides one approach to this problem, but an understanding of routes to chaos provides another. In many experiments there are parameters that are fixed in any realization of the

experiment, but which can be changed. If recognizable routes to chaos are observed when the experiment is repeated at different values of the parameter, then there is a sense in which the presence of chaotic motion has been explained. By the early 1980s, three general 'scenarios' or 'routes to chaos had been identified Eckmann, 1981; Hilborn, 1994 period doubling Feigenbaum, 1979, intermittency and RTN scenario, the third being the most useful instrument for this dissertation (appendix V). As we shall see, in their standard forms each of these transitions uses the term route to chaos in a different way, so care needs to be taken over the interpretation of experimental or numerical observations of these transitions.

0.6.1 Ruelle-Takens-Newhouse (RTN) scenario

In 1971, Ruelle and Takens published a mathematical paper with the title 'On the Nature of Turbulence'. In this paper and a subsequent improvement with Newhouse (1978) Newhouse, Ruelle e Takens, 1978; Ruelle e Takens, 1971, they discuss the Landau's scenario for the creation of turbulence by the successive addition of new frequencies to the dynamics of the fluid. They show that if the attractor of a system has three independent frequencies, then a small perturbation of this system has a strange attractor. The result became known colloquially as "three frequencies implies chaos".

Let's consider a dynamic system in a stationary state (S) that loses its stability and undergoes a first Hopf bifurcation (B_1) as a control parameter μ increases, so that a new oscillatory periodic regime (P) appears, with a characteristic frequency f_1 in the FFT spectrum (figure 13). As μ progressively increases, a second Hopf bifurcation (B_2) produces a new quasiperiodic regime (QP_2), with two incommensurable frequencies f_1 and f_2, whose ratio is an irrational number. A last Hopf bifurcation (B_3) causes the appearance of a quasiperiodic dynamics (QP_3) with a third frequency f_3. This regime is unstable and difficult to observe experimentally (3-torus), and it collapses into a strange attractor, typical of a chaotic dynamic (C), with a broad signal at low frequencies in the FFT spectrum. From a topological point of view, this scenario can be summarized in the following way: *fixed point* $\rightarrow$ *limit cycle* $\rightarrow$ *2-torus* $\rightarrow$ *3-torus* $\rightarrow$ *strange attractor*.

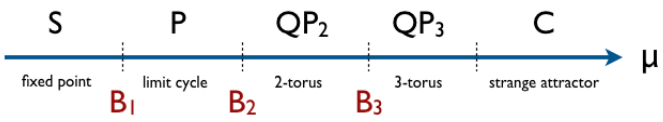

(a)

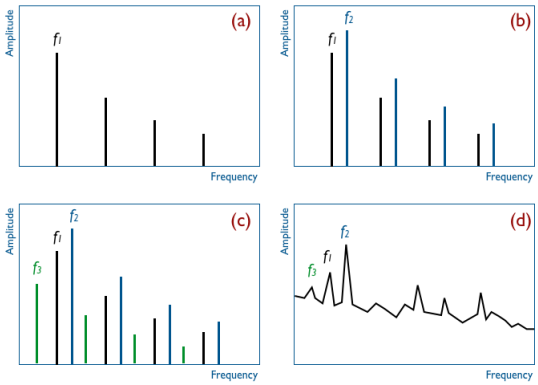

(b)

Figura 13: (a) bifurcation and topological sequence for RTN scenario and (b) the relative FFT spectra.

Oscillating reactions

Oscillations of chemical origin have been present as long as life itself. Every living systems contains hundreds of chemical oscillators. The systematic study of oscillating chemical reactions and of the broader field of nonlinear chemical dynamics is of considerably more recent origin, however. While the study of oscillating reactions did not become well established until the mid-1970s, the first experimental and theoretical works, that led up to the ideas of Prigogine on nonequilibrium thermodynamics and experimental and theoretical work of Belousov, Zhabotinsky, Field, Körös and Noyes, go back to the 19th century.

In 1828, Fechner described an electrochemical cell that produced on oscillating current, this being the first published report of oscillations in a chemical system. Ostwald observed in 1899 that the rate of chromium dissolution in acid periodically increased and decreased. Because both systems were inhomogeneous, it was believed then, and trough much of our own century, that homogeneous oscillating reactions were impossible.

In the last fourty years, very important progresses have been made in nonlinear chemistry and oscillating reactions can be designed *ad hoc* in different forms and studied by coupling chemical kinetics with diffusion (thermic and molecular) and fluidodynamics.

In chapter 0.6.1 we describe the basic concepts of nonlinear chemical kinetics, whilst in chapter 0.8 we will study the Belousov–Zhabotinsky reaction.

0.7 Chemical kinetics

The quantitative interpretation of experimental results in chemical kinetics is frequently based on the constructions and subsequent analysis of *mechanisms* or *models*. Mechanisms typically aim for a semiquantitative match to a particular reaction; models are often deliberately dimpler and attempt to catch the main qualitative features of a broader class of reactions.

0.7.1 Elementary steps

If we propose a sequence of individual reactions which are likely to be significant in carrying the reaction from the original reactant to the final products, the corresponding *reaction rate equations* can then be written out based on the law of mass action. The reaction rate equations specify the rates at which the concentrations of the various chemical species change with time, and how these rates depend upon those concentrations. The idea is to break the overall reaction up into a number

of component reactions. Typical of such a component is an *elementary step*. An example of an elementary step is the following, between a hydrogen atom and an oxygen molecule

$$H + O_2 \rightarrow OH + O^{\bullet} \tag{19}$$

The rate v of an elementary step is given simply in terms of the concentrations of the participating reactants (those on the left-hand side of the reaction step). For the above example

$$v = k[H][O_2] \tag{20}$$

Elementary steps are typically, but not exclusively, bimolecular – involving two species Atkins, 1994; Espenson, 1981. The reaction is envisaged as occurring in a single collision between the reactants. Bimolecular reactions then give rise to a quadratic dependence of rate on concentration, i.e., to an overall second-order process. Equation 20 also involves a coefficient k. This is the reaction rate coefficient or constant. Typically, rate constants are independent of concentration but they may be quite sensitive functions of the temperature. This temperature dependence can frequently be expressed by the Arrhenius law

$$k(T) = Ae^{-\frac{E_a}{RT}} \tag{21}$$

where T is the absolute temperature, $R = 8.314\text{JK}^{-1}\text{mol}^{-1}$ is the universal gas constant, A is the pre-exponential factor and E_a is the activation energy. Many chemical reactions are exothermic or endothermic. The consequent evolution or removal of energy may cause local temperature rises in the reacting mixture and the temperature dependence of k may then have important consequences.

0.7.2 Overall rate equations

The overall rate equations for a given mechanism are derived by combining the rates of all the individual elementary steps. An acceptable mechanism for the hydrogen-oxygen reaction (a valuable example to illustrate this) over a limited range of pressure and temperature involves the elementary steps described in table 1.

(0)	$H_2 + O_2 \rightarrow 2OH$	$v = k_0[H_2][O_2]$
(1)	$OH + H_2 \rightarrow H_2O + H$	$v = k_1[OH][H_2]$
(2)	$H + O_2 \rightarrow OH + O$	$v = k_2[H][O_2]$
(3)	$O + H_2 \rightarrow OH + H$	$v = k_3[O][H_2]$
(4)	$H \rightarrow 1/2H_2$	$v = k_4[H]$

Tabella 1: elementary steps for the hydrogen-oxygen reaction

In each case, the rate of the individual step has been derived from the law of mass action. The rate v is defined as the rate at which the reactant species disappears. In the last step, this means that a noninteger stoichiometric factor arises. The reaction rate equations can now be constructed. As an example, we can consider the rate of change of the hydroxyl radical concentration, $\mathrm{d}[OH]/\mathrm{d}t$. Two OH radicals are

produced in the first step and one is produced in each of steps (2) and (3), while an OH radical is removed in step (1). The rate of equations is thus

$$\frac{\mathrm{d}[OH]}{\mathrm{d}t} = 2k_0[H_2][O_2] - k_1[OH][H_2] + k_2[H][O_2] + k_3[O][H_2] \tag{22}$$

Athough it is necessary to write six rate equations for the six different chemical species, the concentrations of the six chemical species cannot all vary independently. There are two different type of chemical atoms, H and O, from which all the species are formed. As no reaction converts H to O, or vice versa, the total number of each of these atoms must be conserved. With six rate equations and two conservation conditions, the system has four degrees of freedom or four independent concentrations and can be reduced to a set of four rate equations.

0.7.3 Nonelementary processes

In many real situation, a kinetic mechanism involving only true elementary steps is not attainable. Often a number of elementary steps are so intimately coupled that it is only possible to observe their overall effect. In these situations, experimentally-determined empirical rate laws are particularly useful.

The Belousov–Zhabotinsky reaction (see chapter 0.8) is a characteristic example Scott, 1994. As a part of the mechanism for that system, the following processes are important (table 2).

(a)	$BrO_3^- + Br^- + 2H^+ \rightarrow HBrO_2 + HOBr$
(b)	$HBrO_2 + Br^- + H^+ \rightarrow 2HOBr$
(c)	$HOBr + Br^- + H^+ \rightarrow Br_2 + H_2O$

Tabella 2: pseudo-elementary steps for the Belousov–Zhabotinsky reaction

None of these is necessarily believed to be an elementary step even though they have each been written in the same stoichiometric form as the elementary steps seen above in the $H_2 + O_2$ mechanism. Here, the form of reactions (a) - (c) is partly to identify the species that disappear in each process (the reactants) and those that are formed (the products). In some cases, this form is also partly intended to convey information about the empirical rate laws which have been determined for each particular process. Thus, for process (a) the rate of conversion of bromate or bromide ions into the species $HBrO_2$ and $HOBr$ is found to be first order in $[BrO_3^-]$ and in $[Br^-]$ and second order in the concentration of H^+; we can write then for process (a)

$$\begin{aligned} -\mathrm{d}[BrO_3^-]/\mathrm{d}t &= -\mathrm{d}[Br^-]/\mathrm{d}t = -1/2\mathrm{d}[H^+]/\mathrm{d}t \\ &= +\mathrm{d}[HBrO_2]/\mathrm{d}t = +\mathrm{d}[HOBr]/\mathrm{d}t \\ &= k_5[BrO_3^-][Br^-][H^+]^2 \end{aligned} \tag{23}$$

There is no suggestion, however, that this conversion is brought about by a single reactive collision between the four species on the left-hand side of the reaction (a). In general, once all the important processes and their empirical rate laws have been identified, these are again combined to produce the full rate equations for the total rates of change of each concentration.

0.8 Nonlinearity and feedback

The buzzwords *nonlinearity* and *feedback* are the key features of the chemical kinetics underlying all the exotic phenomena such as oscillating reactions. The simplest type of chemical reaction is of the kind

$$A + BC \rightarrow AB + C \tag{24}$$

with rate equations

$$-\,\mathrm{d}[A]/\mathrm{d}t = -\mathrm{d}[BC]/\mathrm{d}t = \mathrm{d}[AB]/\mathrm{d}t = \mathrm{d}[C]/\mathrm{d}t = k[A][BC] \tag{25}$$

In many kinetic studies aimed at determining the reaction rate constant k, the concentration of one of the two reactants, BC say, will be arranged to be in great eccess over that of the other. The concentration of the species in excess can then be treated as a constant, giving a pseudo-first-order reaction. This is the only example of linear system in chemical kinetics. All non-first-order processes are nonlinear and thus nonlinearity is the rule, rather than the exception.

Nonlinearity is of mild interest, while of primary importance is *feedback*, which arises when the products of later steps in the mechanism influence the rate of some of the earlier reactions and, hence, the rate of their own production. This may take the form either of positive feedback (*autocatalysis*) or negative feedback (*autoinhibition*). Several examples of feedback are known in different chemical systems, such as combustion and isomerization processes, gas-liquid partial oxidation processes, gas-solid heterogeneous catalysis, solid-liquid electrodissolution and corrosion, enzyme processes and glycolysis in biological systems.

The Belousov–Zhabotinsky reaction has an autocatalytic step, which is at the very origin of oscillations and other characteristic behaviors, where two moles of $HBrO_2$ are produced from the reaction between one mole of $HBrO_2$ and one mole of BrO_3^-. In the next chapter the Belousov–Zhabotinsky reaction will be analyzed in details.

The Belousov–Zhabotinsky reaction

Boris Pavlovich Belousov began his studies on oscillating reactions in 1950 while head of the Laboratory of Biophysics in the former USSR Ministry of Health. He was looking for an inorganic analog of the Krebs cycle, a key metabolic process in which citric acid is an intermediate. He investigated a solution of bromate, citric acid and ceric ions (Ce^{4+}). He expected to see the monotonic conversion of yellow Ce^{4+} into colorless Ce^{3+}. Instead, the solution repeatedly cleared and then became yellow again! He strove to publish the data observed but different editors refused his manuscript, with the assumption that the supposed reaction and the spontaneous temporal self-organization observed violated the Second Law of Thermodynamics.

In 1961, Anatol Zhabotinsky, a graduate student in biophysics at Moscow State University, began looking at the same system and modified the original recipe, replacing citric with malonic acid. In 1962, Zhabotinsky wrote a manuscript that he sent to Belousov for his comment Zhabotinsky, 1964. After their fructuous epistolary exchange, that brought the Belousov–Zhabotinsky reaction to the attention of several Western chemists, in 1980 the Lenin prize was awarded to Belousov, Zhabotinsky, Krinsky, Ivanitsky and Zaikin for their work on the Belousov–Zhabotinsky reaction Zaikin e Zhabotinsky, 1970.

The Belousov–Zhabotinsky reaction involves the oxidation of an organic species such as malonic acid by an acidified bromate solution in the presence of a metal ion catalyst

$$\begin{aligned} &2BrO_3{}^- + 3CH_2(COOH)_2 + 2H^+ \rightarrow 2CHBr(COOH)_2 \\ &+ 3CO_2 + 4H_2O \end{aligned} \tag{26}$$

Various metal ions can be employed, with the $Ce(III)/Ce(IV)$ Johnson, Scott e Thompson, 1997; Wang, Soerensen e Hynne, 1994, 1995 and $[Fe(II)(phen)]^{2+}/[Fe(III)(phen)]^{3+}$ (ferroin/ferriin) Strizhak e Kawczynski, 1995; Wang *et al.*, 2005 couples most widely used. Cerium and ferroin catalyzed BZ systems show different behaviors both in temporal and spatial evolution, mainly because of the redox potential of the catalysts Ganapathisubramanian e Noyes, 1982; Hegedus *et al.*, 2006; Keki *et al.*, 1992; Smoes, 1979; Taylor, 2002. In a closed system, the reaction typically exhibits a short induction period, followed by an oscillatory phase. The color alternates between red and blue (for the ferroin/ferriin couple, figure 14) with a period of approximately one minute.

The oscillations may last for over two hours during which perhaps a hundred oscillations are observed. Oscillations can arise in a macroscopic medium if the system

Figura 14: color change in a homogeneous BZ system

is sufficiently far from the state of thermodynamic equilibrium Nicolis e Prigogine, 1977. Ultimately, the oscillations die out and the system then drifts slowly and monotonically towards its chemical equilibrium state.

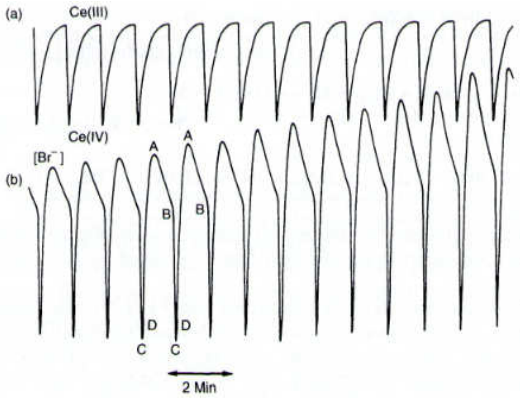

Figura 15: potentiometric records for the BZ reaction

Typical experimental records, as measured by Pt and bromide sensitive electrode, each referenced to a calomel electrode, are shown in figure 15. The Pt electrode responds primarily to the metal ion redox couple: this shows a sharp change from the reduced to the oxidized state followed by a more gradual return. The sharp switch is also associated with the abrupt color change. The bromide electrode responds primarily to $[Br^-]$. A slow decrease AB in $[Br^-]$ can be observed, before the sharp drop BC that accompanies the oxidation of the metal catalyst and the color change. This gives rise to a relaxation waveform, with a second segment of relatively slow evolution CD before the bromide ion concentration increases rapidly again DA.

Although there are oscillatory variations in the concentrations of some intermediate species, it is also important to note that the concentrations of the major reactants, bromate and malonic acid, decrease slowly but continuously during the reaction process. In consequence, the reaction continuously flows in the direction of decreasing free energy: there is no oscillation in the direction of the overall reaction which is always moving inexorably towards the chemical equilibrium state.

The BZ reaction makes it possible to observe propagating chemical waves and development of complex patterns in time and space by naked eye on a very convenient human time scale of dozens of seconds and space scale of several millimeters. The BZ reaction can generate up to several thousand oscillatory cycles in a closed system, which permits studying chemical waves and patterns without constant replenishment of reactants Field e Burger, 1985.

0.9 A mechanism for the BZ reaction

Although its apparent simplicity, the mechanism of the Belousov–Zhabotinsky reaction is very complex (figure 16). The understanding of the Belousov–Zhabotinsky system has been developed primarily in terms of the Field-Körös-Noyes (FKN) me-

(FKN3)	$BrO_3^- + Br^- + 2H^+ \rightarrow HBrO_2 + HOBr$
	$v = k_3[BrO_3^-][Br^-][H^+]^2$
(FKN2)	$HBrO_2 + Br^- + H^+ \rightarrow 2HOBr$
	$v = k_2[HBrO_2][Br^-][H^+]$
Process A	$\mathbf{BrO_3^- + 2Br^- + 3H^+ \rightarrow 3HOBr}$
(FKN5)	$BrO_3^- + HBrO_2 + H^+ \rightarrow 2BrO_2^\bullet + H_2$
	$v = k_5[BrO_3^-][HBrO_2][H^+] - k_5[BrO_2^\bullet]$
(FKN6)	$BrO_2^\bullet + M_{red} + H^+ \rightarrow HBrO_2 + M_{ox}$
	$v = k_6[BrO_2^\bullet][M_{red}][H^+]$
Process B	$\mathbf{BrO_3^- + HBrO_2 + 2M_{red} + 3H^+ \rightarrow 2HBrO_2 + 2M_{ox} + H_2O}$

Tabella 3: scheme for A and B processes

chanism. The major feedback routes arise through Process A, which removes bromide ion, and process B, which provides the autocatalysis. The important steps in Process A are schematized in table 3. These are two electron-transfer processes between the Br(V), Br(III), Br(+I) and Br(-I) oxidation states; subsequent reactions of HOBr become important in resetting the clock. When the bromide ion concentration has fallen sufficiently, the major reaction channel for $HBrO_2$ switches from (FKN2) to the reaction with bromate ion, so initiating Process B (table 3).

The species $BrO_2^\bullet$ involves the Br(IV) oxidation state. Further reaction requires a one-electron transfer step that is provided by the metal ion catalyst. In the simplest case, for which the reverse step (FKN5) can be neglected and $[BrO_2^\bullet]$ can be expressed as a steady-state balance between (FKN5) and (FKN6), the rate at which there is a net formation of $HBrO_2$ is determined by the rate of step (FKN5).

The rate of accumulation thus increases autocatalytically as $[HBrO_2]$ increases. This autocatalytic growth is limited by the self-disproportionation reaction involving $HBrO_2$

$$(FKN4) \qquad 2HBrO_2 \rightarrow BrO_3^- + HOBr + H^+ \qquad v = k_4[HBrO_2]^2 \tag{27}$$

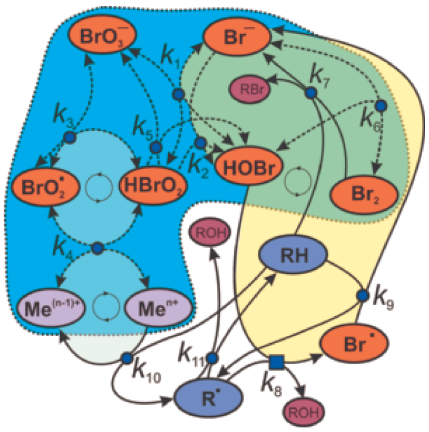

Figura 16: BZ reaction scheme

The switch from Process A to Process B occurs when reactions (FKN2) and (FKN5) are roughly equal. As the bromate concentration remains virtually constant during a given oscillation, the switch to autocatalysis occurs when the $[Br^-]$ has been reduced by Process A to the *critical bromide ion concentration*

$$[Br^-]_{cr} = (k_5/k_2)[BrO_3^-] \approx 1.4 \times 10^{-5}[BrO_3^-] \tag{28}$$

Because bromide ion competes so strongly for $HBrO_2$ it plays the role of an *inhibitor*, delaying the establishment of the autocatalytic feedback via Process B. Processes A and B provide for a classic clock reaction. In the induction period beginning at point A in figure 15, any bromide ion inhibitor (present as impurity or produced in

(FKN5)	$BrO_3^- + HBrO_2 + H^+ \rightarrow 2BrO_2^{\cdot} + H_2$
	$v = k_5[BrO_3^-][HBrO_2][H^+] - k_5[BrO_2^{\cdot}]$
(FKN6)	$BrO_2^{\cdot} + M_{red} + H^+ \rightarrow HBrO_2 + M_{ox}$
	$v = k_6[BrO_2^{\cdot}][M_{red}][H^+]$
Process C	$2M_{ox} + MA + BrMA \rightarrow fBr^- + 2M_{red}+$ other products
	$v = k_c[Org][M_{ox}]$

Tabella 4: scheme for Process C

Rate constants	FKN	Oregonator*
k_1	8.0×10^9 $M^{-2}s^{-1}$	6.4×10^9 $M^{-1}s^{-1}$
k_2	3.0×10^6 $M^{-2}s^{-1}$	2.4×10^6 $M^{-1}s^{-1}$
k_3	2.0 $M^{-3}s^{-1}$	1.3 $M^{-1}s^{-1}$
k_4	3.0×10^3 $M^{-1}s^{-1}$	3.0×10^3 $M^{-1}s^{-1}$
k_5	42.0 $M^{-2}s^{-1}$	33.6 $M^{-1}s^{-1}$
k_c	1.0 $M^{-1}s^{-1}$	1.0 $M^{-1}s^{-1}$

*Assumes $[H^+] = 0.8$ M

Tabella 5: rate constants for FKN and Oregonator models

an earlier cycle of the oscillatory reaction) is removed. At the end of the induction period (point B), the bromide ion concentration has fallen to $[Br^-]_{cr}$ and there is then an autocatalytic acceleratory oxidation of the metal ion catalyst via Process B to point C. In the absence of a resetting mechanism, this would be effectively the end of the story. In order to regenerate the starting conditions, a source of bromide ions is needed and the catalyst must be reduced back to its lower oxidation state. These requirements are met simultaneously through Process C, which involves the organic reactant, malonic acid (MA). A detailed understanding of Process C has only recently begun to emerge Györgyi, Turanyi e Field, 1990. However, the original representation of FKN allows to analyze the different aspects from a qualitative point of view. This proposes that $HOBr$ can give rise to the bromination of MA, perhaps through the formation of Br_2, to produce bromomalonic acid $BrMA$. Both MA and $BrMA$ react with M_{ox} to yield the reduced form of the catalyst and, in the case of $BrMA$, bromide ion. Process C is thus represented as in table 4 The stoichiometric factor f provides something on an 'adjustable' parameter. It represents the number of bromide ions produced as two M_{ox} ions are reduced. If M_{ox} reacts solely with $BrMA$, $f = 2$; for $f > 2/3$ there is a net increase in bromidic ion through each oscillatory cycle. In the simplest analysis, f is taken as a constant: in more sophisticated studies, f is allowed to vary with the instantaneous concentrations of MA, $BrMA$ or of $HOBr$. A chain mechanism involving malonyl radicals $MA^{\bullet}$ and bromine atom radicals $Br^{\bullet}$ has been proposed to account for stoichiometric factors greater than 2. The rate of Process C, as written above, depends on the total concentration of organic species $[Org]$ which early on is approximated by the initial concentration of MA. The rate constants for the steps in the FKN mechanism are given in table 5.

(O3)	$A + Y \rightarrow X + P$	$v = k_3 AY$
(O2)	$X + Y \rightarrow 2P$	$v = k_2 XY$
(O5)	$A + X \rightarrow 2X + 2Z$	$v = k_5 AX$
(O4)	$2X \rightarrow A + P$	$v = k_4 X^2$
(OC)	$B + Z \rightarrow 1/2fY$	$v = k_c BZ$

Tabella 6: the oregonator kinetic scheme

A	BrO_3^-
B	All oxidizable organic species
P	$HOBr$
X	$HBrO_2$
Y	Br^-
Z	M_{ox}

Tabella 7: a simplified notation

0.10 Condition for oscillations: the Oregonator

With a reasonable mechanism and the appropriate values for the reaction rate constants, it should be possible not only to match individual experimental observations but also to predict more generally the experimental conditions under which oscillations might be observed. For this, it is especially convenient to use the *Oregonator* model, developed by Field and Noyes (1974) at University of Oregon and derived from the FKN scheme. This is frequently written in the form reported in table 6 A literal translation is used for chemical species in order to simplify the notation (table 7). The concentrations of the major reactants, A and B, are treated as constants and $[H^+]$ is subsumed into the rate constants. The reaction rate equations for the intermediate species X, Y, Z are

$$\frac{\mathrm{d}X}{\mathrm{d}t} = k_3 AY - k_2 XY + k_5 AX - 2k_4 X^2 \tag{29}$$

$$\frac{\mathrm{d}Y}{\mathrm{d}t} = -k_3 AY - k_2 XY + 1/2fk_c BZ \tag{30}$$

$$\frac{\mathrm{d}Z}{\mathrm{d}t} = 2k_5 AX - k_c BZ \tag{31}$$

The next stage is to transform the concentrations X, Y, Z into *dimensionless variables*. The transformation to be used here involves replacing X, Y, Z and t in equations 29 - 31 by x, y, z and τ, defined by

$$x = 2k_4 X/k_5 A,\ y = k_2 Y/k_5 A,\ z = k_c k_4 BZ/(k_5 A)^2,\ \tau = k_c Bt \tag{32}$$

Essentially, however, these still represent the concentrations of $HBrO_2, Br^-, M_{ox}$ and time, and can be most usefully thought of in these terms. The advantage of these substitutions is that the rate equations now become

$$\frac{\mathrm{d}x}{\mathrm{d}\tau} = \frac{qy - xy + x(1-x)}{\epsilon} \tag{33}$$

$$\frac{\mathrm{d}y}{\mathrm{d}\tau} = \frac{-qy - xy + fz}{\epsilon'} \tag{34}$$

$$\frac{\mathrm{d}z}{\mathrm{d}\tau} = x - z \tag{35}$$

There are three dimensionless parameters

$$\epsilon = k_c B/k_5 A,\ \epsilon' = 2k_c k_4 B/k_2 k_5 A,\ q = 2k_3 k_4/k_2 k_5 \tag{36}$$

The first of these depend on the initial concentrations of bromate ion, MA and H^+; q involves only the reaction rate constants. For typical values, $A = 0.06$M and $B = 0.02$M, we have

$$\epsilon = 10^{-2},\ \epsilon' = 2.5 \times 10^{-5},\ q = 9.0 \times 10^{-5} \tag{37}$$

The autocatalysis in $HBrO_2$ is revealed by the term $x(1-x)$ in equation 33: this has a quadratic form and arises from Process B, step (O5), limited by the disproportionation step (O4). The term $(q-x)y$ in equation 33 arises from the production and removal of $HBrO_2$ via steps (O3) and (O2), i.e. Process A. The other important point involves the size of ϵ and ϵ'. Both of these are small, with ϵ' being much less than 1, and appear in the denominator of a reaction rate equation. Because ϵ' is so small, the concentration of bromide ion y will change quickly in time (i.e. $\mathrm{d}y/\mathrm{d}\tau$ will be large) unless the numerator in equation 34 is also small. This argument is simply a mathematically-based statement of the classic steady-state approximation, so now we assume

$$y = y_{ss} = \frac{fz}{x+q} \tag{38}$$

at all times, i.e. the bromide concentration is in a dynamic steady state relative to the $HBrO_2$ concentration. Substituting this result into the reaction rate equations, we have

$$\frac{\mathrm{d}x}{\mathrm{d}\tau} = \frac{1}{\epsilon}\left[x(1-x) - \frac{x-q}{x+q} fz\right] \tag{39}$$

$$\frac{\mathrm{d}z}{\mathrm{d}\tau} = x - z \tag{40}$$

The two terms in equation 39 represent Process B and Process A respectively, whilst the two terms in equation 40 describe the production of M_{ox} in Process B and its reduction in Process C. We will not apply the staedy-state approximation, based on the magnitude of ϵ, to $HBrO_2$: partly this is because no simple formula for x_{ss} emerges but also we must retain two concentrations to allow oscillatory behavior (see *Cauchy's Theorem*, Appendix V).

Equations 39 and 40 can be integrated numerically for any given choice of f. Figure 17 shows the resulting variation in x and z for different values of f.

a) $f = 0.25$

After some initial transient development, the concentrations settle to constant, steady-state values. Steady states different from the chemical equilibrium state arise in this model because the consumption of the reactants has been

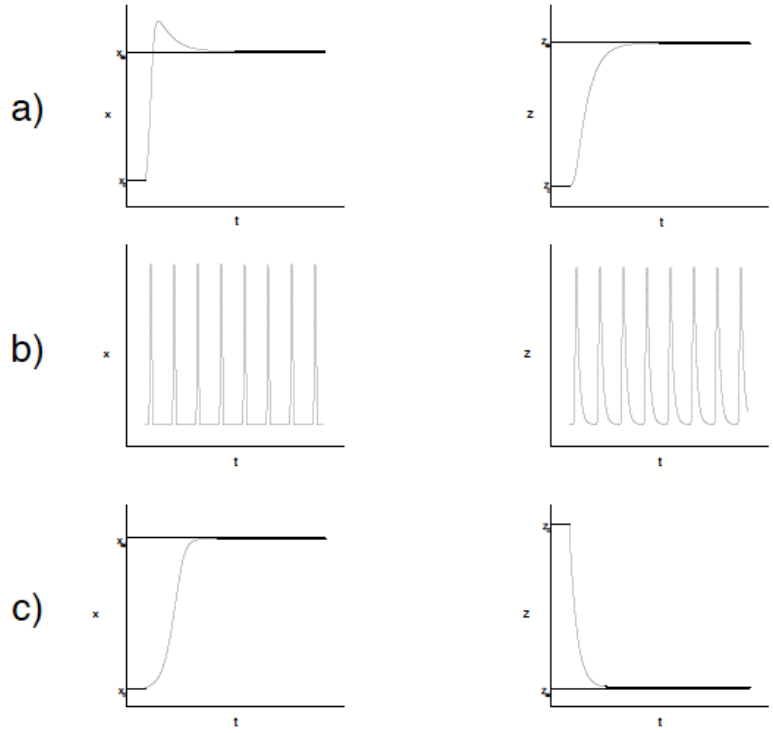

Figura 17: evolution of $HBrO_2$ and M_{ox} concentrations (x and z) for Oregonator model with a) $f = 0.25$; b) $f = 1$; c) $f = 3$.

neglected. Under steady-state conditions, the rates of change of both intermediate concentrations become zero simultaneously, $\mathrm{d}x/\mathrm{d}\tau = \mathrm{d}z/\mathrm{d}\tau = 0$. Thus $z_{ss} = x_{ss}$, where x_{ss} is given by

$$x_{ss} = z_{ss} = 1/2\{1 - f + q + [(f + q - 1)^2 + 4q(1 + f)]^{1/2}\} \qquad (41)$$

A low value for f corresponds to relatively weak resetting Process C, as few bromide ions are produced as the catalyst is reduced. The corresponding steady-state concentrations of $HBrO_2$ and M_{ox} are thus relatively high whilst the steady-state bromide ion concentration y_{ss} is relatively low.

b) $f = 1$

The situation is quite different. A steady-state solution still exists, but the system does not settle to it. Instead a sustained, periodic oscillation in x and z (and hence also in y) about the steady state emerges. The steady state is unstable for this set of parameter values. The computation may be repeated for various other values of f, with oscillatory behavior being observed over the range $1/2 < f < 1 + \sqrt{2}$.

c) $f = 3$

the system has a value for f slightly above the maximum for oscillations and it is said excitable. An excitable system is characterized by having a stable steady state and so is not spontaneously oscillatory. Small perturbation, e.g., by small

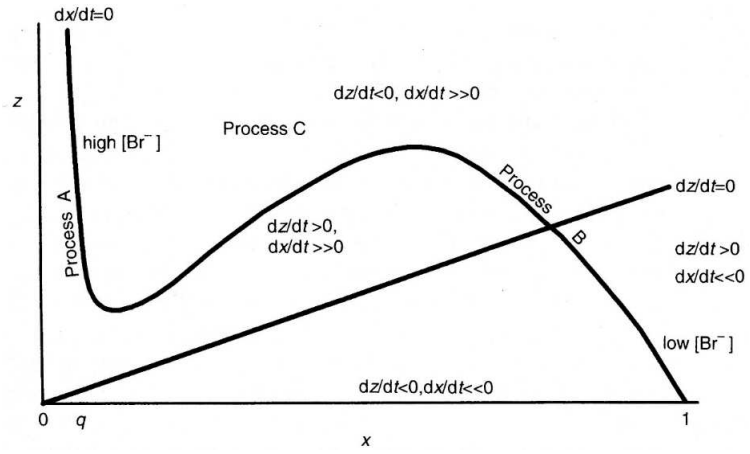

Figura 18: an example of the $x - z$ plane for the Oregonator model showing the $x-$ and $z-$nullclines.

reductions in the bromide concentration, disturbs the system from this state transiently, but the system returns quickly without any change in color. With slightly larger perturbations, the system is stimulated into a single excursion, with a color change and back to the original steady state, with a single large peak in the intermediate concentrations, similar to a single oscillation.

0.11 Oscillating regime

The reason why the steady state loses its stability over the range of f indicated above can be revealed pictorially. For this, we look not at the evolution of x or z as a function of time, but plot the evolution of one concentration as a function of the other. The two concentrations x and z form a *phase plane*: as x and z vary with time, they draw out a curve or *trajectory* on this plane. We can use the properties of the phase plane to graphically solve equations 39 and 40 and thus obtain the conditions for oscillations without recourse to computation. There are two special curves that lie on the phase plane, as indicated in figure 18: these are the *nullclines* that connect x, z pairs for which $\mathrm{d}x/\mathrm{d}\tau = 0$ (the $x-$nullcline) or $\mathrm{d}z/\mathrm{d}\tau = 0$ (the $z-$nullcline). The last is simply the straight line $x = z$ emerging from the origin with unit slope. Any trajectory crossing this line must have a maximum or minimum in z at that point. The $x-$nullcline is determined by the more complex condition

$$\frac{x(x+q)(1-x)}{f(x-q)} = z \tag{42}$$

This is a cubic-type curve which asymptotes to $z \to \infty$ as $x \to q$ and has $z = 0$ for $x = 1$; the range of interest is then $q < x < 1$ and the nullcline has a minimum and a maximum in this range. The two nullclines divide the phase plane into four regions, in which the sign of $\mathrm{d}x/\mathrm{d}\tau$ and $\mathrm{d}z/\mathrm{d}\tau$ vary between positive and negative, indicating the slope of any trajectory in that region. High values for x correspond to low instantaneous concentrations of bromide ion (from equation 38) whilst low $HBrO_2$ concentration correspond to high $[Br^-]$. Remembering that Process A

corresponds to the reduction of $[Br^-]$, we can recognize that this will occur while the system is close to the left-hand branch of the $x-$nullcline. Along the right-hand branch, Process B (oxidation of the catalyst) is important and z increases. Process C corresponds to the oxidation of the organic species by M_{ox} and so occurs at high z. This process reduces $[HBrO_2]$ and increases $[Br^-]$, so causing the system to move to the left and down in the phase plane. The nullclines for $f = 0.25, 1, 3$ are shown in figure 19. In each case, there is a single point at which the $x-$ and $z-$nullclines intersect. At such a point, $\mathrm{d}x/\mathrm{d}\tau = \mathrm{d}z/\mathrm{d}\tau = 0$, so this locates the steady state solution. In the case of figure 19, with $f = 0.25$ (a), the intersection point lies to the right of the maximum. If we start at some arbitrary point (x_0, z_0), corresponding to the initial concentration of x and z, the subsequent evolution may be predicted by the following argument.

If the initial point does not lie on the $x-$nullcline, the right-hand sinde of equation 39 will be nonzero: if the initial point is below the $x-$nullcline, $\mathrm{d}x/\mathrm{d}\tau$ will be positive. Also, because of the small parameter ϵ that effectively occurs as a divisor of the rate expression, $\mathrm{d}x/\mathrm{d}\tau$ will be large in magnitude. This means that the $HBrO_2$ concentration will change rapidly, on a timescale such that z remains effectively constant. This gives rise to a horizontal movement in (a) from (x_0, z_0) to some point on the right-hand branch of the $x-$nullcline. Now $\mathrm{d}x/\mathrm{d}\tau = 0$. Unless the system has actually jumped to the steady state intersection, $\mathrm{d}z/\mathrm{d}\tau$ remains nonzero. This gives rise to a slower evolution: if the system lies below the $z-$nullcline, $\mathrm{d}z/\mathrm{d}\tau$ will be positive, so the concentration of M_{ox} will increase. As z varies, so x will continuously adjust to keep the right-hand side of equation 39 close to zero. Thus the trajectory undergoes a slow evolution along the $x-$nullcline until it approaches the steady-state intersection. The trajectory illustrated in (a) corresponds to the time-series shown in the part (a) of figure 17. A similar argument shows that any initial points finally approach the steady state, although if we start above the $x-$nullcline, the initial jump is to the left-hand branch of the $x-$nullcline, followed by a slower evolution down this branch, a second jump from the minimum onto the right-hand branch of the

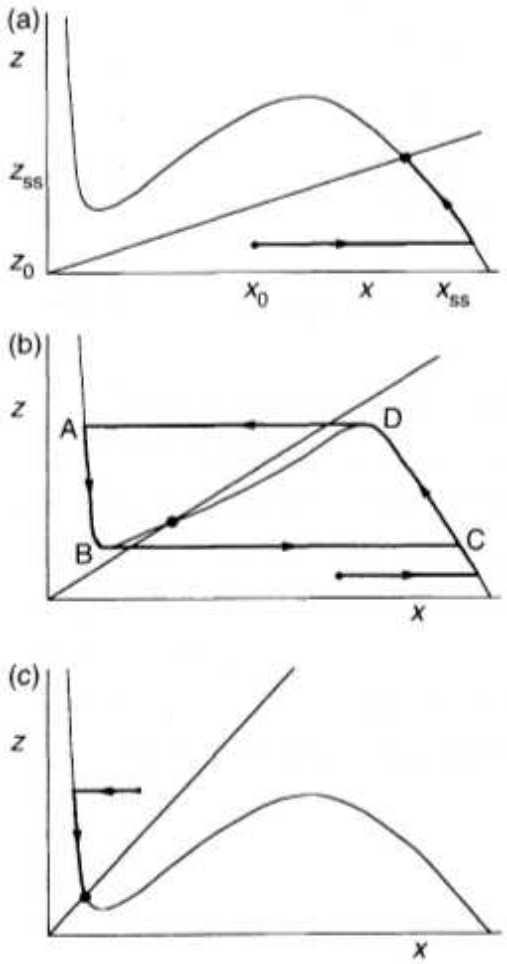

Figura 19: pictorial representation of oscillations in the $x - z$ phase plane

$x-$nullcline and then the final approach to (x_{ss}, z_{ss}).

With $f = 3$, the intersection lies on the left-hand branch of the $x-$nullcine, close to the minimum. Again, we can use the argument that any system lying off the $x-$nullcline will respond by a horizontal jump to one or other of the outer branches of that nullcline, followed by a slower evolution along it. In this way, the steady state is finally reached, as indicated by the trajectory corresponding to the time-series of the part (c) in figure 17.

For the case $f = 1$, however, the situation is different. The intersection point now lies on the middle branch of the $x-$nullcline. If we start at some arbitrary initial point below the $x-$nullcline, the system jumps to the right-hand branch and then moves upwards towards the maximum (as $\mathrm{d}z/\mathrm{d}\tau > 0$). At the maximum, $\mathrm{d}z/\mathrm{d}\tau$ is still positive, so the system must leave the $x-$nullcline. This gives rise to a horizontal jump to the left-hand branch of the $x-$nullcline. Now $\mathrm{d}z/\mathrm{d}\tau < 0$, so the system moves slowly down this branch, towards the minimum. At the minimum, $\mathrm{d}z/\mathrm{d}\tau$ is still negative, so again the system leaves the $x-$nullcline. This causes a new horizontal jump back to the right hand branch and the process repeats. At no time can the system jump to the middle branch, and so the steady-state point is never approached. Instead there is a continuous cycling in the phase plane around the limit cycle ABCD. The system evolves to this limit cycle from all initial conditions, i.e., from all starting points in the $x - z$ phase plane, so the amplitude and period of the oscillation depend only on the kinetics and the experimental conditions, not on the initial conditions. Also, if the system receives some later perturbation, it will return to the same limit cycle and hence to oscillations of the same amplitude and period. This indicates that the limit cycle is stable and is an attractor for the system. The condition for oscillations is simply that the steady state should lie on the middle branch of the $x-$nullcline, i.e., that x_{ss} lies between the minimum and the maximum. The coordinates of minimum and maximum in the $x-$nullcline depend on the parameters q and f, being given approximately by

$$\min = \begin{cases} x = (1+\sqrt{2})q \\ y = 1 + 1/\sqrt{2} \\ z = (1+\sqrt{2})^2 q/f \end{cases} \tag{43}$$

$$\max = \begin{cases} x = 1/2 \\ y = 1/2 \\ z = 1/4f \end{cases} \tag{44}$$

for $q \ll 1$. The condition for the steady state, equation 41, to lie at the minimum is then $f = 1 + \sqrt{2}$, whilst for the steady state to coincide with the maximum, we require $f = 1/2$. The condition for oscillation is thus, as given previously,

$$1/2 < f < 1 + \sqrt{2} \tag{45}$$

In 'chemical' words, oscillations are suppressed if f, the number of bromide ions produced for every two oxidized catalyst ions reduced in Process C, is either too large or too small. A balance between the efficiency of Process C and the rates of Processes A and B must be achieved. If f is too small, the system settles to a steady state corresponding to the oxidized form of the catalyst and low bromide ion

concentration. If f is too large, the build-up of bromide inhibits the autocatalysis and oxidation in Process B and reduced steady state is established. The change from steady state to oscillatory reaction as f enters the above range occurs via a Hopf bifurcation.

Transport phenomena

The FKN and Oregonator kinetic mechanisms contain a unique feedback step, unable to explain the very complex periodic dynamics observed in Belousov–Zhabotinsky experiments. Moreover, besides the temporal oscillations observed in continuous flow reactors, in a thin, unstirred layer of the reaction mixture one can observe propagation waves and chemical patterns. Thus a homogeneous system exhibits not only temporal but also spatial self-organization. This behavior has been justified by considering the coupling between kinetics and transport phenomena, i.e., diffusion and convection.

0.12 Excitable media

Propagating waves may develop in particular systems called *excitable*, i.e., systems in which a group of elements is coupled to each other and each elements can pass informations to its neighbours Kapral e Showalter, 1994; Murray, 1993. In excitable systems, each point is characterized by a *rest* state, that is stable under small perturbations. It means that the response to a small brief perturbation is small, with an amplitude that varies smoothly with the perturbation amplitude. On the contrary, an impulse with a strength greater than a certain *threshold* can cause that point to undergo a large amplitude excursion from, and eventually return to, its rest state value. For spatially extended excitable systems, the subthreshold response is localized, while the suprathreshold response is a traveling wave. The length of time required to return close to the steady state value is a factor that determines the *refractory time* of that point; a refractory point cannot easily undergo another cycle until it recovers. Summarizing, the dynamics described for excitable media, that is characterized by a stable steady state, a threshold and a return to the steady state, is possible if at least two mechanisms occur: a fast nonlinear excitation and a slower recovery process. A wave of activity moving across the excitable media and initiated by an impulse over a certain threshold, propagates with a speed controlled by how fast elements ahead of the wave are induced to cross the threshold. Thus, wave speed is a function of diffusion coefficient (a "passive" property of the media) and the rate of rise of the diffused species of the excited element (an "active" property of the media). A simple and intuitive example of an excitable medium is a wildfire. It travels through the forest as a wave from its initiation point and regenerates with every tree it ignites. Thus, no fire can return to a burnt spot until the vegetation has gone through its refractory period and regrown. In biology field, one of the most widely studied systems with excitable behavior is neural communication by nerve cells via electrical signalling.

In chemical context, among the most studied excitable medium is the Belousov–Zhabotinsky reaction.

0.12.1 Travelling waves

A wave is characterized by the *shape* and *speed* of propagation of the front, that can change continuously. A *travelling wave* is a special case of wave, which does not change shape during its travel and whose speed of propagation is constant. Therefore, travelling wave fronts of chemical reactions are characterized by uniform speed and a constant concentration profile.

More in general, we can deal with three different types of chemical waves

1. *fronts*, that convert reactants in products, so that the composition ahead of and behind the wave is quite different;

2. *pulses*, they occur when an intermediate is firstly produced by a certain front and then it is converted back by a second recovery wave;

3. *periodic wave trains*, i.e., a combination of a series of fronts or pulses which are continuously being initiated at some point or *centre* and which follow each other in the medium.

The pulses can give rise to different types of spatial patterns such as target patterns, spiral waves (one- or multiarmed spirals), Archimedean or inwardly rotating spirals.

0.12.2 Targets and spirals

Reactions that show oscillations in closed systems give rise to a range of interesting behavior in unstirred systems Scott, 1994. Diffusion can interact with nonlinear reaction kinetics to generate propagating waves of chemical reactivity and spatial patterns. The most common kind of chemical wave is the single propagating front, where, in an unstirred medium, there is a relatively sharp boundary between reacted and unreacted material, and this boundary or wavefront moves through the solution at an essentially constant speed. In a uniform two-dimensional medium, such as a Petri dish (figure 20), a wave emanating from a point produces a circular front, since it travels at the same velocity in all directions. If we have a system that generates repeated waves, we obtain a pattern of concentring circles, known as a *target* pattern. When two o more initiation sites are present, waves can collide, which results in annihilation of the colliding waves and can lead to patterns of considerable complexity Epstein e Pojman, 1998.

If target waves are broken, e.g., by gently tilting the reaction mixture, the two ends created respond by curling up to form a pair of counter-rotating spirals. Spiral waves has been observed not only in aqueous solutions but also in a wide range of excitable systems, such as catalytic crystal surfaces Ertle, 1991 and heart muscle Davidenko *et al.*, 1992. Similar structures occur in a great variety of natural environments, like oceans, atmosphere and galaxies Lin e Shu, 1964 (figure 21).

In chemical systems *archimedean* spirals are mainly observed. An archimedean spiral is the locus of points corresponding to the locations over time of a point moving away from a fixed point with a constant speed along a line which rotates

Figura 20: target and spirals in a BZ gel reaction

(a) nautilus shell **(b)** hurricane **(c)** spiral galaxy

Figura 21: spiral shapes in nature

with constant angular velocity. Equivalently, in polar coordinates (r, θ) it can be described by the equation

$$r = a + b\theta \tag{46}$$

with real numbers a and b. Changing the parameter a will turn the spiral, while b controls the distance between successive turnings.

Contrarily to target patterns, which reflect the local heterogeneities such as defects in the surface or dust particles, all spirals in a given BZ reaction mixture rotate with the same period and wavelength, reflecting the bulk kinetics. The advent of modern imaging systems coupled to computer acquisition hardware has led to an increase in the detail with which spirals have been studied. At the centre of a given spiral is a core with a diameter of 30 μm.

The evolution of spiral geometry is followed by studying the *spiral tip*, i.e., the free end of a spiral, defined by

$$\big(\nabla c_1 \times \nabla c_2\big)_{x_{tip}, y_{tip}} = sup\big[(\nabla c_1 \times \nabla c_2)\big], \qquad \forall\ x, y \tag{47}$$

In the simplest form of spiral evolution, the tip of the spiral, where the oxidation front and the reduction back meet, rotates around this circular core with the same frequency as the bulk spiral. As the conditions are varied, however, the spiral tip begins to meander Epstein e Pojman, 1998. Initially, this involves a second oscillation appearing, so the tip describes a quasiperiodic motion. As the behavior becomes more complex, various patterns resembling flowers are described by the tip path Biosa, Bastianoni e Rustici, 2006.

0.13 Diffusion

Molecular or ionic diffusion, often called simply diffusion, is the thermal motion of all (liquid or gas) particles at temperatures above absolute zero. The rate of this

movement is a function of temperature, viscosity of the fluid and the size (mass) of the particles. Diffusion explains the net flux of molecules from a region of higher concentration to one of lower concentration. The result of diffusion is a gradual mixing of material. In a phase with uniform temperature, absent external net forces acting on the particles, the diffusion process will eventually result in complete mixing. Molecular diffusion is typically described mathematically using Fick's laws of diffusion. Fick's first law relates the diffusive flux to the concentration, by postulating that the flux goes from regions of high concentration to regions of low concentration, with a magnitude that is proportional to the concentration gradient (spatial derivative). In one spatial dimension, this is

$$J = -D\frac{\partial c}{\partial x} \tag{48}$$

or, in two or more dimensions,

$$J = -D\nabla c \tag{49}$$

where J is the diffusion flux, D is the *diffusion coefficient* or *diffusivity*, c is the concentration, x is the position. The diffusivity D depends on the temperature, viscosity of the fluid and the size of the particles, according to the Einstein-Stocks relation

$$D = \frac{k_B T}{6\pi\eta r} \tag{50}$$

where k_B is the Boltzmann constant, T is the absolute temperature, η is the viscosity of the medium and r is the radius of the particle. In dilute aqueous solutions the diffusion coefficients of most ions are similar and have values that at room temperature are in the range of $0.6 - 2.0 \times 10^{-5}\mathrm{cm}^2\mathrm{s}^{-1}$.

Fick second law predicts how diffusion causes the concentration to change with time,

$$\frac{\partial c}{\partial t} = D\nabla^2 c \tag{51}$$

where the velocity of variation of concentration is proportional to the second spatial derivative of the concentration.

0.13.1 Turing structures

Original and beautiful spatio-temporal patterns in biological systems, such as leopard spots or zebra stripes, are known as *Turing structures*, in honour of Alan Turing, a british mathematician who provided, in 1952, a simple model for the theory of morphogenesis, i.e. the development of pattern and form in living systems.

Turing suggested that chemicals, which he also called *morphogens*, can react and diffuse in such a way as to produce spatial patterns, stationary in time and periodic in space.

The coupling between kinetics and diffusion can be expressed as

$$\frac{\partial \mathbf{c}}{\partial t} = f(\mathbf{c}) + D\nabla^2 \mathbf{c} \tag{52}$$

where $\mathbf{c}$ is the vector for morphogen concentrations and $f(\mathbf{c})$ represents the reaction kinetics.

Turing surprisingly realized that the competition between diffusion and autocatalysis on two different time scales can lead to the formation of spatial patterns. The key elements, whose suitable combination could give rise to spatial pattern formation, are the diffusion rates of participants. The kinetics should include a positive feedback, such as autocatalysis, on a species called activator and an inhibitory process. The inhibitor's diffusion coefficient should be much greater than the activator's one. The first examples of Turing structures occurring in chemical systems has been evidenced in the chlorite-iodide-malonic acid (CIMA) reaction Castets *et al.*, 1990; Kepper, Boissonade e Epstein, 1990 (figure 22).

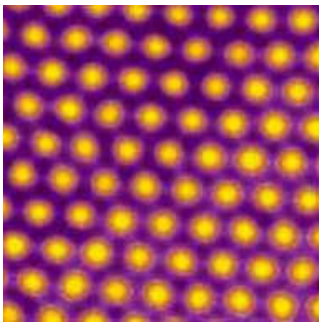

Figura 22: the CIMA reaction

0.14 Convection

The influence of gravity field on the kinetics–diffusion coupling is of great importance. Although simple calculations seems to suggest that gravity should have negligible influence on chemical reactions[1], it can drastically alter the macroscopic transport of heat and matter through *convection*, or macroscopic fluid motion. Natural convection is the movement of fluid as the result of differences in density, so that denser fluid sinks and less dense fluid rises (chapter I, the Bénard instability).This motion is resisted by the viscosity of the medium, which acts like friction does in slowing the motion of solids. Convection is a much more efficient process than diffusion for transporting heat and matter. In a system that exhibits sensitivity to orientation with respect to the force of gravity, wavefronts can propagate up to six time faster when reaction-diffusion mechanism is coupled with convection. In the next section, the equations governing fluid dynamics are illustrated, in order to take into account the effect of natural convection in the evolution of spatio-temporal organization of BZ systems.

0.15 The fundamental equations of hydrodynamics

Mechanics of continuous media is the branch of physics that studies hydrodynamic phenomena and heat flow. The central idea of this discipline is to consider local density, velocity and energy as continuous functions of space and time Chandrasekhar, 1961; Currie, 1993. Due to the molecular nature of matter, it is very hard to rigorously describe these concepts. However, we can define, for instance, local density considering the mass contained in a small element of volume ΔV. This volume contains many molecules and then density can be considered as a continuous function of $\mathbf{r}$, but it is small enough so that the mass divided per V still describes the local density in $\mathbf{r}$. In other words, we are dealing with a 'continuous' matter, other

[1]The mass of a small molecule is on the order of $\approx 10^{-26}$kg, which translates into a gravitational force of about 10^{-25}N; we can compare this with the force of attraction between the electron and the proton in a hydrogen atom, which is of the order of 10^{-8}N. Even allowing for shielding effects, electrostatics forces will always be many orders of magnitude stronger than gravitational forces, so that gravity does not affect directly the fundamental atomic and molecular interactions.

than discrete. Such systems are described by Partial Differential Equation systems (PDEs), in order to evaluate spatial and temporal variations of local density.

The fundamental laws of hydrodynamics are expressed by the following equations

$$\frac{\partial \rho}{\partial t} + \frac{\partial}{\partial x_j}(\rho u_j) = 0 \tag{53}$$

$$P_{ij} = -p\delta_{ij} + 2\mu e_{ij} - \frac{2}{3}\mu\delta_{ij}e_{kk} \tag{54}$$

$$\rho\frac{\partial u_i}{\partial t} + \rho u_j\frac{\partial u_i}{\partial x_j} = \rho X_i + \frac{\partial P_{ij}}{\partial x_j} \tag{55}$$

$$\phi = 2\mu e_{ij}^2 - \frac{2}{3}\mu e_{jj}^2 \tag{56}$$

$$\rho\frac{\partial}{\partial t}(c_V T) + \rho u_j\frac{\partial}{\partial x_j}(c_V T) = \frac{\partial}{\partial x_j}\left(\xi\frac{\partial T}{\partial x_j}\right) - p\frac{\partial u_j}{\partial x_j} + \phi \tag{57}$$

where ρ is the density of the fluid, u_i are the components of velocity in the three spatial directions, x_i are cartesian coordinates, X_i are the components of the resultant of external forces acting on the system. We assume that the internal energy $U = U(T)$ is a function of the temperature only. Equation 53 derives from the principle of mass conservation and is known as *equation of continuity*. Equations 55 and 57 derive from the principle of conservation of momentum and energy, respectively. Equation 54 states the nature of the tensor for viscous stress, while 56 is the term for heat dissipation due to this viscous stress. All these equations are then coupled to the state equations which describe the system along with appropriate boundary conditions. For an incompressible fluid, the velocity field is *solenoidal* because it satisfies the following equation

$$\frac{\partial u_j}{\partial x_j} = 0 \tag{58}$$

This simplifies our system because equations 53 and 55 become

$$\frac{\partial \rho}{\partial t} = -u_j\frac{\partial \rho}{\partial x_j} \tag{59}$$

$$\rho\frac{\partial u_i}{\partial t} + \rho u_j\frac{\partial u_i}{\partial x_j} = \rho X_i - \frac{\partial p}{\partial x_j} + \mu\nabla^2 u_i \tag{60}$$

The last (60) is the original form of the *Navier-Stokes equations*. It is necessary now to define the density as a state function of the system variables. In all chemical reactions we find regions with different density, because density depends on temperature and composition. Temperature is different if the reaction occurs in two contiguous regions of the solution at a different time. The same considerations can be made for composition, because it is impossible to have a solution completely homogeneous. We can thus introduce some coefficients for taking into account the variation of density with temperature T and composition C.

$$\alpha = -\frac{1}{\rho}\frac{\partial \rho}{\partial T} \tag{61}$$

$$\beta_i = \frac{1}{\rho}\frac{\partial \rho}{\partial C_i} \tag{62}$$

where C_i is the molar concentration of the $i-$th species. Thus, in a first approximation, the total density of a solution is given by

$$\rho = \rho_0\Big[1 - \alpha(T - T_0) + \sum_i \beta_i (C - C_0)_i\Big] \tag{63}$$

Further, if we assume that

- viscous dissipation terms are negligible;
- density term can be ignored besides when it influences external acting forces;
- the constants are independent of the state of the system and are invariants during its dynamical evolution;

we then obtain the hydrodynamic equations in the *Boussinesq approximation* Boussinesq, 1903

$$\frac{\partial u_j}{\partial x_j} = 0 \tag{64}$$

$$\frac{\partial u_i}{\partial t} + u_j \frac{\partial u_i}{\partial x_j} = -\frac{1}{\rho_0}\frac{\partial p}{\partial x_i} + \Big(1 + \frac{\delta\rho}{\rho_0}\Big)X_i + \nu\nabla^2 u_i \tag{65}$$

$$\frac{\partial T}{\partial t} + u_j \frac{\partial T}{\partial x_j} = k\nabla^2 T \tag{66}$$

where ρ_0 is the density for the reference state, $\delta\rho$ is the density variation respect to ρ_0, $\nu = \mu/\rho_0$ is the kinematic viscosity and $k = \xi/\rho_0 C_V$ is the thermal diffusivity of the fluid.

Parte II

The Model

The Reaction–Diffusion–Convection System

Instability scenarios by which a nonlinear system is driven to spatio–temporal chaos have been extensively studied , pointing out a strict interplay between kinetics and hydrodynamics.
The emergence of spatio–temporal patterns and self–organized structures like traveling waves and rotating spirals is, in fact, governed by the coupling of chemical reactions and transport phenomena Abramian, Vakulenko e Volpert, 2003; Agladze, Krinsky e Pertsov, 1984; Cross e Hohenemberg, 1993; Gaponenko e Volpert, 2003; Q.Ouyang e J.-M.Flesselles, 1996.
Kinetics–hydrodynamics coupling has also been invoked to explain the onset of temporal chaos in oscillating chemical systems such as Belousov–Zhabotinsky reaction, in which hydrodynamic control seems to regulate the onset of chemical turbulence . This hypothesis is confirmed by experimental evidence for chaotic transients in BZ unstirred systems Agladze, Krinsky e Pertsov, 1984, in which a strict dependence on (i) stirring Biosa, Bastianoni e Rustici, 2006, (ii) viscosity Rustici *et al.*, 2001 and (iii) reactor geometry Liveri *et al.*, 2003 has been observed.

A convenient formalism used to describe such systems is the so called RDC (Reaction-Diffusion-Convection) model, a more general extension of the Reaction–Diffusion (RD) system with a third term (C) that considers the influence exerted by the gravitational field on the RD instabilities Wu *et al.*, 1995. In this way diffusion of the main intermediate species and natural convection are coupled to the kinetic mechanism. To this end, a set of nondimensional equations is derived, coupling oregonator kinetics with diffusion and taking into account, specifically, the convective motions induced by gradients of density only ascribed to concentration inhomogeneities.

In this chapter we present the mathematical model used to describe our RDC system and in the next its translation to an opportune Fortran code for numerical simulations.

0.16 RDC equations

In order to obtain our PDE system, we have to opportunely modify the kinetic equations 39 and 40, by taking into account the concentration of starting reagents

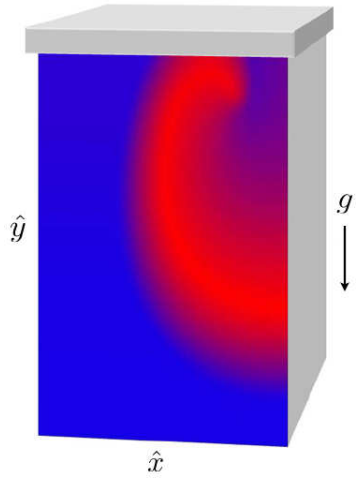

Figura 23: bidimensional representation of a RDC problem

a and b

$$\frac{\mathrm{d}x}{\mathrm{d}\tau} = \frac{1}{\epsilon}\left[x(a-x) - \frac{x-qa}{x+qa}fbz\right] \tag{67}$$

$$\frac{\mathrm{d}z}{\mathrm{d}\tau} = ax - bz \tag{68}$$

We can now couple them to the diffusive term given by Fick's second law (51) and the Navier-Stokes equations (60) , along with the convective term $\mathbf{V}\nabla C_i$, where $\mathbf{V}$ is the velocity field and C_i are the concentrations of intermediate species expressed by x and z. We must also consider the state equations for density (61 - 62) and the hydrodynamic equations formulated in Boussinesq's approximation (64 - 66). For the sake of simplicity, the concentrations of reactants are represented by C_i, the cartesian coordinates by $\hat{x}$ and $\hat{y}$ and $P = p - \rho_0 g\hat{z}$ is the reduced pressure. The problem is then presented by means of the vectorial components of the velocity U (along the $\hat{x}$-axis) and V (along the $\hat{y}$-axis). We are thus approximating a three-dimensional problem to a bidimensional slab in which $\hat{y}$ represents the vertical component along which the gravity force acts Wu *et al.*, 1995 (figure 23).

$$\partial_t C_i + U\partial_{\hat{x}} C_i + V\partial_{\hat{y}} C_i - D_i\nabla^2 C_i = K_i(C_j, \bar{\lambda}) \tag{69}$$

$$\partial_t U + U\partial_{\hat{x}} U + V\partial_{\hat{y}} U + \frac{1}{\rho_0}\partial_{\hat{x}} P - \nu\nabla^2 U = 0 \tag{70}$$

$$\begin{aligned}\partial_t V + U\partial_{\hat{x}} V + V\partial_{\hat{y}} V + \frac{1}{\rho_0}\partial_{\hat{y}} P - \nu\nabla^2 V \\ = -g\sum_{i=1}^{2}\beta_i(C_i - C_{0i})\end{aligned} \tag{71}$$

$$\partial_{\hat{x}} U + \partial_{\hat{y}} V = 0 \tag{72}$$

where C_i and $K_i(C_j, \bar{\lambda})$ are the species concentrations and the kinetic equations of a general chemical process, $\bar{\lambda}$ is the set of kinetic parameters and P is the pressure. D_i is the diffusion coefficient of i^{th} intermediate species, ν is the kinematic viscosity and g the gravitational acceleration. The sum in the right hand of equation 71 substitutes the term $(\rho - \rho_0)/\rho_0$, which is the density variation due to the change of concentration of the i^{th} species with respect to the medium density ρ_0. As a matter of fact, when temperature gradients can be neglected, ρ can be expressed as

$$\rho = \rho_0 \Big[1 + \sum_i \beta_i (C_i - C_{0i}) \Big] \tag{73}$$

To obtain the dimensionless equations we consider the time scale t_0 to be equal to the chemical time scale of the dimensionless kinetic model; the space scale $\hat{x}_0$ measures the spatial domain. We consider the following transformation to dimensionless (barred) variables: $\bar{t} = t/t_0$; $\bar{x} = \hat{x}/\hat{x}_0$; $\bar{u} = U/v_0$; $v_0 = \nu/\hat{x}_0$; $\bar{p} = P/p_0$ with $p_0 = (\rho_0 \hat{x}_0 v_0)/t_0$. Furthermore we write the dimensionless concentrations and the relative kinetic functions in lower case style. The equation system reads:

$$\partial_{\bar{t}} c_i - \frac{D_i t_0}{\hat{x}_0^2} \nabla^2 c_i + \frac{v_0 t_0}{\hat{x}_0} (u \partial_{\bar{x}} c_i + v \partial_{\bar{y}} c_i) = k_i(c_j, \bar{\lambda}) \tag{74}$$

$$\partial_{\bar{t}} \bar{u} - \frac{\nu t_0}{\hat{x}_0^2} \nabla^2 \bar{u} + \frac{v_0 t_0}{\hat{x}_0} (\bar{u} \partial_{\bar{x}} \bar{u} + \bar{v} \partial_{\bar{y}} \bar{u}) + \frac{t_0}{\hat{x}_0 v_0 \rho_0} p_0 \partial_{\bar{x}} \bar{p} = 0 \tag{75}$$

$$\begin{aligned} \partial_{\bar{t}} \bar{v} - \frac{\nu t_0}{\hat{x}_0^2} \nabla^2 \bar{v} + \frac{v_0 t_0}{\hat{x}_0} (\bar{u} \partial_{\bar{x}} \bar{v} + \bar{v} \partial_{\bar{y}} \bar{v}) + \frac{t_0}{\hat{x}_0 v_0 \rho_0} p_0 \partial_{\bar{y}} \bar{p} \\ = -\frac{g t_0}{v_0} \sum_i \beta_i (c_i - c_{0i}) \end{aligned} \tag{76}$$

$$\partial_{\bar{x}} u + \partial_{\bar{y}} v = 0 \tag{77}$$

neglecting the bars upon the dimensionless variables and introducing some new parameters, the system becomes:

$$\partial_t c_i - d_i \nabla^2 c_i + D_\nu (u \partial_{\hat{x}} c_i + v \partial_{\hat{y}} c_i) = k_i(c_j, \bar{\lambda}) \tag{78}$$

$$\partial_t u - D_\nu \nabla^2 u + D_\nu (u \partial_{\hat{x}} u + v \partial_{\hat{y}} u) + \partial_{\hat{x}} p = 0 \tag{79}$$

$$\begin{aligned} \partial_t v - D_\nu \nabla^2 v + D_\nu (u \partial_{\hat{x}} v + v \partial_{\hat{y}} v) + \partial_{\hat{y}} p \\ = -D_\nu \sum_i Gr_i (c_i - c_{0i}) \end{aligned} \tag{80}$$

$$\partial_x u + \partial_y v = 0 \tag{81}$$

where d_i, the **dimensionless diffusion coefficient** and Gr_i, the **Grashof number** of the i^{th} species, are the set of control parameters μ used in our study

$$\mu = \begin{cases} d_i = \dfrac{D_i t_0}{\hat{x}_0^2} \\ Gr_i = \dfrac{g\hat{x}_0^3 \beta_i}{\nu^2} \end{cases} \tag{82}$$

while $D_\nu = \nu t_0/\hat{x}_0^2$ is the dimensionless viscosity. It is worth noticing that the term $(c_i - c_{0i})$, which is normally included in the Grashof number for systems where the concentration gradient is fixed, is here kept out since it dynamically varies in time and space. However Gr_i is still dimensionless since c_i are dimensionless. It represents the entity of convection only ascribed to isothermal density changes Bockmann, Hess e Muller, 1996; Cliffe, Taverner e Wilke, 1998 and is related to the hydrodynamic instability, giving the balance between momentum and viscosity forces acting in the system. The temperature terms are neglected since it has been demonstrated that diffusion of chemicals is two orders of magnitude smaller than thermal diffusivity and has a stronger influence for the onset of convection Pojman e Epstein, 1990; Vasquez, Wilder e Edwards, 1993; Wilder, Edwards e Vasquez, 1992.
The set of equation can be written in the more condensed form:

$$\partial_t c_i - d_i \nabla^2 c_i + D_\nu (\mathbf{v} \cdot \nabla) c_i = k_i(c_j, \bar{\lambda}) \tag{83}$$

$$\partial_t \mathbf{v} - D_\nu \nabla^2 \mathbf{v} + D_\nu (\mathbf{v} \cdot \nabla)\mathbf{v} + \nabla p = -D_\nu \sum_i Gr_i (c_i - c_{0i}) \tag{84}$$

$$\nabla \cdot \mathbf{v} = 0 \tag{85}$$

0.17 The model

The term ∇p can be eliminated by taking the curl of both sides of equation 84. We therefore introduce the *vorticity* as

$$w = \nabla \times \mathbf{v} \tag{86}$$

and the *stream function* as

$$\psi = \begin{cases} u = \partial_y \psi \\ v = -\partial_x \psi \end{cases} \tag{87}$$

and we get the $w - \psi$ form of our Reaction–Diffusion–Convection (RDC) model for a general chemical process[2]

$$\begin{aligned} &\frac{\partial c_i(\hat{x},\hat{y};t)}{\partial t} + D_\nu \left(u \frac{\partial c_i(\hat{x},\hat{y};t)}{\partial \hat{x}} + v \frac{\partial c_i(\hat{x},\hat{y};t)}{\partial \hat{y}} \right) \\ &- d_i \nabla^2 c_i(\hat{x},\hat{y};t) = k_i(c_j, \bar{\lambda}) \end{aligned} \tag{88}$$

$$\begin{aligned} &\frac{\partial w(\hat{x},\hat{y};t)}{\partial t} + D_\nu \Big(u \frac{\partial w(\hat{x},\hat{y};t)}{\partial \hat{x}} + v \frac{\partial w(\hat{x},\hat{y};t)}{\partial \hat{y}} \Big) \\ &- D_\nu \nabla^2 w(\hat{x},\hat{y};t) = -D_\nu \sum_i Gr_i \frac{\partial c_i(\hat{x},\hat{y};t)}{\partial \hat{x}} \end{aligned} \tag{89}$$

$$\frac{\partial^2 \psi(\hat{x},\hat{y};t)}{\partial \hat{x}^2} + \frac{\partial^2 \psi(\hat{x},\hat{y};t)}{\partial \hat{y}^2} = -w(\hat{x},\hat{y};t) \tag{90}$$

$$u = \frac{\partial \psi(\hat{x},\hat{y};t)}{\partial \hat{y}} \tag{91}$$

$$v = -\frac{\partial \psi(\hat{x},\hat{y};t)}{\partial \hat{x}} \tag{92}$$

We also impose the following boundary conditions:

1. *no-flow* (*Dirichlet's condition*) for the chemical concentrations at the wall of the slab (the extremes of the space domain are $0 \le \hat{x} \le a$ and $0 \le \hat{y} \le b$)

$$\left[\frac{\partial c_i(\hat{x},\hat{y};t)}{\partial \hat{x}} \right]_{0,a} = \left[\frac{\partial c_i(\hat{x},\hat{y};t)}{\partial \hat{y}} \right]_{0,b} = 0 \tag{93}$$

2. *no-slip* (*von Neumann's condition*) for the fluid velocity

$$\frac{\partial u}{\partial \hat{x}} + \frac{\partial v}{\partial \hat{y}} = 0 \tag{94}$$

[2]This model has been developed in 2000 by Dr. M. Masia in his MSc degree thesis.

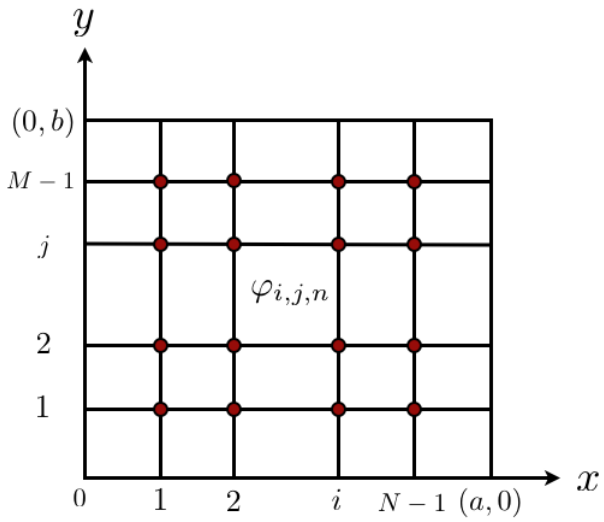

Figura 24: bidimensional integration grid

0.18 Computational methods

The mathematical formulation of our problem is thus defined by a set of *parabolic* partial differential equations, because of the presence of first order temporal and second order spatial derivatives

$$\frac{\partial \varphi}{\partial t} = \left(\frac{\partial^2 \varphi}{\partial x^2} + \frac{\partial^2 \varphi}{\partial y^2}\right) \tag{95}$$

Such kind of problems are generally integrated over spatio-temporal grids to obtain numerical solutions with different numerical methods (see appendix 0.36), once initial and boundary conditions are known Smith, 1965.

0.18.1 Alternating direction implicit method

This section is concerned with the numerical solution method adopted in our model - the ADI (*alternating direction implicit*) method - to solve a parabolic equation of this kind

$$\frac{\partial \varphi}{\partial t} = \left(\frac{\partial^2 \varphi}{\partial x^2} + \frac{\partial^2 \varphi}{\partial y^2}\right) \tag{96}$$

over a rectangular region $0 \leq x \leq a$, $0 \leq y \leq b$, where φ is known initially at all points within and on the boundary of the rectangle, and is known subsequently at all points on the boundary. The coordinates (x, y, t) of the nodes of the solution domain are $x = i\delta x$, $y = j\delta y$, $t = n\delta t$, where i, j, n are positive integers; we also denote the values of φ at these nodes by $\varphi(i\delta x, j\delta y, n\delta t) = \varphi_{i,j,n}$ (figure 24). The explicit finite-difference representation of equation 96

$$\begin{aligned} \frac{\varphi_{i,j,n+1} - \varphi_{i,j,n}}{\delta t} =& \frac{k}{(\delta x)^2}(\varphi_{i-1,j,n} - 2\varphi_{i,j,n} + \varphi_{i+1,j,n}) \\ &+ \frac{k}{(\delta y)^2}(\varphi_{i,j-1,n} - 2\varphi_{i,j,n} + \varphi_{i,j+1,n}) \end{aligned} \tag{97}$$

appears attractively simple but is computationally laborious because the condition for its validity, which is

$$k\Big[\frac{1}{(\delta x)^2}+\frac{1}{(\delta y)^2}\Big]\delta t \leq \frac{1}{2} \tag{98}$$

necessitates extremely small values for δt. For most problems it is an impractical method. The Crank-Nicolson method, namely

$$\begin{aligned}\frac{\varphi_{i,j,n+1}-\varphi_{i,j,n}}{\delta t} =& \frac{k}{2}\Big[(\frac{\partial^2\varphi}{\partial x^2}+\frac{\partial^2\varphi}{\partial y^2})_{i,j,n} \\ &+(\frac{\partial^2\varphi}{\partial x^2}+\frac{\partial^2\varphi}{\partial y^2})_{i,j,n+1}\Big]\end{aligned} \tag{99}$$

is valid for all values of $x = i\delta x$, $y = j\delta y$ and $t = n\delta t$, but it requires the solution of $(M-1)(N-1)$ simultaneous algebraic equations for each step forward in time, where $N\delta x = a$ and $M\delta y = b$. Unlike the 1-dimensional case they cannot be solved by a simple recursive process. For large values of M and N they would usually be solved iteratively.

The most efficient method at present, for rectangular regions, is the ADI method proposed by Peaceman and Rachford in 1955 [Peaceman e Rachford, 1955] it involves about twenty-five time less work than the explicit method and seven times less work than the Crank-Nicolson method. Let assume that the solution is known for time $t = n\delta t$. The ADI method consists of replacing only one of the second-order derivatives, $\partial^2\varphi/\partial x^2$ say, by an implicit difference approximation in terms of unknown values of φ from the $(n+1)$th time-level, the other second-order derivative, $\partial^2\varphi/\partial y^2$, being replaced by an explicit finite-difference approximation. Application of the corresponding finite-difference equation to each of the $(N-1)$ nodes along a row parallel to the x-axis (figure 24) gives $(N-1)$ equations for the $(N-1)$ unknown values of φ at these nodes for time $t = (n+1)\delta t$. When there are $(M-1)$ rows parallel to the x-axis, the advancement of the solution over the whole rectangle to the $(n+1)$th time steps involves the solution of $(M-1)$ independent systems of equations, each system containing $(N-1)$ unknowns.

$$\begin{aligned}\frac{\varphi_{i,j,n+1}-\varphi_{i,j,n}}{k\delta t} =& \frac{\varphi_{i-1,j,n+1}-2\varphi_{i,j,n+1}+\varphi_{i+1,j,n+1}}{(\delta x)^2} \\ &+\frac{\varphi_{i,j-1,n}-2\varphi_{i,j,n}+\varphi_{i,j+1,n}}{(\delta y)^2}\end{aligned} \tag{100}$$

The advancement of the solution to the $(n+2)$th time level is then achieved by replacing $\partial^2\varphi/\partial y^2$ by an implicit finite-difference approximation and $\partial^2\varphi/\partial x^2$ by an explicit one, and writing down the finite-difference equation corresponding to each node along columns paralles to the y-axis. This gives $(N-1)$ independent systems of equations, each system involving $(M-1)$ unknowns. The time interval δt must be the same for each advancement.

$$\begin{aligned}\frac{\varphi_{i,j,n+2}-\varphi_{i,j,n+1}}{k\delta t} =& \frac{\varphi_{i-1,j,n+1}-2\varphi_{i,j,n+1}+\varphi_{i+1,j,n+1}}{(\delta x)^2} \\ &+\frac{\varphi_{i,j-1,n+2}-2\varphi_{i,j,n+2}+\varphi_{i,j+1,n+2}}{(\delta y)^2}\end{aligned} \tag{101}$$

The solution of these systems is much easier than the solution of the $(M-1)(N-1)$ algebraic equations associated with fully implicit methods. The system of equations involved is symmetric and tridiagonal (banded with bandwidth 3), and is typically solved using tridiagonal matrix algorithm. It can be shown that this method is unconditionally stable and second order in time and space.

The code

The mathematical model used in our study has been translated to an opportune code that solves partial differential equations with the method of finite difference with alternating direction Press *et al.*, 1992. It has been developed in a Fortran 77 language[3] and modified in a vectorizable Fortran 90 code[4], in order to reduce the simulation time required for a calculation. At this moment, a 30 million temporal steps simulation can be carried out in 24 hours, instead of some months. The name of last version of the code used in the nonlinear dynamics group is `oregon.f90`.

0.19 The concentration functions

Let's discuss the application of ADI method to one of the equations of the Reaction-Diffusion-Convection PDE system (equations 88 - 94), namely equation 88 and its kinetic relative 39.
We run over the discretized x-axis (i cursor) to solve the system for the time $n+1/2$:

$$\begin{aligned}&\frac{\xi_{i,j}^{n+1/2}-\xi_{i,j}^{n}}{\tau/2}-D_i\left[\frac{\xi_{i+1,j}^{n+1/2}-2\xi_{i,j}^{n+1/2}+\xi_{i-1,j}^{n+1/2}}{h2}\right.\\&\left.-\frac{\xi_{i+1,j}^{n}-2\xi_{i,j}^{n}+\xi_{i-1,j}^{n}}{h2}\right]+D_\nu\left[u_{i,j}^{n}\frac{\xi_{i+1,j}^{n+1/2}-\xi_{i-1,j}^{n+1/2}}{2h}\right.\\&\left.+v_{i,j}^{n}\frac{\xi_{i,j+1}^{n}-\xi_{i,j-1}^{n}}{2h}\right]=\frac{1}{\epsilon}\left[\xi_{i,j}^{n}(1-\xi_{i,j}^{n})+f\chi_{i,j}^{n}\frac{q-\xi_{i,j}^{n}}{q+\xi_{i,j}^{n}}\right]\end{aligned}\tag{102}$$

where $\xi = c_1$ and $\chi = c_2$ refer to $HBrO_2$ and Ce^{4+}, respectively. We now proceed over the discretized y-axis (j cursor) to solve the system for the time $n+1$

$$\begin{aligned}&\frac{\xi_{i,j}^{n+1}-\xi_{i,j}^{n+1/2}}{\tau/2}-D_i\left[\frac{\xi_{i+1,j}^{n+1/2}-2\xi_{i,j}^{n+1/2}+\xi_{i-1,j}^{n+1/2}}{h2}\right.\\&\left.-\frac{\xi_{i+1,j}^{n+1}-2\xi_{i,j}^{n+1}+\xi_{i-1,j}^{n+1}}{h2}\right]+D_\nu\left[u_{i,j}^{n}\frac{\xi_{i+1,j}^{n+1/2}-\xi_{i-1,j}^{n+1/2}}{2h}\right.\\&\left.+v_{i,j}^{n}\frac{\xi_{i,j+1}^{n+1}-\xi_{i,j-1}^{n+1}}{2h}\right]=\frac{1}{\epsilon}\left[\xi_{i,j}^{n}(1-\xi_{i,j}^{n})+f\chi_{i,j}^{n}\frac{q-\xi_{i,j}^{n}}{q+\xi_{i,j}^{n}}\right]\end{aligned}\tag{103}$$

[3]Prof. V. Volpert, Université de Lyon
[4]Dr. P. C. Cresto, Universitá di Sassari

Clearly, in the first step terms in x direction are calculated by means of the implicit approximation, while explicit approximation is used proceeding along the y direction. Viceversa, for the second time step, the computation is explicit while running over the x direction and implicit in the y direction.

Equation 102, and similarly equation 103, can be re–written with the unknown terms for the time $(n+1/2)$ as a function of known terms at time n.

$$\begin{aligned} \frac{\xi_{i,j}^{n+1/2}}{\tau/2} - D_i \left[\frac{\xi_{i+1,j}^{n+1/2} - 2\xi_{i,j}^{n+1/2} + \xi_{i-1,j}^{n+1/2}}{h^2} \right] \\ + D_\nu u_{i,j}^n \left[\frac{\xi_{i+1,j}^{n+1/2} - \xi_{i-1,j}^{n+1/2}}{2h} \right] \\ = \frac{\xi_{i,j}^n}{\tau/2} + D_i \left[\frac{\xi_{i+1,j}^n - 2\xi_{i,j}^n + \xi_{i-1,j}^n}{h^2} \right] \\ - D_\nu v_{i,j}^n \left[\frac{\xi_{i+1,j}^n - \xi_{i-1,j}^n}{2h} \right] + \frac{1}{\epsilon} \left[\xi_{i,j}^n (1 - \xi_{i,j}^n) + f\chi_{i,j}^n \frac{q - \xi_{i,j}^n}{q + \xi_{i,j}^n} \right] \end{aligned} \tag{104}$$

We have then to deal with 3 fundamental unknowns for time $(n+1/2)$:

$$\xi_{i+1}^{n+1/2},\ \xi_i^{n+1/2} \text{ and } \xi_{i-1}^{n+1/2}$$

where j is fixed. In other terms the problem can be re–written in the form

$$A_{(i-1,j)}\xi_{i-1,j} + B_{(i,j)}\xi_{i,j} + C_{(i+1,j)}\xi_{i+1,j} = F_{i,j} \tag{105}$$

where $A_{(i-1,j)}$, $B_{(i,j)}$, $C_{(i+1,j)}$ represent the expression for $\xi_{i-1,j}$, $\xi_{i,j}$ and $\xi_{i+1,j}$ respectively, while $F_{i,j}$ includes the known terms for the time level n. This formula, extended to all the points of the j–th row, generates a *tridiagonal* matrix $\mathcal{M}$, so that we can re–write equation 105 as

$$\mathcal{M}\bar{\xi} = \bar{F} \tag{106}$$

In this notation j is neglected, i is the cursor along x direction and k is the index of the m terns $(A_{(i-1,j)}, B_{(i,j)}, C_{(i+1,j)})$ to be considered to solve the concentration profile over the j–th row. The solution of this linear system of equations requires the imposition of suitable boundary conditions. In this case we can use Dirichlet boundary conditions,that sets the borders of the spatial domain equal to zero: $\xi_{(1,j)} = 0$ and $\xi_{(m,j)} = 0$, along the x direction and $\xi_{(i,1)} = 0$ and $\xi_{(i,n)} = 0$, along the y direction. We can also impose the Von Neumann (no–flow) boundary conditions by which a concentration plateau is introduced at the borders of the spatial domain: $\xi_1 = \xi_2$ and $\xi_{m-1} = \xi_m$ along the x axis and $\xi_1 = \xi_2$ and $\xi_{n-1} = \xi_n$ along the y direction. This condition allows us to write the form

$$\xi_{m-1} = Aa_{(m-1)}\xi_m + Bb_{(m-1)} \tag{107}$$

and, being $\xi_{m-1} = \xi_m$, then

$$\xi_{m-1} = \frac{Bb_{(m-1)}}{(1 - Aa_{(m-1)})} \tag{108}$$

The result of these considerations leads to the *bidiagonal* form of the previous matrix

$$\mathcal{M} = \begin{pmatrix} 1 & Aa_{(1,2)} & 0 & \cdots & \cdots & 0 & 0 & 0 \\ 0 & 1 & Aa_{(2,3)} & 0 & \cdots & 0 & 0 & 0 \\ 0 & 0 & 1 & Aa_{(3,4)} & 0 & 0 & 0 & 0 \\ & & & & & & & \\ 0 & 0 & \vdots & \vdots & \vdots & 0 & 0 & 0 \\ 0 & \cdots & 0 & 0 & 1 & Aa_{(k,i+1)} & 0 & 0 \\ & & & & & & & \\ & & & \vdots & \vdots & \vdots & & \\ 0 & \cdots & 0 & \vdots & \vdots & & 0 & 0 \\ 0 & \cdots & 0 & 0 & 0 & 1 & Aa_{(m-1,m-2)} & 0 \\ 0 & \cdots & 0 & 0 & 0 & 0 & 0 & 1 \end{pmatrix} \tag{109}$$

and consequently

$$\mathcal{M}\bar{\xi} = \begin{pmatrix} 0 \\ Bb_{(2)} \\ Bb_{(3)} \\ \vdots \\ Bb_{(i)} \\ \vdots \\ Bb_{(m-1)} \\ 0 \end{pmatrix} \tag{110}$$

which can be directly solved starting from the boundary value ξ_m and following the algorithm

$$\xi_{m-1} \quad = \quad Aa_{(m-1)}\xi_m + Bb_{(m-1)} \tag{111}$$

0.20 The output files

The spatial configurations of concentrations of $HBrO_2$ and Ce^{4+} are recorded in output files named `bro(ce)________.dat` at a time specified by the parameter `wrstep` (see appendix 0.36.5). The dashed line in the filename is a eight-digits integer given by 100×`ht`, where `ht` is the temporal integration step. This operation is also reiterated along the y direction for all j, in order to scan the entire solving grid and to build up the temporal evolution for the concentrations. In appendix 0.36.5 an example of the implementation of the algorithm in the FORTRAN 90 programming language is described. The same method is used to solve equations for vorticity w and stream function ψ (see equations 86-94). The temporal evolution of chemical oscillations is written in the output file `timeav.dat`, which contains the average values for concentrations of $HBrO_2$ and Ce^{4+} (see appendix 0.36.5). This file contains also the temporal average values of vorticity and stream function (`psi________.dat`), as described in table 8.

0.21 Initial conditions

The initial distribution of concentrations over the integration grid is formulated in order to produce a dishomogeneous situation, typical of reaction–diffusion system. In this way, convective motions occur under the influence exherted by gravitational field and opportune conditions of the medium viscosity. Therefore the functions describing initial concentrations were set according to the model for a reaction-diffusion BZ system proposed in Jahnke, Skaggs e Winfree, 1989, the so-called *step*

Columns	*Contents*
1	`wrstep`
2	$[HBrO_2]_{\text{av}}$
3	$[Ce^{4+}]_{\text{av}}$
4	$[HBrO_2]_{\text{stdev}}$
5	$[Ce^{4+}]_{\text{stdev}}$
6	w_{av}
7	ψ_{av}

Tabella 8: the structure of output file timeav.dat

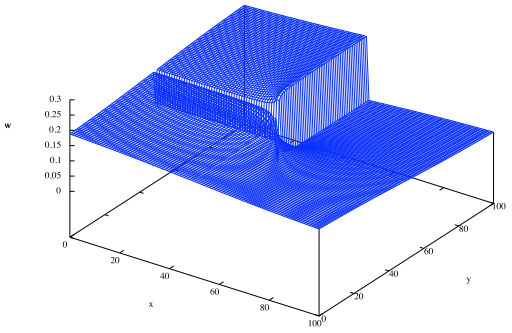

Figura 25: initial $[Ce^{4+}]$ distribution

functions, used in the simulation of spiral waves (figure 25)

$$c_1^0 = \begin{cases} 0.8, & 0 < \theta < 0.5 \\ c_{1(ss)}, & \text{elsewhere.} \end{cases} \tag{112}$$

$$c_2^0 = c_{2(ss)} + \frac{\theta}{8\pi f} \tag{113}$$

where $c_{2(ss)} = c_{1(ss)} = q(f+1)/(f-1)$, θ is the polar coordinate angle and, as suggested by the experimental results about the influence of the initial concentrations on the onset of chaos, the original function for c_2^0 was multiplied by a factor of 1.3. The resulting Fortran translation is in appendix 0.36.5.

0.22 The input file

The input file `param.dat` allows the regulatation of the following set of values

- initial parameters;
- kinetic parameters, useful to control the chemistry of our system, so that it can be set to an opportune region of the phase space;
- hydrodynamic parameters;

- dimensionless diffusivity d_i and Grashof numbers Gr_i: they constitute the set of μ control parameters considered in this study in order to follow the dynamical evolution of our system.

The input file is structured in a manner that makes possible to evaluate the different effects of reaction–diffusion–convection on system dynamics in a separate way

```
m = 101
nf = 150000001
wrstep = 10001

Gr1 = 10.00000
Gr2 = 10.00000
d1 = 0.02000
visc = 1.00000

eps = 0.00005
ff = 1.60000
q = 0.01000
A = 1.00000
B = 1.00000
t1_default_value = 0.80000
init_ce = 1.33333
```

The first three parameters represent: the number `m` of points in the integration grid, the number `nf` of temporal steps in a single simulation and `wrstep` is the time every spatial configuration is recorded. The second group of parameters are the Grashof number Gr_i for the two main intermediate species, the dimensionless diffusivity d_i and the dimensionless viscosity D_ν.
Lastly, we have the kinetic parameters for oregonator model: ϵ, f, q.
`A` is the initial concentration of BrO_3^-, `B` the initial concentration of malonic acid, `init_ce` the initial concentration of the catalyst Ce^{4+}, `t1_default_value` the standard value for step functions.

Numerical integration was performed using the time step of 1.0×10^{-6} on a square grid of 100 points in each direction. The temporal scale applied to the system is the same imposed in the dimensionless form of the kinetic oregonator functions ($t_0 = 1/(k_0 B = 21\text{s} =$ oregonator time unit, otu). The spatial scale x_0 is arbitrarily set to 0.06 cm, equal to the minimum spatial domain for which we experimentally observe chaotic dynamics in a Belousov–Zhabotinsky unstirred system. Dimensionless viscosity $D_\nu = 58.50$, ν being the kinematic viscosity set equal to the water viscosity 0.01 cm^2s^{-1}. Grashof numbers and diffusivities range $Gr_i \in \{0.00, 12.50\}$ and $d_i \in \left\{1.5 \times 10^{-7}, 1.5 \times 10^{-6}\right\}$ where, for sake of simplicity, we set $Gr_1 = Gr_2$ and $d_1 = d_2$. Diffusivity in `param.dat` file is expressed as d_f and ranges from 0.01 to 0.10, due to the fact that $d_f = d_i/(1.5 \times 10^{-5}\text{cm}^2\text{s}^{-1})$.

The decision to use a range for d_i from one to two orders of magnitude inferior to the value of $1.5 \times 10^{-5}\text{cm}^2\text{s}^{-1}$ indicated in Jahnke, Skaggs e Winfree, 1989; Wu *et al.*, 1995 arises from the fact that in our simulations any RDC coupling hasn't never been observed for this value. Probably, the order of magnitude reported in literature for BZ active species is greater than that accessible by convective motions resulting from concentration gradients.

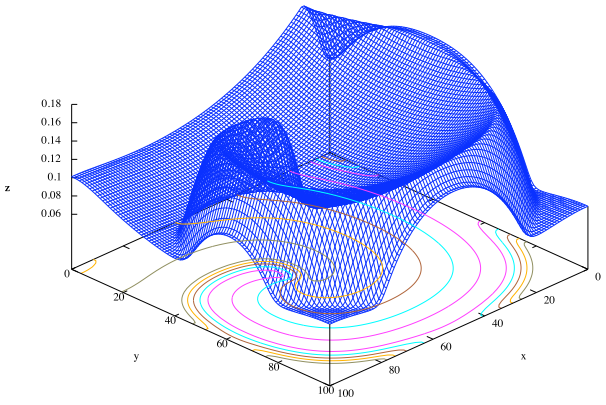

Figura 26: $[Ce^{4+}]$ spatial distribution at $d_i = 6.0 \times 10^{-7}$

0.23 The model at work

The formulation of the code and the structure of the input file provide a very functional way to study a complex RDC system, breaking it into simpler forms Budroni *et al.*, 2008; Marchettini *et al.*, 2010.
In other words, we can neglect the influence of convection and deal with a reaction–diffusion (RD) system, or even ignore the coupling with diffusion, in order to study only chemical oscillations (R system). For instance, setting Grashof numbers Gr_i and diffusivities d_i equal to zero, the plot of temporal evolution file `timeav.dat` for chemical spatial concentrations allows one to immediately perform important qualitative analysis. A simpler R system will give periodic temporal chemical oscillations of the two main intermediate species $[HBrO_2]$ and $[Ce^{4+}]$ (figure 48), characterized by a single main frequency of $\omega_1 = 0.394$ ofu and its principal harmonics in the FFT amplitude spectrum. The (c_1, c_2) phase space will show a limit cycle attractor, typical of periodic dynamics. The 3d plot of the spatial concentration of the intermediate species has the shape as in figure 25.

Keeping fixed $Gr_i = 0$ and increasing d_i, we observe the coupling between oregonator kinetic functions and diffusivity. The 3d spatial configuration of intermediates immediately changes, giving rise to a well-shaped spiral wave, typical of a reaction-diffusion (RD) system (figure 26). In figure 27 we also show temporal series and fft spectrum for the RD system. It is clear that dynamics continues to be periodic, with a decrease in the amplitude of the oscillations and a shift in the frequency of limit cycle to higher values ($\omega_1 = 0.740$ ofu), as shown in fft spectrum, due to the effective coupling between kinetics and diffusion. To be more precise, a frequency shift occurs in fft spectrum when diffusivity increases, as shown in figure 28. This behavior seems to be related to the increase in rotational speed of spiral waves, when diffusivity change (figure 29).

Things dramatically change when we introduce the convective term, so that a RD system becomes a RDC one. The next chapter reports in detail the qualitative study carried out in this project, where we show that natural convection, modeled according to our PDE system, is the main responsible for the transition to chemical

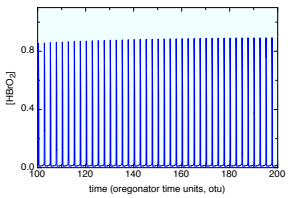

(a) temporal evolution of concentration

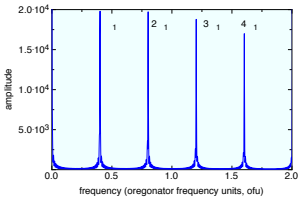

(b) FFT amplitude spectrum

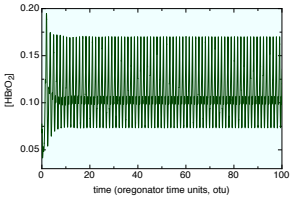

(c) temporal evolution of concentration

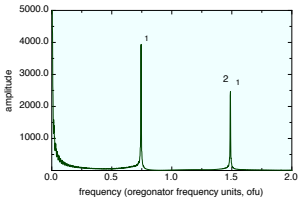

(d) FFT amplitude spectrum

Figura 27: the R (a–b) and RD (c–d) systems

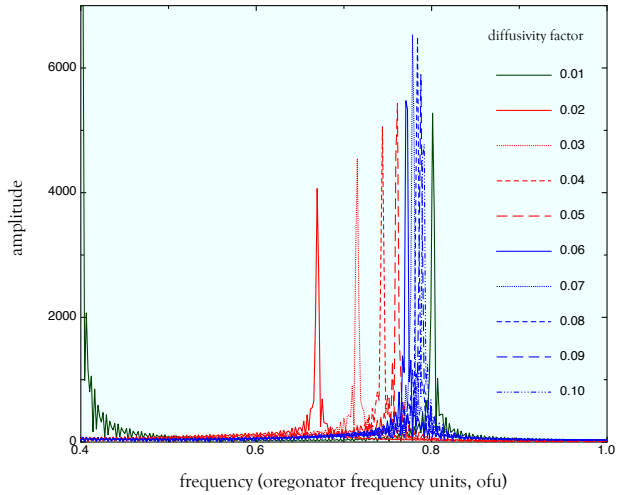

Figura 28: frequency shift for $d_i = 1.5 \times 10^{-7} - 10^{-6}$ and $Gr_i = 0$

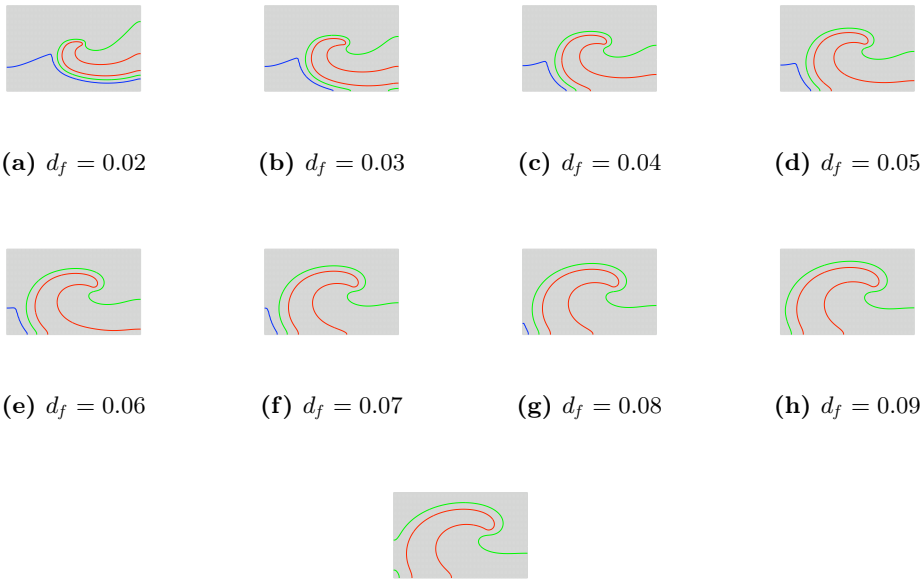

(a) $d_f = 0.02$ **(b)** $d_f = 0.03$ **(c)** $d_f = 0.04$ **(d)** $d_f = 0.05$

(e) $d_f = 0.06$ **(f)** $d_f = 0.07$ **(g)** $d_f = 0.08$ **(h)** $d_f = 0.09$

(i) $d_f = 0.10$

Figura 29: increase in rotation speed of spiral waves induced by variation of diffusivity in the range 3.0×10^{-7} (a) – 1.5×10^{-6} (i) for a pure RD system ($Gr_i = 0$)

chaos observed experimentally in Belousov–Zhabotinsky unstirred systems. Moreover, we notice a hydrodynamic competition between diffusivity and Grashof number for the stability states of our dynamic model, both in temporal and spatio-temporal evolution.

Parte III

Results

Spatio-Temporal chaos

In a RD model, the diffusion breaks the symmetry of the kinetic system and introduces an instability that leads to new stable solutions, which have the form of characteristic dissipative structures. Therefore, we can imagine the reaction-diffusion-convection (RDC) system as an extension of the reaction-diffusion model, in which the addiction of a convective term will result in a sort of competition with diffusion for the new states of stability for the system Q.Ouyang e J.-M.Flesselles, 1996.

However, a range of values of Grashof numbers Gr_i will exist, for which the RDC coupling corresponds to a kind of inertia respect to the diffusive regime: the rotating solution imposed by diffusion still assumes a preminent role. As Grashof numbers increase, the system will reach a critical point in which the instability due to the convective motions assumes a prevaricating character and the system dynamics will evolve to new regimes driven by hydrodynamics, with a route to chaos similar to the transition to turbulence observed in fluids Belk e Volpert, 2004; Ducrot e Volpert, 2005; Gaponenko e Volpert, 2003; Gollub e Benson, 1980; Guzmán e Amon, 1994; McLaughlin e Orszag, 1982; Molenaar, Clercx e Heijst, 2005.

In figure 30 we illustrate the effect induced by convection on the shape of spiral wave concentration: as Grashof number increases, distortion and also breaking of the spiral wave occurs Budroni *et al.*, 2009; Jahnke, Skaggs e Winfree, 1989, resulting in spatio–temporal chaos Biktashev, Holden e Tsyganov, 1998; Pérez-Villar *et al.*, 2002; Ramos, 2001; Sandstede, Scheel e Wulff, 1999.

Although the effects of hydrodynamics in a oscillating RDC system has been extensively studied, a comprehensive understanding on the relative, separate role played by diffusion and convection in terms of stability of periodic solutions is missing. Experimental attempts to shed light on these aspects (see for example Rossi *et al.*, 2005) have pointed out the difficulty to control the species diffusivity without affecting other variables and suggest that a numerical approach is in this context not only convenient but necessary.

In this chapter we give a comparative overview of the effect associated to the main transport phenomena on system dynamic evolution, by extending the exploration of the RDC system 88–94, to a significant domain of the (Gr_i,d_i) parameter space.
To this end we perform a set of numerical simulations of the RDC model, ranging $Gr_i \in [0.00, 12.50]$ and $d_i \in [10^{-7}, 10^{-6}] \times 1.5$, setting, for sake of simplicity, $Gr_1 = Gr_2$ and $d_1 = d_2$. In detail the dynamic evolution of the system is followed by the variation of one parameter, holding the other fixed at a determined value.

In previous studies we interestingly pointed out that local and spatially averaged properties of the oscillating RDC system behave coherently to each other Budroni,

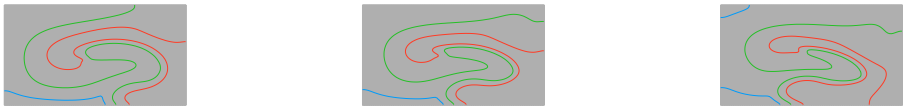

(a) $Gr_i = 2.0$ **(b)** $Gr_i = 4.0$ **(c)** $Gr_i = 6.0$

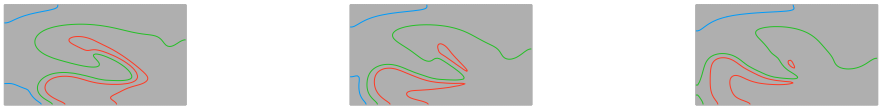

(d) $Gr_i = 9.8$ **(e)** $Gr_i = 9.9$ **(f)** $Gr_i = 10.0$

Figura 30: distortion and breaking of spiral waves induced by convection ($Gr_i > 0$) at $d_i = 6.0 \times 10^{-7}$

Rustici e Tiezzi, 2011. In this way all the information on the system dynamics is preserved if we record the species concentration averaged over the spatial domain $\langle c_i(\hat{x}, \hat{y}; t)\rangle$ as a function of time. As a matter of fact it is what one experimentally does following spectrophotometrically the Belousov–Zhabotinsky reaction in a closed and unstirred reactor. The resulting time series are directly analyzed by means of Fast Fourier Transform (FFTs), in order to detect the emergence of new dynamical regimes as the control parameters are varied. Chaotic series are characterized calculating the Maximal Lyapunov Exponent (MLE) λ_i using the Kantz's algorithm (see appendix V).

0.24 Grashof number as control parameter

We observe that when Gr_i lies in the interval $(0.00 - 9.70)$, intermediate species (and coherently all the system properties) oscillate according to a periodic or biperiodic dynamics for the whole range of d_i examined. To be more precise, the FFT spectra of $\langle c_i(x, y; t)\rangle$ temporal series reveal one distinct main frequency $\omega_1 = 0.394$ ofu (oregonator frequency units) for Gr_i up to 9.00. Along with $\omega_1 = 0.394$ we can recognize a frequency halving $n \times \frac{\omega_1}{2}$ ($n \in \mathbb{N}^+$) as $Gr_i = 9.40$ (figure **??**, appendix **??**). The periodicity of the new solution presents a retard with respect to the convectionless stationary state probably because of the hydrodynamic inertia.

The interesting part of the bifurcation diagram is concentrated in the range $Gr_i \in [9.40, 10.00]$ and $d_i \in [3.0 \times 10^{-7}, 1.5 \times 10^{-6}]$, where the system exhibits transitions to complex oscillations, as illustrated in appendix **??** by the following

- figure **??**,
- figure **??**,
- figure **??**

For instance, if we fix $d_i = 6 \times 10^{-7}$ and increase the hydrodynamic parameter up to the value 9.70, a first supercritical Hopf bifurcation occurs, driving the system from periodic to quasi-periodic dynamics. System oscillations are characterized by the appearance of a new frequency $\omega_2 = 0.536$ ofu in the FFT spectrum, (typical of a toroidal attractor in the phase space), whose ratio to ω_1 is an irrational number (figure **??**).
As the Grashof numbers are further increased up to $Gr_i = 9.80$, the quasiperiodic dynamics is forced to temporal chaos: the system dynamics undergoes to a series of supercritical pitchfork bifurcations, clearly shown in the FFT spectrum (figure **??**) where the main frequency ω_1 and the relative subharmonics $n \times \frac{\omega_1}{2^m}$ $(m, n \in \mathbb{N}^+)$ are present in addition to ω_2. This dynamics is associated with a multi–periodic toroidal-like attractor that eventually collapses into a strange attractor (figure **??**). The route to chaotic oscillations can be schematized as follows: P (periodic) $\rightarrow QP^2$ (quasiperiodic) $\rightarrow mP - QP^2$ (m–period quasiperiodic) $\rightarrow C$ (chaotic).

Typically quasi–periodic forced systems follow a topological transition to chaos (*i*) by a destruction of the torus–2 to simple cycle and than through some standard route Ott, 1993 or (*ii*) through the emergence of an unstable torus–3, which collapses into a fractal, chaotic object: the RTN scenario Rustici *et al.*, 1996. Here the global transition cannot be pertinently classified into a pure RTN scenario since from quasi–periodicity the system undergoes a sequence of period–doubling bifurcations to aperiodicity, combining a pure RTN with a period–doubling path of bifurcations. This singular scenario has been shown for electronic systems (see for example Chan e Tse, 1997), but it is quite rare for chemical oscillators.

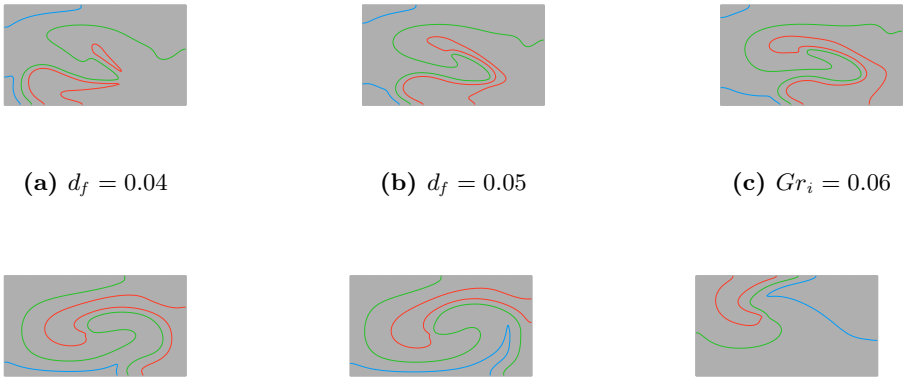

(a) $d_f = 0.04$ **(b)** $d_f = 0.05$ **(c)** $Gr_i = 0.06$

(d) $d_f = 0.07$ **(e)** $Gr_i = 0.08$ **(f)** $d_f = 0.09$

Figura 31: the shape of spiral wave is restored when d_i increases and Gr_i is fixed

0.25 Diffusivity as control parameter

Things drastically change when diffusion coefficient varies: starting from the chaotic state previously found (let say $Gr_i = 9.90$) and keeping Gr_i fixed, an inverse transition is observed as d_i increases from 6×10^{-7} to 1.5×10^{-6}. In particular the system dynamics moves from chaos to periodicity according to a pure RTN scenario Rustici *et al.*, 1999. In appendix **??**, figures **??**, **??** and **??** illustrate the fundamental steps of this second transition, that can be summarized in the following way: C (chaotic) $\rightarrow QP^2$ (quasi–periodic) $\rightarrow BP$ (bi–periodic) $\rightarrow P$ (periodic).

In details, from aperiodicity (figure **??**) at $Gr_i \in [9.90, 10.00]$ and $d_i = 6 \times 10^{-7}$, the system dynamics is switched to a quasiperiodic regime via a supercritical Hopf bifurcation at $d_i = 7.5 \times 10^{-7}$ (figure **??**). As a matter of fact a new frequency ω_3, whose ratio to ω_1 is an irrational number, appears in the FFT spectrum at 0.505 ofu. Main linear combinations of two frequencies are also evidenced in figure **??**, appendix **??**, and listed in table 9. When diffusivity rises up to 9×10^{-7} a periodic (period–2) solution is found, characterized by ω_1 and the harmonics $n \times \frac{\omega_1}{2}$ (figure **??**). For $d_i = 1.35 \times 10^{-6}$ the system finally returns to simple periodic oscillations (figure **??**).

Signal	Linear combination	Frequency (ofu)
ω_1	-	0.394
ω_2	-	0.536
ω_3	-	0.505
α	$\omega_2 - \omega_1$	0.142
β	$2\omega_1 - \omega_2$	0.252
γ	$3\omega_1 - \omega_2$	0.646
δ	$\omega_1 + \omega_2$	0.930
ϵ	$\omega_2 - \omega_1$	0.111
ζ	$2\omega_1 - \omega_2$	0.283
η	$\omega_2 - 0.5\omega_1$	0.308
θ	$2.5\omega_1 - \omega_2$	0.480
ι	$3\omega_1 - \omega_2$	0.677
κ	$\omega_2 + 0.5\omega_1$	0.702
λ	$3.5\omega_1 - \omega_2$	0.874
μ	$\omega_1 + \omega_2$	0.899

Tabella 9: FFT spectra frequencies

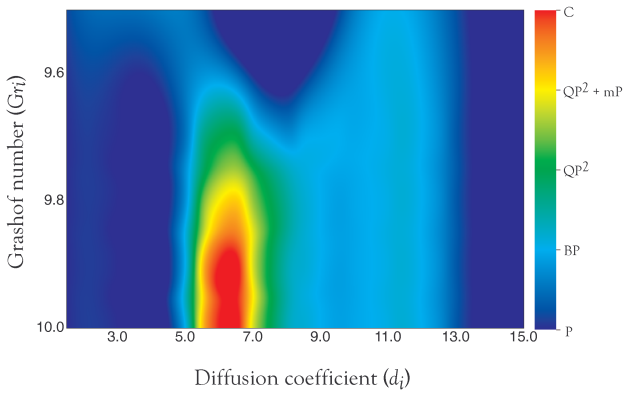

Figura 32: Bifurcation diagram in the $(Gr_i, d_i)-$plane. Transitions are evidenced in blu (P, periodic), cyano (BP, biperiodic), green (QP^2, quasiperiodic), yellow (mP+ QP^2, complex periodicity), red (C, chaos).

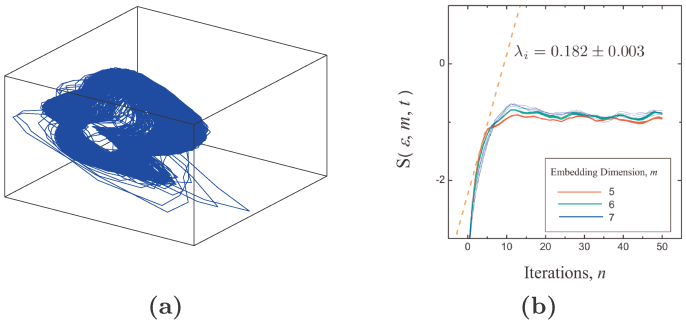

Figura 33: attractor at $Gr_i = 9.9$ (a) and its related Maximal Lyapunov Exponent (b)

0.26 Characterization of chaotic regimes

Figure 32 summarizes the results of our simulations, sketching dynamics transformations of the RDC system in the two–dimensional (Gr_i, d_i) bifurcation diagram Ciotti *et al.*, 2011. It represents the core of table **??** in appendix **??**, where qualitative aspects of system dynamics are listed. Here each color defines a dynamical regime as specified in the figure caption.

The chaotic regime, characterized by an infinite series of frequencies in the amplitude spectrum, emerges in the range $Gr_i \in [9.90, 10.00]$ (figure **??**, appendix **??**).

The chaoticity of the system in this (d_i, Gr_i) domain has been tested by calculating the maximal Lyapunov exponent ($\lambda = 0.182 \pm 0.003$) by means of the Kantz's algorithm (figure 33). A further qualitative feature of chaos is shown in figure 34, where two distinct simulations have been carried out with a difference in the fifth digit in the initial catalyst concentration: sensitivity to initial conditions for a chaotic state is there clearly evidenced.

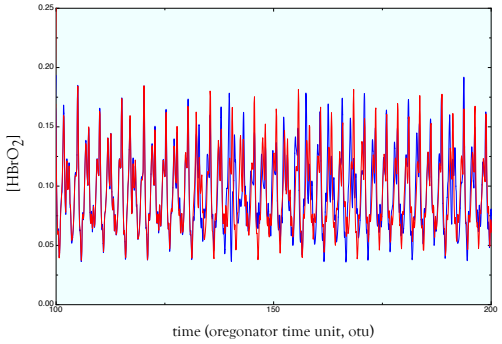

Figura 34: sensitivity to inital conditions for the chaotic state at $Gr_i = 9.9$ when $[Ce^{4+}] = 1.33333$ (blue curve) and 1.33339 (red curve)

0.27 Frequency locking

A circle map is given by iterating the map

$$\theta_{n+1} = \theta_n + \Omega - \frac{K}{2\pi}\sin(2\pi\theta_n) \tag{114}$$

where $0 < \theta < 1$ is the polar angle, K is the coupling strength and Ω the driving phase. For small to intermediate values of K (that is, in the range $0 < K < 1$) and certain values of Ω, the map exhibits a phenomenon called *phase-locking*.

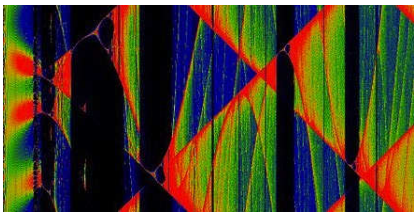

Figura 35: bifurcation diagram for circle maps

In a phase-locked region, the values θ_n advance essentially as a rational multiple of n, although they may do so chaotically on the small scale. The phase-locked regions, or *Arnold tongues*, are illustrated in black in the bifurcation diagram showed in figure 35, for Ω held fixed at 1/3, and K running from 0 to 4π (horizontal axis). ap also exhibits subharmonic routes to chaos, that is, period doubling of the form 3, 6, 12, 24, ...

In the description of both diffusion and convection driven transitions, we intentionally neglect to discuss narrow parameter windows within the quasiperiodic – chaotic regions, where periodicity is found. The original route to chaos evidenced and the occurrence of periodic intervals (figure 36) suggests that, similarly as in circle maps Ott, 1993, there must be some characteristic relationship among critical parameters which determines *frequency-locking* phenomena and deserves more detailed investigation. This singular scenario has been shown for electronic systems (see for example Chan e Tse, 1997) but is quite rare for chemical oscillators.

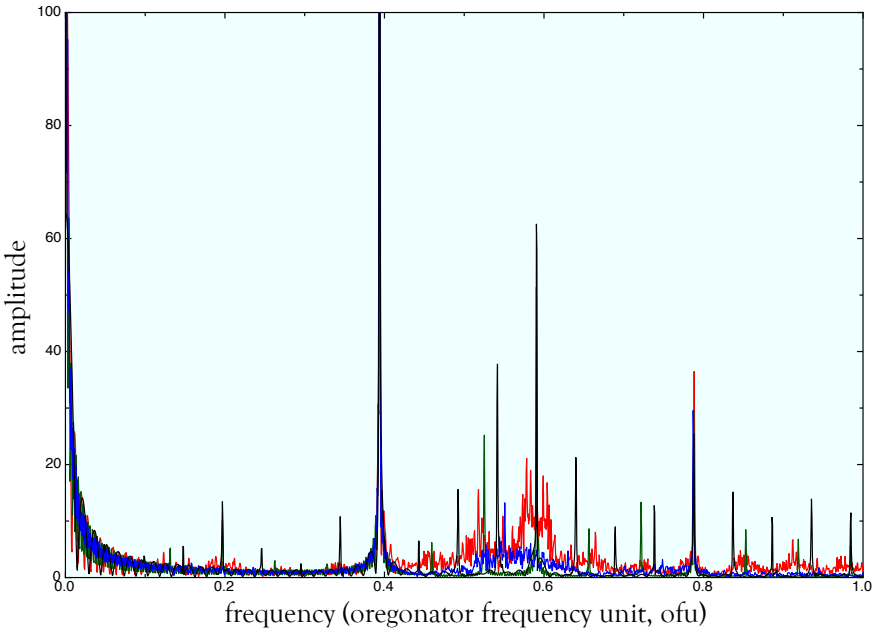

Figura 36: periodic windows within the quasiperiodic – chaotic regions for $d_i = 0.0401$ (black curve) and $d_i = 0.0402$ (green curve) at $Gr_i = 10.0$.

Diffusion coefficients and Molecular dynamics

In the previous chapter, we investigated the system dynamics in a particular range of diffusion coefficients of intermediate species. We pointed out that reaction-diffusion coupling does not occur if we assume a value of diffusion coefficient $D_i = 1.5 \times 10^{-5}\text{cm}^2\text{s}^{-1}$, as indicated in Jahnke, Skaggs e Winfree, 1989; Wu *et al.*, 1995.

In this last chapter we would like to illustrate the results obtained from molecular dynamics simulations in the prediction of a dynamic property such as diffusion coefficient, in order to extend our discussions to the analysis of the RDC model in exam, with particular attention to the experimental results obtained in our research group.

This chapter is structured in the following way: in every section we briefly discuss some basic concepts of molecular dynamics approach and we attach the results obtained in our simulations for Ce^{3+} and $HBrO_2$.[5]

0.28 Molecular Dynamics

Molecular dynamics (MD) simulation is an essential technique to study a variety of molecular properties including molecular diffusion Wang e Hou, 2011. It is useful to study diffusion process not only in atomic details, but also under thermodynamic conditions not easily reachable by experiments.

Concerning our study, we carried out molecular dynamics calculations of the diffusion coefficients of Ce^{3+} and $HBrO_2$. Every set of simulations, at different levels of a potential hypersurface, has been carried out for 216 molecules of water and 1 molecule of the intermediate species in the *microcanonical ensemble*. The temperature fluctuations for every run is shown in figure 37.

For Ce^{3+} we used a force field consisting of a polarizable term, as reported in M. Souaille, Spezia e Cartailler, 2007.

Concerning $HBrO_2$, we used a GAFF potential Wang *et al.*, 2004, whose van der Waals parameters are inherited from traditional Amber force field Cornell *et al.*, 1995

[5] MD simulations have been carried only for Ce^{3+} and not for Ce^{4+}, due to the lack of parameters of force field potential for the last.

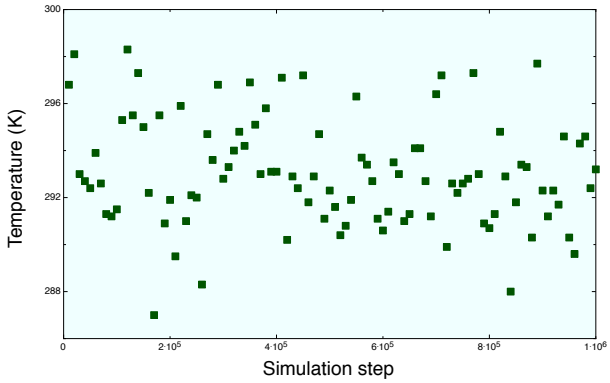

Figura 37: temperature fluctuations in NVE ensemble

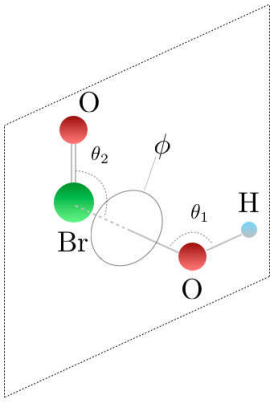

Figura 38: bending and torsional angles in $HBrO_2$

$$E_{pot} = \sum_{bonds} k_r(r - r_{eq})^2 + \sum_{angles} k_\theta(\theta - \theta_{eq})^2 + \sum_{dihedrals} \frac{v_n}{2}[1 + \cos(n\phi - \gamma)] + \sum_{i<j} \left\{ 4\epsilon_{ij} \left[\left(\frac{\sigma_{ij}}{r_{ij}} \right)^{12} - \left(\frac{\sigma_{ij}}{r_{ij}} \right)^{6} \right] + \frac{q_i q_j}{r_{ij}} \right\} \tag{115}$$

where θ and ϕ are defined as in figure 48.

The set of molecular dynamics parameters used in our simulations are summarized in appendix 0.36.5.

0.29 The radial distribution function

The radial distribution function (or RDF) is an example of a pair correlation function, which describes how, on average, the atoms in a system are radially packed around each other. This proves to be a particularly effective way of describing the average structure of disordered molecular systems such as liquids.

The RDF can be deduced also experimentally from x-ray or neutron diffraction studies, thus providing a direct comparison between experiment and simulation. It can also be used in conjunction with the interatomic pair potential function to calculate the internal energy of the system, usually quite accurately. To construct a RDF, we choose an atom in the system and draw around it a series of concentric spheres, set at a small fixed distance $\Delta\mathbf{r}$ apart (see figure 39). At regular intervals a snapshot of the system is taken and the number of atoms found in each shell is counted and stored. At the end of the simulation, the average number of atoms in each shell is calculated. This is then divided by the volume of each shell and the average density of atoms in the system. Mathematically the formula is

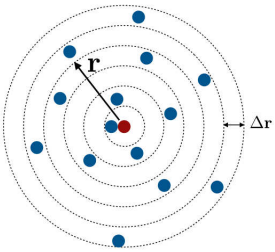

Figura 39: RDF schematic representation

$$g(\mathbf{r}) = \frac{1}{\rho} \frac{n(\mathbf{r})}{4\pi r^2 \Delta\mathbf{r}} \tag{116}$$

where $g(\mathbf{r})$ is the radial distribution function, $n(\mathbf{r})$ is the mean number of atoms in a shell of width $\Delta\mathbf{r}$ at distance $\mathbf{r}$, ρ is the mean atom density. All the atoms in the system can be treated in this way, leading to an improved determination of the RDF as an average over many atoms.

The RDF is usually plotted as a function of the interatomic separation $\mathbf{r}$. A typical RDF plot shows a number of important features. Firstly, at short separations (small $\mathbf{r}$) the RDF is zero. This indicates the effective width of the atoms, since they cannot approach any more closely. Secondly, a number of obvious peaks appear, which indicate that the atoms pack around each other in *shells* of neighbours. The occurrence of peaks at long range indicates a high degree of ordering. Usually,

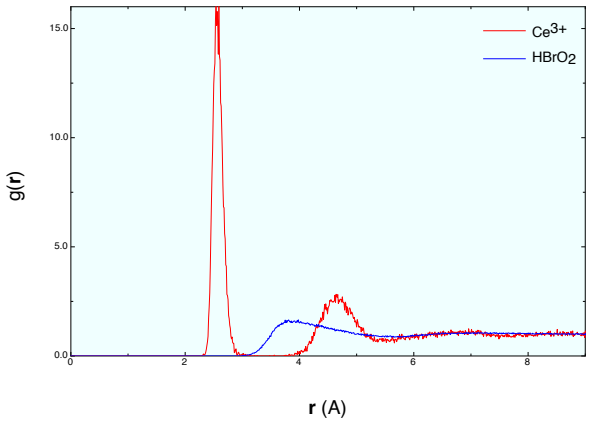

Figura 40: RDF for Ce^{3+} and $HBrO_2$

at high temperature the peaks are broad, indicating thermal motion, while at low temperature they are sharp. They are particularly sharp in crystalline materials, where atoms are strongly confined in their positions. At very long range every RDF tends to a value of 1, which happens because the RDF describes the average density at this range. In figure 40 a comparison plot for RDF of Ce^{3+} and $HBrO_2$ shows an important feature of our chemical system: cerium ions are geometrically well-packed with water molecules in at least two different coordination spheres, as shown by a first sharp peak that decays to zero and a second well-defined peak, whilst bromous acid seems to be quite "hydrophobic", showing a broad band at short distance.

0.30 The mean square displacement

Molecules in liquids and gases do not stay in the same place, but move about constantly. The motion of an individual molecule in a dense fluid does not follow a simple path. As it travels, the molecule is jostled by collisions with other molecules which prevent it from following a straight line. If the path is examined in close detail, it will be seen to be a good approximation to a random walk. Mathematically, a random walk is a series of steps, one after another, where each step is taken in a completely random direction from the one before. This kind of path was analyzed by Albert Einstein in a study of Brownian motion and he showed that the mean square of the distance travelled by particle following a random walk is proportional to the time elapsed. This relationship can be written as

$$\text{MSD} = \left\langle r^2\left(t\right)\right\rangle \quad = \quad 6D_i t + C \tag{117}$$

where $\left\langle r^2\right\rangle$ is the mean square displacement (or distance) and t is time. The symbol $\langle\rangle$ stand for an average over the number N of the particles of the system considered.

$$\text{MSD} = \left\langle r^2\left(t\right)\right\rangle \quad = \quad \frac{1}{N}\sum_{i=1}^{N} {r_i}^2(t) \tag{118}$$

D_i and C are constants. The constant D_i is the most important of these and defines the diffusion rate. It is called the *diffusion coefficient*.

What is the mean square distance and why is it significant? Imagine a single particle undertaking a random walk. For simplicity we assume this is a walk in one dimension. Each consecutive step may be either forward or backward, we cannot predict which, though we can say we are equally likely to step forward as to step back: a drunk man comes to mind! From a given starting position, the distance we are likely to travel can be determined simply by adding together the steps, taking into account the fact that steps backwards subtract from the total, while steps forward add to the total. But since both forward and backward steps are equally probable, we will come to the surprising conclusion that the probable distance travelled sums up to zero. If however, instead of adding the distance of each step, we add the square of the distance, we realize that we will always be adding positive quantities to the total. In this case the sum will be some positive number, which grows larger with every step. This obviously gives a better idea about the distance (squared in this case) that a particle moves. If we assume that each step takes place at regular time intervals, we can easily see how the square distance grows with time. In a molecular system a molecule moves in three dimensions, but the same principle applies. Also, since we have many molecules to consider, we can calculate a square displacement for all of them. The average square distance, taken over all molecules, gives us the mean square displacement. This is what makes the mean square displacement (or MSD for short) significant in science: through its relation to diffusion it is a measurable quantity, one which relates directly to the underlying motion of the molecules.

The linear dependence of the MSD plot is apparent. If the slope of this plot is taken, the diffusion coefficient D_i may be readily obtained from Einstein's equation

$$\frac{\partial \left\langle r^2\left(t\right)\right\rangle}{\partial t} = 6D_i \tag{119}$$

At very short times however, the plot is not linear. This is because that the path a molecule takes will be an approximate straight line until it collides with its neighbour. Only when it starts the collision process its path will resemble a random walk. Until it makes that first collision, we may say it moves with approximately constant velocity, which means the distance it travels is proportional to time, and its MSD is therefore proportional to the time squared. Thus at very short time, the MSD resembles a parabola. This is of course a simplification - the collision between molecules is not like the collision between two pebbles, it is not instantaneous in space or time, but is "spread out" a little in both. This means that the behaviour of the MSD at short time is sometimes more complicated than this MSD plot shows.

The implementation of a fortran 90 algorithm to calculate MSD is reported in appendix 0.36.5. Figure 41 illlustrates the comparison between mean square displacement plots calculated for the intermediate species of Belousov–Zhabotinsky reaction.

0.31 The velocity autocorrelation function

The velocity autocorrelation function (VACF) is a prime example of a time dependent correlation function, and is important because it reveals the underlying na-

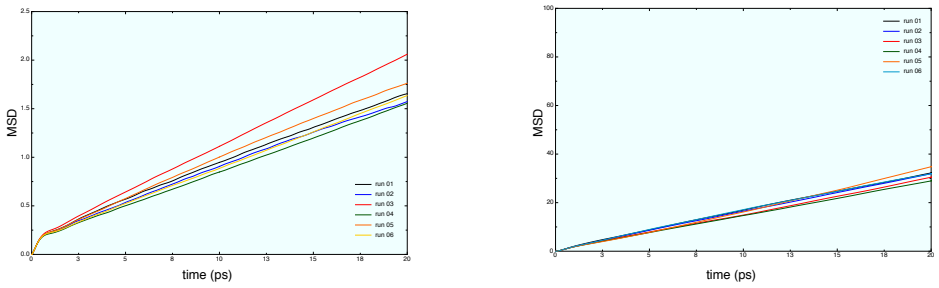

(a) **(b)**

Figura 41: mean square displacement for Ce^{3+} (a) and $HBrO_2$ (b)

ture of the dynamical processes operating in a molecular system. There is a special case of a more general relationship between the VACF and the mean square displacement, and belongs to a class of properties known as the *Green-Kubo* relations, which relate correlation functions to so-called transport coefficients.

We can describe the distance $r(t)$ a molecule moves in time as an integral of its velocity $v(t)$

$$r(t) = \int_0^t v(u)du \tag{120}$$

The square of this distance is thus

$$r^2(t) = \int_0^t \int_0^t v(u) \cdot v(u')dudu' \tag{121}$$

defining $u' = u + s$ and integrating over u, results in the following form where the ensemble average has also been taken

$$\left\langle r^2(t) \right\rangle = 2 \int_0^t (t - s) \left\langle v(0) \cdot v(s) \right\rangle ds \tag{122}$$

In this equation $\langle v(0) \cdot v(s) \rangle$ is the velocity autocorrelation function VACF, so the relationship between MSD and VACF is now apparent. This can also be written as

$$\left\langle r^2(t) \right\rangle = 2t \int_0^t \left\langle v(0) \cdot v(s) \right\rangle ds - 2 \int_0^t s \left\langle v(0) \cdot v(s) \right\rangle ds \tag{123}$$

What this integral shows is that the MSD is comprised of two parts. The first term on the right includes the time t explicitly and if we assume that when t is large, the VACF decays to zero (as it usually does) then the integral here will have a fixed value. Since the second term also integrates to a fixed value for large t, we can see that this equation is equivalent to Einstein's, provided we assume that

$$3D_i = \int_0^t \left\langle v(0) \cdot v(s) \right\rangle ds \tag{124}$$

and

$$C = -2 \int_0^t s \left\langle v(0) \cdot v(s) \right\rangle ds \tag{125}$$

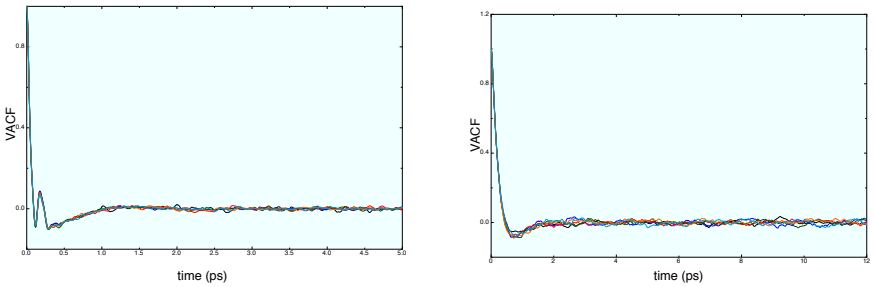

(a) **(b)**

Figura 42: velocity autocorrelation function for Ce^{3+} (a) and $HBrO_2$ (b)

when t is large. This is a very important result, as it shows how the diffusion coefficient can be obtained from both the VACF and the MSD.

Consider a single atom at time zero. At that instant the atom i will have a specific velocity v_i. If the atoms in the system did not interact with each other, the Newton's Laws of motion tell us that the atom would retain this velocity for all time. This of course means that all our points of VACF would have the same value, and if all the atoms behaved like this, the plot would be a horizontal line. It follows that a VACF plot that is almost horizontal, implies very weak forces are acting in the system.

On the other hand, what happens to the velocity if the forces are small but not negligible? Then we would expect both its magnitude and direction to change gradually under the influence of these weak forces. In this case we expect the scalar product $\langle v(0) \cdot v(s) \rangle$ to decrease on average, as the velocity is changed. In such a system, the VACF plot is a simple exponential decay, revealing the presence of weak forces slowly destroying the velocity correlation. Such a result is typical of the molecules in a gas.

What happens when the interatomic forces are strong? Strong forces are most evident in high density systems, such as solids and liquids, where atoms are packed closely together. In these circumstances the atoms tend to seek out locations where there is a near balance between repulsive forces and attractive forces, i.e., the most energetically stable positions. In solids these locations are extremely stable, and the atoms cannot escape easily from their positions. Their motion is therefore an oscillation: the atom vibrate backwards and forwards, reversing their velocity at the end of each oscillation. If we now calculate the VACF, we will obtain a function that oscillates strongly from positive to negative values and back again. The oscillations will not be of equal magnitude however, but will decay in time, because there are still perturbative forces acting on the atoms to disrupt the perfection of their oscillatory motion. So what we see is a function resembling a damped harmonic motion. Liquids behave similarly to solids, but now the atoms do not have fixed regular positions. A diffusive motion is present to destroy rapidly any oscillatory motion. The VACF therefore may perhaps show one very damped oscillation (a function with only one minimum) before decaying to zero. In simple terms this may be considered a collision between two atoms before they rebound from one another

and diffuse away. Figure 42 illustrate the different VACF calculated from MD simulations for both Ce^{3+} and $HBrO_2$. For cerium atoms we can observe the so-called *back scattering* configuration, that suggests a well-packed coordination with water molecules.

0.32 Prediction of diffusion coefficients

Table 10 summarizes the diffusion coefficients estimated by MSD and VAC calculations for intermediate Ce^{3+} and $HBrO_2$. We can immediately see that Ce^{3+} ions diffuse about 20 times slower than $HBrO_2$. This behavior can be justified considering well-packed water-cerium ions and slightly hydrophobic bromous acid molecules, as it results from RDF and VAC plots (figures 40 and 42) . The mean value between VAC and MSD estimations corresponds to $1.38 \times 10^{-6}\mathrm{cm}^2\mathrm{s}^{-1}$ ($d_f = 0.09$). This value is a bifurcation point *periodic*$\leftrightarrow$*biperiodic* in our numerical study of stability, as results from the second RTN scenario evidenced, with diffusivity as control parameter and Grashof number fixed.

The range of D_i exhamined in our nonlinear dynamical simulations finds a counterpart in molecular dynamics calculations. The lower value of diffusion rate for Ce^{3+} ions seems therefore to control the entity of RDC coupling and can be considered as the main responsible for the route to chaos observed when d_i varies.

	VACF	MSD
Ce^{3+}	0.1450 ± 0.0265	0.1310 ± 0.0210
$HBrO_2$	2.5827 ± 0.4795	2.6023 ± 0.4255

Tabella 10: average diffusion coefficients ($10^{-5}\mathrm{cm}^2\mathrm{s}^{-1}$)

From an experimental point of view, we can hence imagine that starting from a value of cerium diffusivity of $< 1.38 \times 10^{-6}\mathrm{cm}^2\mathrm{s}^{-1}$, the system can be switched through different dynamical scenarios by the variation of temperature Masia *et al.*, 2001, concentration of reactants Biosa *et al.*, 2005, medium viscosity Rossi *et al.*, 2005. At this point, it becomes important to understand how the system dynamics is affected by different diffusion coefficients and Grashof numbers: this will constitute the natural extension of this work.

Parte IV

Conclusions

Future perspectives

The study carried out for my doctoral dissertation has reached some interesting goals and evidenced

- a competition between diffusion and convection for the dynamical stability of a RDC system;
- a new route to spatio-temporal chaos in a chemical nonlinear system;
- a first estimation of diffusion coefficients of intermediate species of Belousov–Zhabotinsky reaction by molecular dynamics simulations.

All the theoric results obtained have an important experimental interpretation within the research in nonlinear chemistry carried out by our group.

The discussed pathway to chaos *via* a combined Hopf–Pitchfork bifurcation, observed from a numerical point of view when Gr_i varies and D_i is fixed, constitutes a new achievement and deserves deeper and formal studies, as it is quite unusual for chemical systems. Also some small windows of periodicity within quasiperiodic–chaotic regions, which are fairly reminiscent of frequency–locking phenomena, should be investigated in more detail in order to evaluate whether an RDC system can be reasonably reduced to a particular case of a circle map.

The values of diffusion coefficients for intermediate species Ce^{3+} and $HBrO_2$ in Belousov–Zhabotinsky reaction, that have been estimated by MD simulations using VAC and MSD calculations, indicate that the lower diffusion rate of Ce^{3+} controls, in fact, the RDC coupling. These values should be now used for a comprehensive study of our proposed RDC model, performing new simulations in which both intermediate species have different diffusivity and also different Grashof numbers.

Parte V

Appendix

Nonlinear Analysis

0.33 Stability

Consider a system – dissipative or conservative – evolving according to equation 123. We suppose that the system has reached, after a certain lapse of time, a 'reference' state $\mathbf{X}_s$ on an invariant manifold. In principle, the system will remain therein for ever and will undergo a dynamic behavior dictated by the particular type of manifold considered.

In actuality, a real-world system never stays in a single state as time varies. As a result the instantaneous state $\mathbf{X}(t)$ will continuously deviate from $\mathbf{X}_s$ by an amount $\mathbf{x}(t)$, referred to as the perturbation

$$\mathbf{X}(t) = \mathbf{X}_s + \mathbf{x}(t) \qquad (126)$$

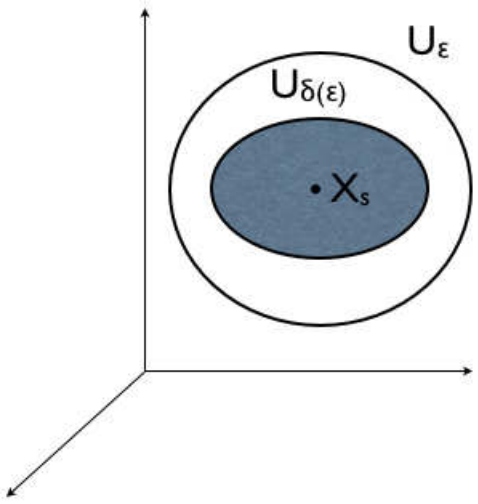

Figura 43: geometric view of stability

$\mathbf{X}_s$ is stable in the sense of Lyapunov if, for any given neighborhood U_ϵ of $\mathbf{X}_s$ there esists a certain neighborhood $U_{\delta(\epsilon)}$ such that any trajectory emanating from the interior of $U_{\delta(\epsilon)}$ never leaves U_ϵ. $\mathbf{X}_s$ is unstable if no such neighborhood $U_{\delta(\epsilon)}$ can be found. $\mathbf{X}_s$ is asymptotically stable if it is stable and if, in addition, any trajectory emanating from the interior of $U_{\delta(\epsilon)}$ tends to $\mathbf{X}_s$ as $t \to \infty$. In other words, there is Lyapunov stability if, for any $\epsilon > 0$, there exists a $\delta(\epsilon) > 0$ such that for any $\mathbf{X}(0)$ with $|\mathbf{X}(0) - \mathbf{X}_s| < \delta$, one has $|\mathbf{X}(t) - \mathbf{X}_s| < \epsilon$ for all $t \geq 0$. Asymptotic stability if, in addition, $|\mathbf{X}(t) - \mathbf{X}_s| \to 0$ as $t \to \infty$. In this latter case $\mathbf{X}_s$ will be an attractor of the dynamic system. Clearly then, asymptotic stability can hold only in dissipative systems.

0.33.1 The principle of linearized stability

The starting point is to substitute equation 126 into 123. Using the fact that the reference state $\mathbf{X}_s$ is itself a particular solution of these latter equations one obtains

$$\frac{d\mathbf{x}}{dt} = \mathbf{F}(\mathbf{X}_s + \mathbf{x}, \mu) - \mathbf{F}(\mathbf{X}_s, \mu) \qquad (127)$$

We assume that $\mathbf{F}$ can be Taylor expanded in formal power series of $\mathbf{x}$ around $\mathbf{X}_s$.

$$\mathbf{F}(\mathbf{X}_s + \mathbf{x}, \mu) = \mathbf{F}(\mathbf{X}_s, \mu) + \left(\frac{\partial \mathbf{F}}{\mathbf{X}}\right)_{\mathbf{X}_s} \cdot \mathbf{x} + \frac{1}{2}\left(\frac{\partial^2 \mathbf{F}}{\partial \mathbf{X} \partial \mathbf{X}}\right)_{\mathbf{X}_s} \cdot \mathbf{x}\mathbf{x} + \dots \tag{128}$$

Substituting equation 128 into 127

$$\frac{d\mathbf{x}}{dt} = \mathcal{L}(\mu) \cdot \mathbf{x} + \mathbf{h}(\mathbf{x}, \mu) \tag{129}$$

where we introduce the short hand notation

$$\mathcal{L}(\lambda) = \left(\frac{\partial \mathbf{F}}{\partial \mathbf{X}}\right)_{\mathbf{X}_s} \mathbf{h}(\mathbf{x}, \mu) = \frac{1}{2}\left(\frac{\partial^2 \mathbf{F}}{\partial \mathbf{X} \partial \mathbf{X}}\right)_{\mathbf{X}_s} \cdot \mathbf{x}\mathbf{x} + \dots \tag{130}$$

The linear operator $\mathcal{L}(\mu)$ is simply the Jacobian matrix of $\mathbf{F}$ evaluated at the reference state, whereas $\mathbf{h}(\mathbf{x}, \mu)$ contains contributions that are nonlinear in $\mathbf{x}$. A useful example is illustrated in appendix V.
Comparing the equations 130 and 123 we can see that the former is an equivalent version of the latter in which the origin of coordinates in phase space has been placed on $\mathbf{X}_s$. In dynamic systems involving a finite number of degrees of freedom, $\mathbf{h}(\mathbf{x}, \mu)$ is a vector in phase space, whereas $\mathcal{L}(\mu)$ is a $n \times n$ matrix whose elements are given by $\mathcal{L}_{ij} = (\partial \mathbf{F}_i / \partial X_j)_{X_{js}}$, $(i, j = 1, \dots, n)$. However, equation 130 still constitutes a highly nonlinear problem which, as a rule, is as intractable as the original problem (123).
At this point, a most important result can be invoked to enable further progress.

Theorem 1. *If the trivial solution $\mathbf{x} = 0$ of the linearized problem (131) is asymptotically stable, then $\mathbf{x} = 0$ (or equivalently $\mathbf{X} = \mathbf{X}_s$) is an asymptotically stable solution of the nonlinear problem (130 or 123). If the trivial solution $\mathbf{x} = 0$ of the linearized problem is unstable, then $\mathbf{x} = 0$ (or equivalently $\mathbf{X} = \mathbf{X}_s$) is an unstable solution of the nonlinear problem.*

This theorem, also known as the **principle of linearized stability**, compares the stability properties of the following two problems

- the original, fully nonlinear problem (130);
- the 'auxiliary' linearized problem, in which high order terms are omitted

$$\frac{d\mathbf{x}}{dt} = \mathcal{L}(\mu) \cdot \mathbf{x} \tag{131}$$

0.33.2 Linear stability analysis of fixed points

The objective is to set up quantitative criteria of stability of the fixed points of a dynamic system. This will be possible thanks to the principle of linearized stability which reduces stability to a linear problem (equation 131). This set of ordinary differential equations admits solutions that depend on time exponentially

$$\mathbf{x} = \mathbf{u} e^{\omega t} \tag{132}$$

Substituting into 131

$$\frac{d\mathbf{u}e^{\omega t}}{dt} = \mathcal{L}(\mu)\mathbf{u}e^{\omega t} \tag{133}$$

we have that $\mathbf{u}$ and the characteristic exponent ω must satisfy the relations

$$\mathcal{L}(\mu) \cdot \mathbf{u} = \omega\mathbf{u} \tag{134}$$

or, in more explicit form

$$\sum_j \mathcal{L}_{ij}(\mu)u_j = \omega u_i \tag{135}$$

In other words $\mathbf{u}$ and ω are, respectively, eigenvectors and eigenvalues of $\mathcal{L}(\mu)$ and stability is thus reduced to an eigenvalue problem. An important point is that independently of the properties of $\mathbf{u}$, which takes into account the structure of $\mathbf{x}$ as a vector in phase space, the knowledge of eigenvalue ω provides a full solution of the problem of stability. Indeed, separating ω into real and imaginary part

$$|\mathbf{x}| \approx e^{(Re\omega)t}e^{i(Im\omega)t} \tag{136}$$

it follows that

- if $Re\omega < 0$, $|\mathbf{x}|$ is exponentially decreasing and hence the reference state $\mathbf{x} = 0$ (or $\mathbf{X} = \mathbf{X}_s$) is *asymptotically stable*;
- if $Re\omega > 0$, the perturbation grows exponentially and hence the reference state is *unstable*.

These two regimes, for which the principle of linearized stability applies, are separated by the regime where $Re\omega = 0$. This borderline state – between asymptotic stability and instability – is known as *marginal stability*.

Notice that the occurrence of instability and marginal stability is compatible with both conservative and dissipative systems. In contrast, asymptotic stability implies by necessity a contraction of phase space volumes and can therefore occur only in dissipative systems. The eigenvalue problem (134) allows to better understand the importance of the control parameters μ. Indeed, a variation of μ induces a variation of $\mathcal{L}$ and, through it, of the eigenvalue ω. Two typical possibilities are depicted by curves (a) and (b) of figure 44. In (a), ω crosses the μ-axis with a positive slope. This will be reflected by the fact that as μ increases, the system will switch from asymptotic stability to instability. As the reference fixed point will no longer

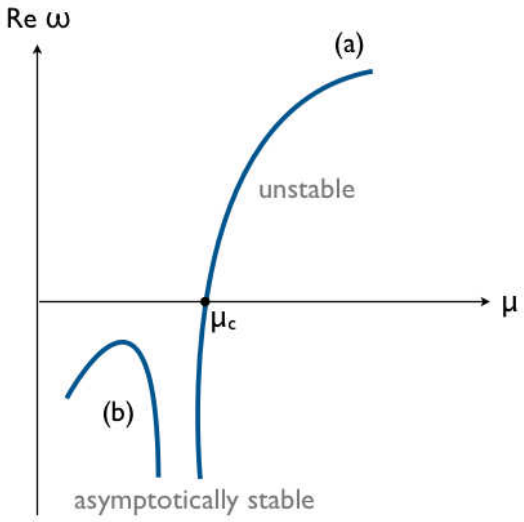

Figura 44: real part of eigenvalue ω versus μ

be a physically legitimate solution for
$\mu > \mu_c$, a qualitative change of behavior is to be expected when μ_c is crossed. For this reason we shall refer to λ_c as the *critical value* of the control parameter. In constast, in (b) the real part of eigenvalue ω remains negative for all values of μ: the fixed point is always asymptotically stable and no qualitatively new regime is expected to arise spontaneously from the action of perturbations. It is clear by now that the central problem of stability theory is the determination of eigenvalue ω of the operator $\mathcal{L}(\mu)$. An explicit calculation can be carried out from equation 135

$$\begin{array}{ccccccccc} l_{11}u_1 & + & l_{12}u_2 & + & \dots & + & l_{1n}u_n & = & \omega u_1 \\ l_{21}u_1 & + & l_{22}u_2 & + & \dots & + & l_{2n}u_n & = & \omega u_2 \\ \vdots & & \vdots & & \ddots & & \vdots & & \vdots \\ l_{n1}u_1 & + & l_{n2}u_2 & + & \dots & + & l_{nn}u_n & = & \omega u_n \end{array} \tag{137}$$

where a generic row has the following form

$$\sum_{j=1}^{n} \mathcal{L}_{ij}(\mu)u_j = \omega u_i \tag{138}$$

which we write in the more suggestive form

$$\sum_{j=1}^{n} (\mathcal{L}_{ij}(\mu) - \omega\delta_{ij}^{kr})u_j = 0, \qquad i = 1, \dots, n \tag{139}$$

This set of homogeneous algebraic equations for u_j admits a nontrivial solution provided that the determinant of the matrix of coefficients of u_j vanishes. This gives rise to the *characteristic equation*

$$det|(\mathcal{L}_{ij}(\mu) - \omega_m(\mu)\delta_{ij}^{kr})| = 0 \tag{140}$$

where we have introduced the index m to account for the fact that equation 140, which is an algebraic equation for ω_m, will in general admits several solutions. Unless the matrix $\mathcal{L}(\mu)$ has some remarkable symmetries built in, the eigenvalues ω_m will be distinct.

0.34 Bifurcation analysis

The linear stability analysis is a powerful instrument to depict the qualitative behavior of a dynamic system around a critical value of the control parameter μ_c, known as a *bifurcation point*. We have already shown how it is possible to obtain useful informations from a bifurcation diagram (figure 41), in which a variable of the system (the angle θ) is plotted against a control parameter (the angular velocity ω). However, as soon as one enters the domain of instability, the linearized equations become inadequate, as they predict runaway to infinity. In order to investigate the

existence of new physically acceptable solutions which emerge beyond the threshold of instability, the full nonlinear equations will have to be analyzed.
The starting point is given by equations

$$\frac{d\mathbf{x}}{dt} = \mathcal{L}(\mu) \cdot \mathbf{x} + \mathbf{h}(\mathbf{x}, \mu) \tag{141}$$

We suppose that linear stability analysis performed on these equations has established the existence of a critical value μ_c such that the linearized operator $\mathcal{L}(\mu_c)$ admits an eigenvalue with vanishing real part, $Re\omega_c = Re\omega(\mu_c) = 0$. The linearized version of 141

$$\frac{d\mathbf{x}}{dt} = \mathcal{L}(\mu) \cdot \mathbf{x} \tag{142}$$

then admits at $\mu = \mu_c$ a solution of the form

$$\mathbf{x} = \mathbf{u}e^{i(Im\omega_c)t} = \mathbf{u}e^{i\Omega_c t} \tag{143}$$

Substituting into 142 and setting $mu = \mu_c$,

$$[i\Omega_c \mathbb{I} - \mathcal{L}(\mu_c)] \cdot \mathbf{u} = 0 \tag{144}$$

where $\mathbb{I}$ is the identity matrix. In other words, the operator

$$\mathbf{J}_c = i\Omega_c \mathbb{I} - \mathcal{L}(\mu_c) \tag{145}$$

admits at least one eigenvector $\mathbf{u}$ corresponding to a zero eigenvalue. We also express this property by the statement that $\mathbf{J}_c$ admits a *nontrivial null space*. The question is now what is the behavior of solutions of the full nonlinear problem (141) for values of the control parameter μ in a certain neighborhood of μ_c. The following two theorems give a surprisingly comprehensive answer.

Theorem 2. *If $\mathbf{x} = 0$ remains a solution of 141 in a neighborhood of μ_c, ω_c is a simple eigenvalue that is a simple root of the characteristic equation, then $\mu = \mu_c$ is a bifurcation point, in the sense that there is at least one new branch of solutions outgoing from $(\mathbf{x} = 0, \mu_c)$. This branch either extends to infinity or meets another bifurcation point.*

Theorem 3. *If ω_c is a simple eigenvalue and the additional transversality condition is satisfied,*

$$\left[\frac{d}{d\lambda} Re\omega(\mu)\right]_{\mu=\mu_c} \neq 0 \tag{146}$$

guaranteeing that the $Re\omega$ versus μ curve in figure 44 crosses the μ-axis at $\mu = \mu_c$, then:

- *the bifurcating solutions will be stationary if $\Omega_c = 0$ in equation 144;*
- *the bifurcating solutions will be time-periodic if $\Omega_c \neq 0$ in equation 144 (Hopf bifurcation).*

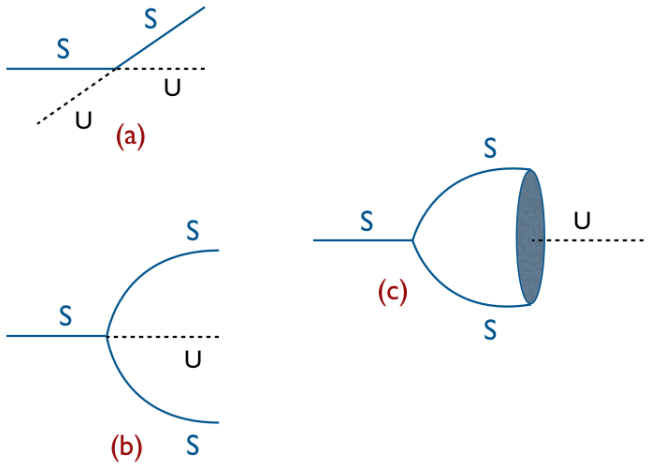

Figura 45: (a) transcritical; (b) pitchfork; (c) Hopf bifurcation

In both of the above cases *supercritical* branches (bifurcating in the region of μ-values for which the reference state has lost its stability) are stable and *subcritical* ones (bifurcating in the region of μ-values for which the reference state is stable) are unstable, provided that the remaining eigenvalues of $\mathcal{L}(\mu_c)$ have negative real parts. Figure 45 summarizes the various possibilities: full and dotted lines represent, respectively, asymptotically stable (S) and unstable (U) branches of solutions. In curves (a) and (b) the amplitude of the solution is plotted versus the control parameter; in curve (c) the continuous family of solutions corresponding to the different values of the phase of the oscillatory motion is schematically depicted.

0.35 Lyapunov exponents

The Lyapunov exponent λ_i of a dynamical system is a quantity that characterizes the rate of separation of infinitesimally close trajectories (figure 46).

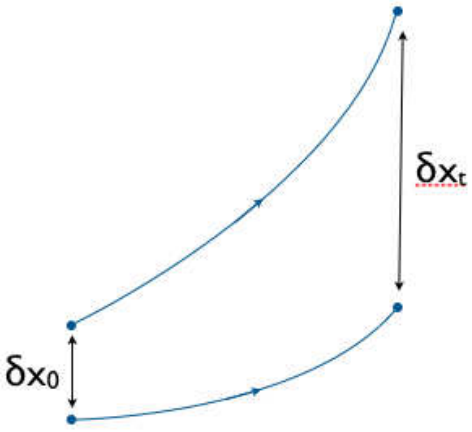

Figura 46: Lyapunov exponents

Quantitatively, two trajectories in phase space with initial separation vector $\delta \mathbf{x}_0$ diverge according to

$$|\delta \mathbf{x}_t| \approx e^{\lambda_i t} |\delta \mathbf{x}_0| \qquad (147)$$

The rate of separation can be different for different orientations of initial separation vector . Thus, there is a spectrum of Lyapunov exponents λ_i, equal in number to the dimensionality of the phase space Γ. It is common to refer to the largest one as the Maximal Lyapunov exponent (MLE), because it determines a notion of predictability for a dynamical system

$$MLE = \lim_{t\to\infty} \frac{1}{t} \ln \frac{|\delta \mathbf{x}_t|}{|\delta \mathbf{x}_0|} \tag{148}$$

A positive MLE is usually taken as an indication that the system is chaotic (provided some other conditions are met, e.g., phase space compactness, sensitivity to initial conditions, etc.).

The maximal Lyapunov exponent has been calculed using the Kantz algorithm from TISEAN package *TISEAN software package*; Hegger, Kantz e Schreiber, 1999. The algorithm looks for exponential perturbation growth by implementing the formula

$$S(\epsilon, m, t) = \left\langle \ln(\frac{1}{U_n} \sum_{s_{n'} \in U_n} |s_{n+t} - s_{n'+t}|) \right\rangle_n \tag{149}$$

where $s_{n'}$ represents a return point in the phase space close to the point s_n visited previously by the system; m is the embedding dimension and U_n the neighborhood with diameter ϵ. The maximal Lyapunov exponent λ is given by the slope of the pencil derived by $S(\epsilon, m, t)$ for different m, where it exhibits a linear increase, identical for each m.

0.36 Period doubling scenario

Feigenbaum, Coullet and Tresser discovered this route to chaos: the resulting dynamics is the consequence of subsequent period-doubling bifurcations. This behavior can be easily followed by an FFT amplitude spectrum, where a signal doubling is produced when the system becomes unstable and two new steady states appear Feigenbaum, 1979. In 1976 the biologist Robert May presented the *logistic map* as a plausible population model with a period-doubling cascade of bifurcations and chaotic trajectories

$$x_{n+1} = r x_n (1 - x_n) \tag{150}$$

where x_n is a number between zero and one, and represents the ratio of existing population to the maximum possible population at year n, r is a positive number and represents a combined rate for reproduction and starvation.

Figure 47 shows the attractor of the logistic map (150) as a function of the parameter r, for $2.4 < r < 4.0$. We can observe that for small r, the attractor is always periodic and has period 2^n, with n increasing as r increases. Beyond some critical value $r = r_c$, with $r_c \approx 3.57$, the attractor may be more complicated and it seems to be contained in 2^n bands that merge as r increases.

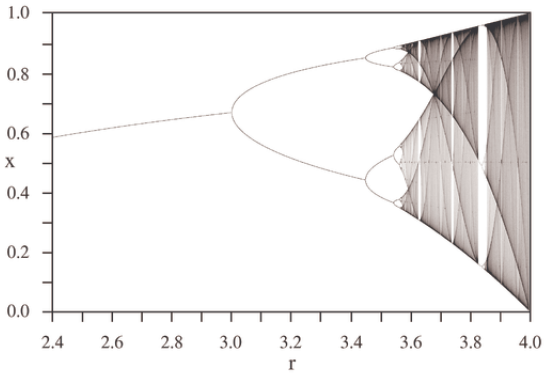

Figura 47: logistic map attractor

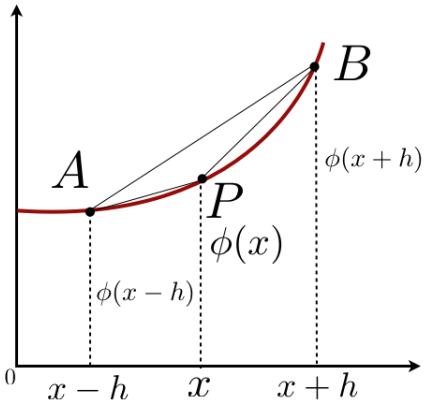

Figura 48: finite difference method

Numerical methods

0.36.1 Finite difference method

Assuming the function $\varphi(x)$, whose derivatives are to be approximated, is properly-behaved, by Taylor's theorem we have

$$\varphi(x+h) = \varphi(x) + h\varphi^{'}(x) + 1/2h^2\varphi^{''}(x) + 1/6h^3h\varphi^{'''}(x) + \dots \tag{151}$$

$$\varphi(x-h) = \varphi(x) - h\varphi^{'}(x) + 1/2h^2\varphi^{''}(x) - 1/6h^3h\varphi^{'''}(x) + \dots \tag{152}$$

and adding the two equations

$$\varphi(x+h) + \varphi(x-h) = 2\varphi(x) + h^2\varphi^{''}(x) + o(h^4) \tag{153}$$

If we neglect orders greater than 2, we also have

$$\varphi^{''}(x) \approx \frac{1}{h^2}[\varphi(x+h) - 2\varphi(x) + \varphi(x-h)] \tag{154}$$

Subtracting 152 from 151, we obtain

$$\varphi^{'}(x) \approx \frac{1}{2h}[\varphi(x+h) - \varphi(x-h)] \tag{155}$$

Equation 155 approximates the slope of tangent to the curve with the slope of the chord joining the points $\varphi(x-h)$ and $\varphi(x+h)$ (figure 48) and is said *central*

difference approximation. The slope of the tangent can be also approximated by a *forward difference*, i.e., the slope of the chord joining the points $\varphi(x)$ and $\varphi(x+h)$

$$\varphi'(x) \approx \frac{1}{h}[\varphi(x+h) - \varphi(x)] \tag{156}$$

or by a *backward difference*, between the points $\varphi(x-h)$ and $\varphi(x)$

$$\varphi'(x) \approx \frac{1}{h}[\varphi(x) - \varphi(x-h)] \tag{157}$$

Both equation 156 and 157 can be obtained from 151 and 152 ignoring derivatives beyond the second order: this methods imply then a first order error.

0.36.2 Notation for multiple variables

Let φ be a function of independent variables x and t. We divide the $x-t$ plane in a grid of regular rectangles of sides $\delta x = h$ and $\delta y = k$. The coordinates (x,t) of a point or *node* P will be $x = ih$ and $t = jk$, with i, j integers. The value of φ at point P is then $\varphi_P = \varphi(ih, jk) = \varphi_{i,j}$. From equation 154 we have

$$\left(\frac{\partial^2\varphi}{\partial x^2}\right)_{i,j} \approx \frac{\varphi_{i+1,j} - 2\varphi_{i,j} + \varphi_{i-1,j}}{h^2} \tag{158}$$

Analogically for the t variable,

$$\left(\frac{\partial^2\varphi}{\partial t^2}\right)_{i,j} \approx \frac{\varphi_{i+1,j} - 2\varphi_{i,j} + \varphi_{i-1,j}}{k^2} \tag{159}$$

with errors $O(h^2)$ and $O(k^2)$, respectively. Using this notation, the forward difference approximation for $\partial\varphi/\partial t$ at point P is

$$\left(\frac{\partial\varphi}{\partial t}\right)_{i,j} \approx \frac{\varphi_{i,j+1} - \varphi_{i,j}}{k} \tag{160}$$

with a $O(k)$ error.

0.36.3 Explicit methods

Using a forward difference at time t_j and a second-order central difference for the space derivative at position x_i (according to equations 160 and 158), an explicit solution for the parabolic partial differential equation 95 is given by the recurrence equation

$$\frac{\varphi_{i,j+1} - \varphi_{i,j}}{k} = \frac{\varphi_{i+1,j} - 2\varphi_{i,j} + \varphi_{i-1,j}}{h^2} \tag{161}$$

Therefore we can obtain a formula for the unknown quantity $\varphi_{i,j+1}$ from the value of the function at the time j

$$\varphi_{i,j+1} = \varphi_{i,j} + r(\varphi_{i+1,j} - 2\varphi_{i,j} + \varphi_{i-1,j}) \tag{162}$$

where $r = k/h^2$. So, with this recurrence relation, and knowing the values at time j, one can obtain the corresponding values at time $j+1$. The values $\varphi_{0,j}$ and $\varphi_{i,j}$ must be replaced by the boundary conditions. This explicit method is known to be numerically stable and convergent whenever $r \leq 1/2$. The numerical errors are proportional to the time step and the square of the space step $\Delta\varphi = O(k) + O(h^2)$. This method is said *explicit* because allows the calculation of an unknown quantity in function of known values.

0.36.4 Implicit methods

If we use the backward difference at time t_{j+1} and a second-order central difference for the space derivative at position x_i we get the recurrence equation

$$\frac{\varphi_{i,j+1} - \varphi_{i,j}}{k} = \frac{\varphi_{i+1,j+1} - 2\varphi_{i,j+1} + \varphi_{i-1,j+1}}{h^2} \tag{163}$$

We can obtain $\varphi_{i,j+1}$ from solving a system of linear equations

$$(1 + 2r)\varphi_{i,j+1} - r\varphi_{i-1,j+1} - r\varphi_{i+1,j+1} = \varphi_{i,j} \tag{164}$$

The scheme is always numerically stable and convergent but usually more numerically intensive than the explicit method as it requires solving a system of numerical equations on each time step. The errors are linear over the time step and quadratic over the space step.

0.36.5 The Crank-Nicolson method

If we use the central difference at time $t_{j+1/2}$ and a second-order central difference for the space derivative at position x_i we get the recurrence equation

$$\begin{aligned}\frac{\varphi_{i,j+1} - \varphi_{i,j}}{k} =& \frac{1}{2}\Big(\frac{\varphi_{i+1,j+1} - 2\varphi_{i,j+1} + \varphi_{i-1,j+1}}{h^2} \\ &+ \frac{\varphi_{i+1,j} - 2\varphi_{i,j} + \varphi_{i-1,j}}{h^2}\Big)\end{aligned} \tag{165}$$

This formula is known as the *Crank–Nicolson method*. We can obtain $\varphi_{i,j+1}$ from solving a system of linear equations

$$\begin{aligned}&(2 + 2r)\varphi_{i,j+1} - r\varphi_{i-1,j+1} - r\varphi_{i+1,j+1} = \\ &(2 - 2r)\varphi_{i,j} + r\varphi_{i-1,j} - r\varphi_{i+1,j}\end{aligned} \tag{166}$$

The scheme is always numerically stable and convergent but usually more numerically intensive as it requires solving a system of numerical equations on each time step. The errors are quadratic over the time step and formally are of the fourth degree regarding the space step, $\Delta\varphi = O(k^2) + O(h^4)$. However, near the boundaries, the error is often $O(h^2)$. Usually the Crank–Nicolson scheme is the most accurate scheme for small time steps. The explicit scheme is the least accurate and can be unstable, but is also the easiest to implement and the least numerically intensive. The implicit scheme works the best for large time steps.

The Fortran 90 Code

0.37 The concentration functions

In this section we describe how the `oregon.f90` code implements the ADI method applied on concentration functions, as expressed by equation 88 and its kinetic relative 39.

```
DO j=2,m-1
**** DIRICHLET BOUNDARY CONDITIONS ****
Aa(1,j)=ONE
Bb(1,j)=ZERO
**** FROM TRIDIAGONAL TO BIDIAGONAL MATRIX ****
DO i=2,m-1
A(i,j) = Di/(hx*hx)+Dv*U(i,j)
B(i,j) = -2*TWO*Di/(hx*hx)-TWO/h
C(i,j) = Di/(hx*hx)-Dv*U(i,j)
F(i,j) = (-TWO/ht)*T1(i,j)+
Dv/2hx*V(i,j)*(T1(i,j+1)-T1(i,j-1))-
Di/(hx*hx)*(T1(i,j+1)-T1(i,j)-T1(i,j)+T1(i,j-1))-
1/q1*(T1(i,j)*(ONE-T1(i,j))+S1(i,j)*q3*
(q2-T1(i,j))/(q2+T1(i,j)))
Aa(i,j)=C(i,j)/(A(i,j)*Aa(i-1,j)+B(i,j))
Bb(i,j)= (F(i,j)-A(i,j)*Bb(i-1,j))/
(A(i,j)*Aa(i-1,j)+B(i,j))
END DO
**** VON NEUMANN BOUNDARY CONDITIONS ****
T2(m,j)=Bb(m-1,j)/(ONE-Aa(m-1,j))
**** FINAL RECONSTRUCTION OF THE CONCENTRATION
PROFILE OVER X DIRECTION ****
DO i=1,m-1
T2(m i,j)=Aa(m-i,j)*T2(m-i+1,j)+Bb(m-i,j)
END DO
END DO
```

Chemical oscillations are considered as spatial averages `Tav` and `Sav` of configurations provided by `bro(ce)________.dat` respectively, in which every point (i, j) of the grid is associated with a value of concentration for the two species, `T3(i,j)` and `S3(i,j)`. The resulting code is

```
Tav = 0
Sav = 0
DO i = 2,m-1
DO j = 2,m-1
Tav = Tav + T3(i,j)
```

```
Sav = Sav + S3(i,j)
END DO
END DO
Tav = Tav/npoints
Sav = Sav/npoints
```

0.38 Initial conditions

The concentration functions describing the initial conditions are

$$c_1^0 = \begin{cases} 0.8, & 0 < \theta < 0.5 \\ c_{1(ss)}, & \text{elsewhere.} \end{cases} \tag{167}$$

$$c_2^0 = \left[c_{2(ss)} + \frac{\theta}{8\pi f} \right] \times 1.3 \tag{168}$$

where θ is the polar coordinate angle and f the oregonator kinetic parameter. The polar coordinate is defined, respect to the center of the grid (mid, mid) as

$$\arctan \left[\frac{(j - \text{mid})}{(i - \text{mid})} \right] \tag{169}$$

and the Fortran 90 translation is

```
DO i=1,m
DO j=1,m
IF((i.GT.mid).AND.(j.GT.mid)) THEN
ratio=(j-mid)/(i-mid)
theta=ATAN(ratio)
ELSE IF((i.LT.mid).AND.(j.GT.mid))
THEN
ratio=(j-mid)/(i-mid)
theta=ATAN(ratio)+PG
ELSE IF((i.LT.mid).AND.(j.LT.mid)) THEN
ratio=(j-mid)/(i-mid)
theta=ATAN(ratio)+PG
ELSE IF((i.GT.mid).AND.(j.LT.mid))
THEN
ratio=(j-mid)/(i-mid)
theta=ATAN(ratio)+TWO*PG
END IF
T1(i,j) =ss
IF((theta.GE.ZERO).AND.(theta.LE.HALF))
T1(i,j)=T1 DEFAULT VALUE
T1(mid,mid)=ss
S1(i,j) =ss+theta*ONE/(EIGHT*PG*f)
S1(mid,mid)=ss
END DO
END DO
```

0.39 Molecular Dynamics Simulations

In this section we report the force field parameters used in our simulations, in order to predict the diffusion coefficients of intermediate species Ce^{3+} and $HBrO_2$ participating to Belousov–Zhabotinsky reaction.

0.39.1 Ce^{3+} MD input parameters

```
INTERACTION PARAMETERS:

        The input Lennard Jones functional were introduced
        in the sigma-epsilon notation

        Lennard-Jones parameters: sigma (angstrom)

              O            H            Ce
   O    3.1655000   0.0000000   0.0000000
   H    0.0000000   0.0000000   0.0000000
   Ce   0.0000000   0.0000000   0.0000000

        Lennard-Jones parameters: epsilon (kJ mol-1)

              O            H            Ce
   O    0.6500000   0.0000000   0.0000000
   H    0.0000000   0.0000000   0.0000000
   Ce   0.0000000   0.0000000   0.0000000

        Additional potential functions where introduced
        for some pairs
        The overall number of additional functions is:   1
        In particular they are: 1  Buckingham interaction


        Added Buckingham parameters: A (kJ mol-1)

                  O                   H                   Ce
   O      0.0000000E+00     0.0000000E+00     1.0040000E+06
   H      0.0000000E+00     0.0000000E+00     0.0000000E+00
   Ce     1.0040000E+06     0.0000000E+00     0.0000000E+00

        Added Buckingham parameters: B (1/angstrom)

                  O                   H                   Ce
   O      0.0000000E+00     0.0000000E+00     3.5000000E+00
   H      0.0000000E+00     0.0000000E+00     0.0000000E+00
   Ce     3.5000000E+00     0.0000000E+00     0.0000000E+00

        Added Buckingham parameters: C (kJ mol-1 angstrom^6)

                  O                   H                   Ce
   O      0.0000000E+00     0.0000000E+00     3.6280000E+04
   H      0.0000000E+00     0.0000000E+00     0.0000000E+00
   Ce     3.6280000E+04     0.0000000E+00     0.0000000E+00


  Partial charges on atoms (Coulomb):
```

```
          O            H            Ce
-0.7300000    0.3650000    3.0000000
```

0.39.2 $HBrO_2$ MD input parameters

```
INTERACTION PARAMETERS:

        the input Lennard Jones functional were introduced
        in the sigma-epsilon notation

        Lennard-Jones parameters: sigma (angstrom)

              O            H            O            Br           OH           HO
   O    3.1506000    0.0000000    3.0552000    3.5530000    3.1075500    0.0000000
   H    0.0000000    0.0000000    0.0000000    0.0000000    0.0000000    0.0000000
   O    3.0552000    0.0000000    2.9598000    3.4576000    3.0121500    0.0000000
   Br   3.5530000    0.0000000    3.4576000    3.9554000    3.5099500    0.0000000
   OH   3.1075500    0.0000000    3.0121500    3.5099500    3.0645000    0.0000000
   HO   0.0000000    0.0000000    0.0000000    0.0000000    0.0000000    0.0000000

        Lennard-Jones parameters: epsilon (kJ mol-1)

              O            H            O            Br           OH           HO
   O    0.6361960    0.0000000    0.7477885    0.9230902    0.7485004    0.0000000
   H    0.0000000    0.0000000    0.0000000    0.0000000    0.0000000    0.0000000
   O    0.7477885    0.0000000    0.8789550    1.0850056    0.8797917    0.0000000
   Br   0.9230902    0.0000000    1.0850056    1.3393600    1.0860385    0.0000000
   OH   0.7485004    0.0000000    0.8797917    1.0860385    0.8806292    0.0000000
   HO   0.0000000    0.0000000    0.0000000    0.0000000    0.0000000    0.0000000


        Partial charges on atoms (Coulomb):

              O            H            O            Br           OH           HO
      -0.8340000    0.4170000   -0.2930000    0.3720000   -0.4360000    0.3570000


S t r e t c h i n g   P o t e n t i a l :

            U = 1/2*k_2(r - r_0)^2 + 1/3*k_3(r - r_0)^3 + 1/4*k_4(r - r_0)^4

            n. stretchings =   3

              1   atom 1 =   1        atom 2 =   2
                 r_0 =      1.80000    (Angstroem)
                 k_2 =   2418.38190    (kJ/mol/A^2)
                 k_3 =      0.00000    (kJ/mol/A^3)
                 k_4 =      0.00000    (kJ/mol/A^4)

              2   atom 1 =   2        atom 2 =   3
                 r_0 =      1.86600    (Angstroem)
                 k_2 =   1985.60120    (kJ/mol/A^2)
                 k_3 =      0.00000    (kJ/mol/A^3)
                 k_4 =      0.00000    (kJ/mol/A^4)

              3   atom 1 =   3        atom 2 =   4
                 r_0 =      0.97400    (Angstroem)
                 k_2 =   3093.92160    (kJ/mol/A^2)
                 k_3 =      0.00000    (kJ/mol/A^3)
                 k_4 =      0.00000    (kJ/mol/A^4)



            B e n d i n g   P o t e n t i a l :
```

```
U = 1/2*k_2(A - A_0)^2 + 1/3*k_3(A - A_0)^3 + 1/4*k_4(A - A_0)^4

n. bendings =   2

  1   atom 1 =   1        atom 2 =   2        atom 3 =   3
     A_0 =      1.77325    (Radians)          101.60    (Degrees)
     k_2 =    352.83765    (kJ/mol/rad^2)
     k_3 =      0.00000    (kJ/mol/rad^3)
     k_4 =      0.00000    (kJ/mol/rad^4)

  2   atom 1 =   2        atom 2 =   3        atom 3 =   4
     A_0 =      1.77325    (Radians)          101.60    (Degrees)
     k_2 =    352.83765    (kJ/mol/rad^2)
     k_3 =      0.00000    (kJ/mol/rad^3)
     k_4 =      0.00000    (kJ/mol/rad^4)


D i h e d r a l   P o t e n t i a l :

U = A*[1+cos(m*phi-delta)]

n. dihedrals =   1

       A =     20.92750     (kJ/mol)
     phi =      3.14159    (Radians)          180.00    (Degrees)
       m =      2.00000
```

0.39.3 The mean square displacement

We consider a discrete physical system composed only by a single particle randomly moving in a unidimensional box of lenght L. In this case the mean square displacement is not a function of the time but a vector of j temporal components ranging from 0 to $n-1$ (for simplicity we consider $n = 5$ temporal instants and $j = 0, \ldots, n-1 = 4$ temporal steps ($j = \delta t$)):

$$\begin{aligned} MSD =& \vec{r^2}(t_0, \ldots, t_{n-1}) \\ =& \Big(\left\langle r^2\left(t_0\right)\right\rangle, \ldots, \left\langle r^2\left(t_{n-1}\right)\right\rangle \Big) \end{aligned} \tag{170}$$

where the j^{th}component of the vector is given by

$$\left\langle r^2\left(j\right)\right\rangle = \frac{1}{n-j} \sum_{k=1}^{n-j} [x(k+j) - x(k)]^2 \tag{171}$$

and $\frac{1}{n-j}$ is a factor for the average over the number of configurations within the sum.

Let now calculate from 171 the components of $\vec{r^2}(t_0,\ldots,t_{n-1})$ vector:

$$
\begin{aligned}
\left\langle r^2\,(0)\right\rangle &= \frac{1}{5-0}\sum_{k=1}^{5-0}[x(k+0)-x(k)]^2 = 0 \\
\left\langle r^2\,(1)\right\rangle &= \frac{1}{5-1}\sum_{k=1}^{5-1}[x(k+1)-x(k)]^2 = \\
&= \frac{1}{4}\big\{[x(2)-x(1)]^2+[x(3)-x(2)]^2+ \\
&\quad +[x(4)-x(3)]^2+[x(5)-x(4)]^2\big\} \\
\left\langle r^2\,(2)\right\rangle &= \frac{1}{5-2}\sum_{k=1}^{5-2}[x(k+2)-x(k)]^2 = \\
&= \frac{1}{3}\big\{[x(3)-x(1)]^2+[x(4)-x(2)]^2+ \\
&\quad +[x(5)-x(3)]^2\big\} \qquad (172) \\
\left\langle r^2\,(3)\right\rangle &= \frac{1}{5-3}\sum_{k=1}^{5-3}[x(k+3)-x(k)]^2 = \\
&= \frac{1}{2}\big\{[x(4)-x(1)]^2+[x(5)-x(2)]^2\big\} \\
\left\langle r^2\,(4)\right\rangle &= \frac{1}{5-4}\sum_{k=1}^{5-4}[x(k+4)-x(k)]^2 = \\
&= \frac{1}{1}\big\{[x(5)-x(1)]^2\big\}
\end{aligned}
$$

The translation into an opportune Fortran 90 code is quite simple.

```
DO i=1,n
READ(10,*) x(i)
IF (i>1) THEN
IF (x(i)-x(i-1) > L/2) THEN

! periodic boundary conditions for a simulation box
! of length L centered in 0:  - L/2 < x < + L/2

jump = jump - L
ELSE IF (x(i)-x(i-1)< -L/2) THEN
jump = jump + L
END IF
xn(i)=x(i)+jump
ELSE
xn(i) = x(i)
END IF

WRITE(30,100) x(i), jump, xn(i)
100 FORMAT (1x, f16.7, 1x, f16.7, 1x, f16.7)
END DO
```

```
DO j=0,n-1
r2 = 0.0d0
DO k=1,n-j
r=xn(k+j)-xn(k)
r2=r2 + r*r
END DO

!******************************
!MEAN SQUARE DISPLACEMENT

r2 = r2/(n-j)

!******************************

write (20,110) j, r2
110 format(1x, i6, 1x, f12.5)

END DO
```

Bibliografia

Abramian, A., S. Vakulenko e V. Volpert
2003 *Patterns and Waves*, AkademPrint, Saint Petersburg. (Citato a p. lxi.)

Agladze, K.I., V.I. Krinsky e A.M. Pertsov
1984 , *Nature*, 308, 834-835. (Citato a p. lxi.)

Atkins, P. W.
1994 *Physical Chemistry, 5th edition*, Oxford University Press, Oxford. (Citato a p. xxxvi.)

Belk, M. e V. Volpert
2004 , *Chaos*, 14, 263. (Citato a p. lxxix.)

Biktashev, J. N., A. V. Holden e M. A. Tsyganov
1998 , *Phys. Rev. Lett.*, 81, 2815. (Citato a p. lxxix.)

Biosa, G., S. Bastianoni e M. Rustici
2006 , *Chemistry-A Eur. J.*, 12, 13, p. 3430. (Citato alle pp. liii, lxi.)

Biosa, G. *et al.*
2005 , *Chem. Phys.*, 308, 7. (Citato a p. xciv.)

Bockmann, M., B. Hess e S.C. Muller
1996 , *Phys. Rev. E*, 53, 5498. (Citato a p. lxiv.)

Boussinesq, J.
1903 *Théorie Analytique de la Chaleur*, 2, Gauthier-Villars, Paris. (Citato a p. lvii.)

Budroni, M. A., M. Rustici e E. Tiezzi
2011 , *Math. Model. Nat. Phenom.*, 6, 226. (Citato a p. lxxix.)

Budroni, M. A. *et al.*
2008 , *J. Phys. Chem.*, 128, 111102. (Citato a p. lxxiv.)

Budroni, M. A. *et al.*
2009 , *J. Phys. Chem.*, 130, 024902. (Citato a p. lxxix.)

Castets, V. *et al.*
1990 , *Phys. Rev. Lett.*, 64, 24. (Citato a p. lv.)

Chan, W. e C. Tse

1997 , *IEEE Trans. Circuits and System-I*, 44, 12, p. 1129. (Citato alle pp. lxxxi, lxxxiv.)

Chandrasekhar, S.

1961 *Hydrodynamic and hydromagnetic stability*, Oxford University Press, Oxford. (Citato a p. lv.)

Ciotti, L. *et al.*

2011 , *Chem. Phys, Lett.*, 512. (Citato a p. lxxxiii.)

Cliffe, K.A., S.J. Taverner e H. Wilke

1998 , *Phys. Fluids*, 10, 173023. (Citato a p. lxiv.)

Cornell, W. D. *et al.*

1995 , *J. Am. Chem. Soc.*, 117, pp. 5179–5197. (Citato a p. lxxxvii.)

Cross, M.C. e P.C. Hohenemberg

1993 , *Rev. Mod. Phys.*, 65, 3. (Citato a p. lxi.)

Currie, I. G.

1993 *Fundamental of mechanics of fluids*, McGraw-Hill, New York. (Citato a p. lv.)

Davidenko, J. M. *et al.*

1992 , *Nature*, 355, pp. 349–351. (Citato a p. lii.)

Ducrot, A. e V. Volpert

2005 , *J. Tech. Phys.*, 46, 129. (Citato a p. lxxix.)

Eckmann, J. P.

1981 , *Rev. Mod. Phys.*, 643, 53, pp. 740–749. (Citato a p. xxxiii.)

Epstein, I. R. e J. A. Pojman

1998 *An introduction to nonlinear chemical dynamics*, Oxford University Press, Oxford. (Citato alle pp. lii, liii.)

Ertle, G.

1991 , *Science*, 254, p. 1750. (Citato a p. lii.)

Espenson, J. H.

1981 *Chemical kinetics and reaction mechanism*, McGraw-Hill, New York. (Citato a p. xxxvi.)

Feigenbaum, M. J.

1979 , *J. Stat. Phys.*, 699, 21, pp. 740–749. (Citato alle pp. xxxiii, cvii.)

Field, R.J. e M. Burger

1985 *Oscillations and Travelling Waves in Chemical Systems*, Wiley, New York. (Citato a p. xl.)

Ganapathisubramanian, N. e R. M. Noyes

1982 , *J. Phys. Chem.*, 86, 26. (Citato a p. xxxix.)

Gaponenko, Y. e V. Volpert

2003 *Numerical Simulations of Convective Turing Structures, Pattern and Waves*, a cura di A. Abramian, S. Vakulenko e V. Volpert, AkademPrint, St. Petersburg. (Citato alle pp. lxi, lxxix.)

Gollub, J. P. e S. H. Benson

1980 , *J. Fluid. Mech.*, 100, 449. (Citato a p. lxxix.)

Guzmán, A. M. e C. H. Amon

1994 , *Phys. Fluids*, 6. (Citato a p. lxxix.)

Györgyi, L., T. Turanyi e R. J. Field

1990 , *J. Phys. Chem.*, 94, 7162. (Citato a p. xlii.)

Hegedus, L. *et al.*

2006 , *J. Phys. Chem. A*, 110, 47. (Citato a p. xxxix.)

Hegger, R., H. Kantz e T. Schreiber

TISEAN software package, Publicly available at http://www.mpipks-dresden.mpg.de/~tisean. (Citato a p. cvii.)

1999 , *Chaos*, 9, 413. (Citato a p. cvii.)

Hilborn, R. H.

1994 *Chaos and nonlinear dynamics*, Oxford University Press, New York-Oxford. (Citato a p. xxxiii.)

Jahnke, W., W.E. Skaggs e A.T. Winfree

1989 , *J. Phys. Chem.*, 93, 2, pp. 740–749. (Citato alle pp. lxxi, lxxiii, lxxix, lxxxvii.)

Johnson, B. R., S. K. Scott e B. W. Thompson

1997 , *J. Nonlinear Sci.*, 2, 350. (Citato a p. xxxix.)

Kapral, R. e K. Showalter

1994 *Chemical waves and patterns*, Kluwer Academic Publishers, Dordrecht, Boston e London. (Citato a p. li.)

Keki, S. *et al.*

1992 , *J. Phys. Chem.*, 96, 4. (Citato a p. xxxix.)

Kepper, P. De, J. Boissonade e I. R. Epstein

1990 , *J. Phys. Chem.*, 94, pp. 6525–6536. (Citato a p. lv.)

Lin, C. C. e F. H. Shu

1964 , *Astrophys.J.*, 140, pp. 646–655. (Citato a p. liii.)

Liveri, M.L. Turco *et al.*

2003 , *J. Phys. Chem. A*, 107, 4834. (Citato a p. lxi.)

Lorenz, E.
1963 , *J. Atmos. Sci.*, 20, pp. 130–141. (Citato a p. xxi.)

M. Souaille, M. Duvail qnd, R. Spezia e T. Cartailler
2007 , *J. Chem. Phys.*, 127, 034503, pp. 1157–1174. (Citato a p. lxxxvii.)

Mandelbrot, B.
1982 *The fractal geometry of nature*, W. H. Freeman, San Francisco. (Citato a p. xxx.)

Marchettini, N. *et al.*
2010 , *Phys. Chem. Chem. Phys.*, 12, 11062. (Citato a p. lxxiv.)

Masia, M. *et al.*
2001 , *Chem. Phys. Lett.*, 341, 285. (Citato a p. xciv.)

McLaughlin, J. B. e S. A. Orszag
1982 , *J. Fluid. Mech.*, 122, 123. (Citato a p. lxxix.)

Molenaar, D., H. J. Clercx e G. J. F. van Heijst
2005 , *Phys. Rev. Lett.*, 95, 104503. (Citato a p. lxxix.)

Murray, J.
1993 *Mathematical Biology*, Springer, Berlin, Heidelberg e New York. (Citato a p. li.)

Newhouse, S., D. Ruelle e F. Takens
1978 , *Comm. Math. Phys.*, 64, 1, pp. 35–40. (Citato a p. xxxiii.)

Nicolis, G.
1995 *Introduction to nonlinear science*, Cambridge University Press, Cambridge. (Citato alle pp. xxiv, xxvii.)

Nicolis, G. e I. Prigogine
1977 *Self-organization in nonequilibrium systems*, Wiley, New York. (Citato alle pp. xxiv, xl.)

Ott, E.
1993 *Chaos in dynamical system*, Cambridge University Press, New York. (Citato alle pp. lxxxi, lxxxiv.)

Peaceman, D. W. e H. H. Rachford
1955 "The numerical solution of parabolic and elliptic differential equations", *J. Soc. Indust. Appl. Math.*, 3, pp. 28–41. (Citato a p. lxvii.)

Pérez-Villar, V. *et al.*
2002 , *Phys. Rev. E*, 66, 036309. (Citato a p. lxxix.)

Pojman, J. A. e I. Epstein
1990 , *J. Phys. Chem.*, 4966, 94, pp. 740–749. (Citato a p. lxiv.)

Press, W. H. *et al.*
1992 *Numerical recipes in Fortran: the art of scientifing computing*, Cambridge University Press, Cambridge. (Citato a p. lxix.)

Prigogine, I.
1947 *Etude thermodynamique des processus irreversibles*, Desoer, Liège. (Citato a p. xxiii.)

Q.Ouyang e J.-M.Flesselles
1996 , *Nature*, 379, 143. (Citato alle pp. lxi, lxxix.)

Ramos, J. I.
2001 , *Chaos, Solitons and Fractals*, 12, 1897. (Citato a p. lxxix.)

Rossi, F. *et al.*
2005 , *Chem. Phys.*, 313, 101. (Citato alle pp. lxxix, xciv.)

Ruelle, D. e F. Takens
1971 , *Comm. Math. Phys.*, 20, 3, pp. 167–192. (Citato a p. xxxiii.)

Rustici, M. *et al.*
1996 , *Chem. Phys. Lett.*, 263, 429. (Citato a p. lxxxi.)

Rustici, M. *et al.*
1999 , *J. Phys. Chem.*, 103, 6564. (Citato a p. lxxxii.)

Rustici, M. *et al.*
2001 , *Faraday Discuss.*, 120, 39. (Citato a p. lxi.)

Sandstede, B., A. Scheel e C. Wulff
1999 , *J. Nonlinear. Sci.*, 9, 439. (Citato a p. lxxix.)

Scott, S. K.
1994 *Oscillations, waves and chaos in chemical kinetics*, Oxford University Press, Oxford. (Citato alle pp. xxxvii, lii.)

Smith, G. D.
1965 *Numerical solution of partial differential equations*, Oxford University Press, London. (Citato a p. lxvi.)

Smoes, M.
1979 , *J. Phys. Chem.*, 71, 11. (Citato a p. xxxix.)

Strizhak, P. E. e A. L. Kawczynski
1995 , *J. Phys. Chem.*, 99, 27. (Citato a p. xxxix.)

Strogatz, S. H.
1994 *Nonlinear dynamics and chaos*, Addison-Wesley, Cambridge. (Citato a p. xxvii.)

Taylor, A. F.
2002 , *Prog. React. Kinet. Mech.*, 27, 4. (Citato a p. xxxix.)

Vasquez, D.A., J.W. Wilder e B.F. Edwards
1993 , *J. Chem. Phys.*, 98, 3, p. 2138. (Citato a p. lxiv.)

Wang, J. e T. Hou
2011 , *J. Comp. Chem.*, 32, 16, pp. 3505–3519. (Citato a p. lxxxvii.)

Wang, J., P. G. Soerensen e F. Hynne
1994 , *J. Phys. Chem.*, 98, 3. (Citato a p. xxxix.)
1995 , *J. Phys. Chem.*, 192, 63. (Citato a p. xxxix.)

Wang, J. *et al.*
2004 , *J. Comp. Chem.*, 25, 9, pp. 1157–1174. (Citato a p. lxxxvii.)

Wang, J. *et al.*
2005 , *J. Phys. Chem. A*, 109, 7. (Citato a p. xxxix.)

Wilder, J.W., B.F. Edwards e D.A. Vasquez
1992 , *Phys. Rev. A*, 45, 2320. (Citato a p. lxiv.)

Wu, Y. *et al.*
1995 , *Phys. Rev. E*, 51, 1119, pp. 740–749. (Citato alle pp. lxi, lxii, lxxiii, lxxxvii.)

Zaikin, A.N. e A.M. Zhabotinsky
1970 , *Nature (London)*, 225, 535. (Citato a p. xxxix.)

Zhabotinsky, A. M.
1964 , *Proc. Acad. Sci. USSR*, 157, 392. (Citato a p. xxxix.)

Dichiarazione

This doctoral thesis is a presentation of my original research work. Wherever contributions of others are involved, every effort is made to indicate this clearly, with due reference to the literature, and acknowledgement of collaborative research and discussions. The work was done under the guidance of my Advisor, Professor Mauro Rustici, at the Physical Chemistry Department, University of Sassari, within the Doctoral School of Chemical Sciences, Director Professor G. B. Suffritti.

Sassari, novembre 2011

Luigi Ciotti